DESIGN AND MECHANICAL EVALUATION OF AN ARTIFICIAL MENISCUS IMPLANT

A Thesis
Presented to
The Academic Faculty

by

Jonathan William Schwartz

In Partial Fulfillment
of the Requirements for the Degree
Master of Science in the
School of Mechanical Engineering

Georgia Institute of Technology
May 2018

DESIGN AND MECHANICAL EVALUATION OF AN ARTIFICIAL MENISCUS IMPLANT

Approved by:

Dr. David N. Ku, Advisor
School of Mechanical Engineering
Georgia Institute of Technology

Dr. Robert Guldberg
School of Mechanical Engineering
Georgia Institute of Technology

Dr. Johnna Temenoff
School of Biomedical Engineering
Georgia Institute of Technology

Date Approved: April 23, 2018

ACKNOWLEDGEMENTS

I would like to thank my advisor, Dr. David Ku, for allowing me to join his lab and giving me this research opportunity. His guidance and advice throughout my time at Georgia Tech has added significant value to my graduate school experience and has set me up for future success. Working in his lab and on this project has strengthened my critical thinking and problem solving ability more than I could have imagined and has given me skills that I will use for the rest of my career. I will always be thankful for my time here and his mentorship.

I would also like to thank my lab mates, both past and present, for their help along the way. Although we all had different projects, the discussion and advice you all provided allowed me to find a solution whenever I was stuck on something. I enjoyed working around you all throughout this graduate school experience and wish you all the best of luck in life.

I would like to thank all the friends I've made since moving to Atlanta and the friends I've had all along. Although graduate school had its busy times, the breaks spent with them provided stress relief when it was needed most.

Finally, I would like to thank my parents, Jeff and Vicki, and my sister, Kristina, for always supporting me through the good times and bad and for pushing me to do my best. I wouldn't be where I am today if it weren't for your love and support, and I'm very lucky to have such a great family behind me.

TABLE OF CONTENTS

LIST OF TABLES

LIST OF FIGURES

SUMMARY

The menisci are wedges of fibrocartilage in the knee joint that help to redistribute compressive loads by increasing the contact area within the joint. Meniscus tears are among the most common orthopedic injuries, but shortcomings with the current treatments leave a clinical need for a new method for repair or replacement. The meniscal tissue can only be repaired in limited cases due to its healing capacity and no artificial meniscal replacement is currently approved by the FDA. The most common treatment for meniscal tears is removal of the damaged tissue, or a meniscectomy. The contact stress in the joint increases proportionally with the amount of meniscus tissue removed due to the decrease in contact area, and the changes in contact stress leads to articular cartilage damage and the development of osteoarthritis. This work explores the use of an artificial composite material with the shape, strength, properties, and contact mechanics needed to serve as a meniscal replacement implant following injury.

In this research, a proposed artificial meniscus implant design is made from an aramid fiber-reinforced composite of polyvinyl alcohol (PVA) hydrogel, which is a promising biomaterial for orthopedic applications. A set of functional requirements and design specifications are created from literature values related to the loading experienced on the menisci in the knee joint and the mechanical properties of the natural menisci. Samples of the composite material underwent a series of tests to determine if the design specifications could be met. The ultimate strength (tensile and shear), the elastic modulus (tensile and compressive), resistance to change after cyclic loading, resistance to change after high magnitude compressive loading, and fiber tear out strength were evaluated. The

pressure distributing properties of various meniscus implant prototypes and conditions in a knee joint model were also assessed.

All design specifications were met using the composite material and the proposed implant design restored the contact mechanics within the knee joint model to natural conditions. The results of this work show that the right combination of material, structure, and shape for an artificial meniscus implant can provide the functional and mechanical properties needed to serve as a suitable meniscus replacement following injury. The artificial implant can be a possible treatment for damaged menisci that overcomes the deficiencies associated with the current options.

CHAPTER 1. INTRODUCTION AND BACKGROUD

1.1 Meniscus Structure and Function

The lateral and medial menisci are two semilunar wedges of dense fibrocartilage in the knee joint between the tibia and femur. The shape of the menisci allow conformity between the femoral condyles and the tibial plateaus. They are attached to the tibia and femur through various ligaments, with the main attachment points being to the tibia at the posterior and anterior horns (see Figure 1), but have mobility within the knee [1]. The lateral and medial menisci have different dimensions within the joint, with the lateral meniscus being approximately 34.8-37.0 mm long and 28.4-29.8 mm wide and the medial meniscus being 43.8-45.1 mm long and 29.5-32.2 mm wide [2]. In addition to having a wider variety of shape, size, and thickness, the lateral meniscus also occupies a larger portion of the tibial plateau area at 75-93% when compared to the medial meniscus at 51-74% [3].

The adult menisci are separated into distinct regions when it comes to vascularization, as shown in Figure 2. The peripheral “red zone” contains a blood supply and nerves while the central “white zone” is avascular and aneural, which negatively affects the healing capacity within this central region of the menisci. The two regions are separated by a transitional “red-white zone” that has limited healing ability [4]. Water makes up most of the meniscal tissue, accounting for about 72% of its weight. It is also composed of fibrochodrocyte cells and an extracellular matrix consisting mainly of a collagen fiber network (75% dry weight) along with proteoglycans, glycoproteins, and elastin [5], [6].

The collagen fibers within the menisci have a specific arrangement that contribute directly to the tensile properties of the meniscus tissue (see Figure 3). A random woven mesh of fibers is present at the surface for low friction articulation with surrounding articular cartilage [7]–[9]. Circumferentially oriented fibers in the deep layers of the meniscus follow the peripheral border and extend beyond the meniscal horns to form the ligamentous attachments to the tibia [10], [11]. These circumferential fibers allow the meniscus to withstand tensile hoop stresses that develop in the tissue under compressive loading. There are also radially oriented "tie" fibers interspersed between circumferential fibers that provide the meniscal tissue with structural integrity and prevent splitting of circumferential fibers [12].

The menisci withstand tensile, compressive, and shear forces and have various roles within the knee joint such as joint stability, shock absorption, joint lubrication, load bearing, and chondroprotection by distributing loads over a broad area of articular cartilage [7], [13]–[16]. The primary function of the menisci is to redistribute the axial compressive load from the femur across the tibial plateau. Due to the wedge shape of the meniscus, it extrudes radially under compressive force. This extrusion is prevented by the circumferential fibers and their ligamentous attachments at the horns, which develop tensile hoop stresses to resist the radial displacement, as shown in Figure 4 [17]–[19].

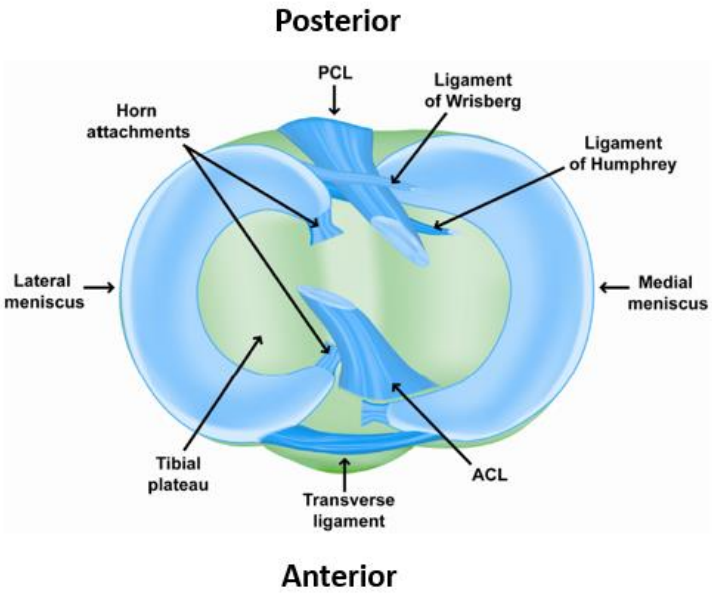

Figure 1: The menisci and their anterior and posterior horn attachments. Also shown are associated ligaments within the knee joint. [20]

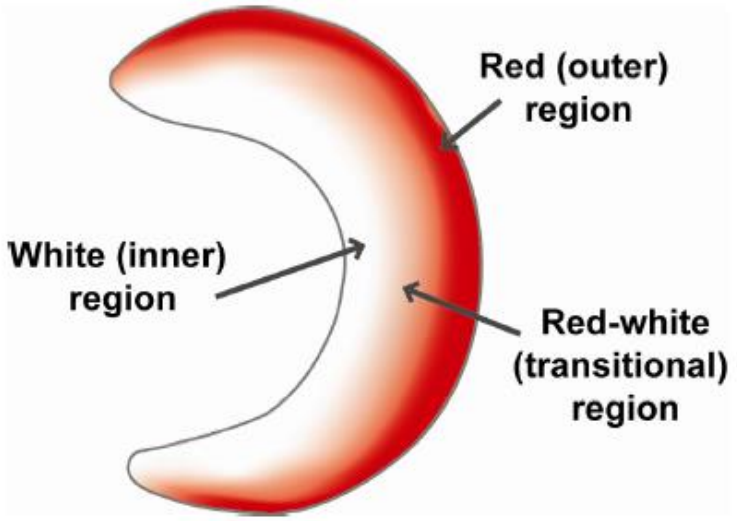

Figure 2: Vascularization of the meniscus. The peripheral red region has vasculature and nerves and the central white region does not. [20]

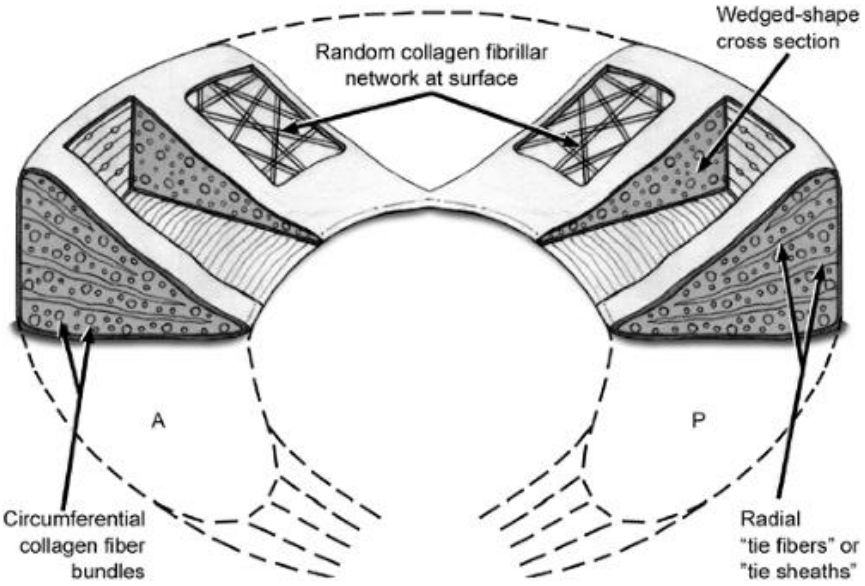

Figure 3: The collagen fiber structure of the meniscus. A random network is at the surface while circumferential and radial fibers are in the deeper tissue layers. [21]

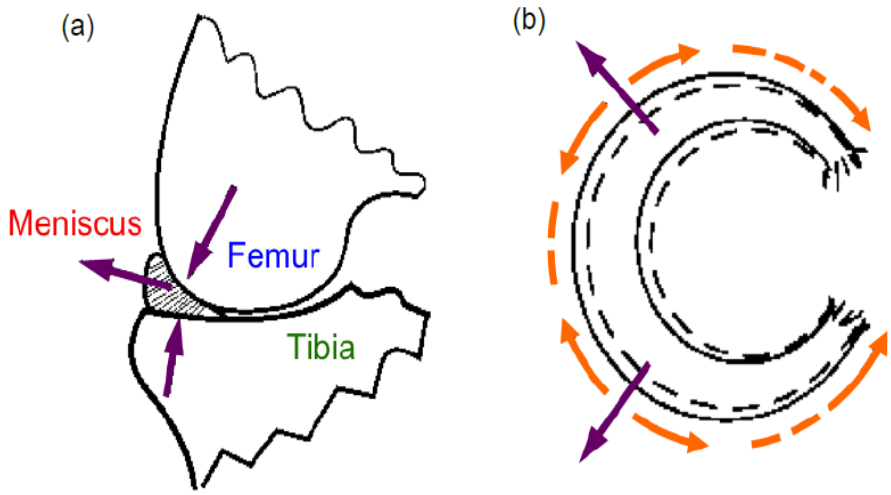

Figure 4: The loading of the meniscus from the side (a) and from above showing hoop stress development in orange and radial displacement in purple (b). [22]

1.2 Meniscus Pathophysiology

1.2.1 Prevalence

Meniscal lesions or tears are one of the most common injuries of the knee, with 15% of all knee injuries involving one or both menisci and around 850,000 meniscal injury related surgeries occurring in the USA annually [23]–[25]. Due to western culture's growing desire to stay active even at a high age, the number of meniscus related injuries continues to grow. The rates of hospital admission after meniscal injury is 0.35-0.7 per 1000 person-years, and this incidence is even higher for active US military service men at 8.27 per 1000 person-years [26]–[28].

1.2.2 Injuries

There are two types of meniscal lesions: acute/traumatic tears from forced movement of the knee joint and chronic/degenerative tears from deterioration of tissue due to aging. Traumatic tears occur from sharp movements and actions of great force, and usually occur in younger people [29]. The symptoms associated with meniscal injury include pain, mechanical impairment, tenderness, and swelling in the knee joint area [30]. In addition to the symptoms associated with the initial injury, osteoarthritis can develop due to meniscal pathology or after a meniscectomy, which is the surgical removal of all or part of the meniscus [31], [32]. Once the meniscus is torn or damaged, its chondroprotective function is compromised, which leads to the progression of osteoarthritis [33]. There are many different types of meniscal tears and they can be classified by location, thickness, depth, and pattern [34]. Some common tear patterns include longitudinal/bucket handle, oblique, radial/transverse, horizontal, and complex (see Figure 5) [35]. The location of the tear is

important for their ability to heal, since only tears in vascularized regions have healing capabilities [36].

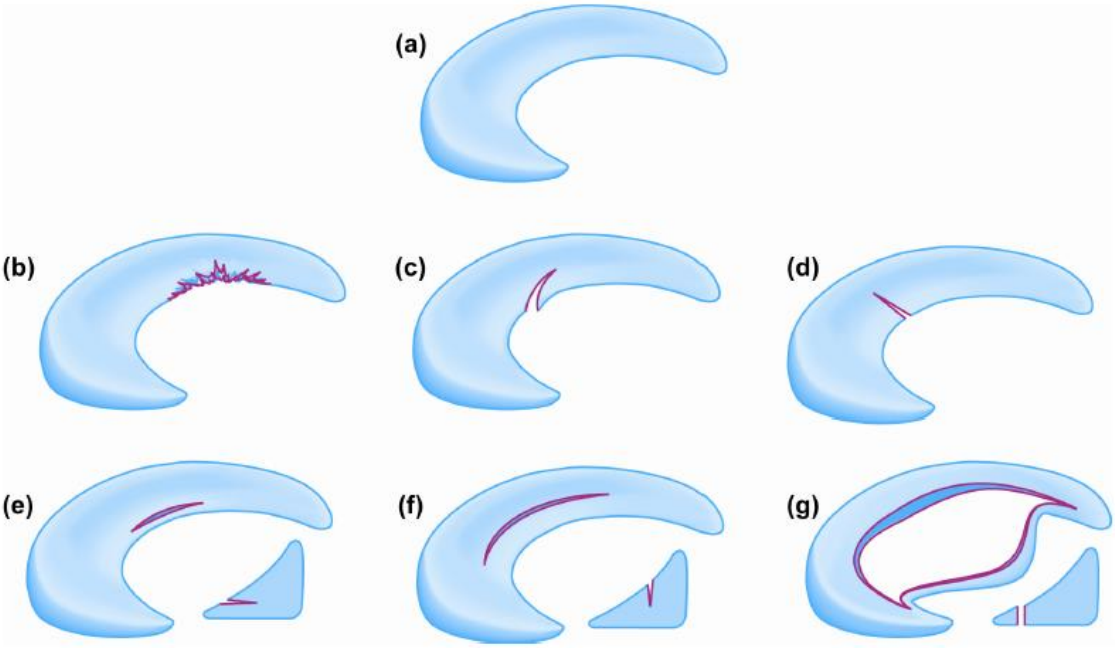

Figure 5: Meniscal tear patterns. The healthy meniscus (a) can experience complex/degenerative (b), oblique (c), radial (d), horizontal (e), and longitudinal (f) tears. A longitudinal tear passing through the entire thickness results in a bucket-handle tear (g). [20]

1.3 Current Treatments and Issues

1.3.1 Repair

Surgical repair on the meniscus following a tear can be achieved arthroscopically using sutures, staples, anchors, or similar methods, as shown in Figure 6 [37], [38]. There are many factors that come into play when assessing whether a meniscus tear can heal via repair or not including the type of tear, its location, the age of the patient, and various other

factors. [39]. The criteria for meniscal tear repair is limited due to the nature of meniscus tissue, since only 10% to 30% of the tissue is vascularized and can heal [40]. For this reason, only 3-5% of tears are currently considered for repair [41].

1.3.2 Meniscectomy

A meniscal tear can be treated by partial removal of the portion of the meniscus containing the tear (see Figure 6) or total removal of the meniscus, both of which are referred to as a meniscectomy. With an annual incidence of meniscal legions in the USA being 66 per 100,000 inhabitants, 61 of them result in meniscectomy [42], [43]. It is the most common treatment for meniscus injuries since menisci can only be repaired if the injury is in the peripheral vascularized region. Although they are a common treatment due to the disappearance of pain and impairment, meniscectomies can cause joint space narrowing, femoral condyle flattening, and ridge formation due to an increase in the contact stresses from the femur onto the tibial plateau [44]. These contact stresses increase proportionally with the amount of meniscus tissue removed and can increase by up to 235% due to the approximately 75% reduction in contact area on the tibial plateau following a meniscectomy (see Figure 7) [45]–[47]. The changes in contact stress distribution has also been suggested to lead to the progression of osteoarthritis in the joint and a direct relation between resection of the meniscus and the risk to develop radiographic osteoarthritis has been established [48]–[51]. Studies have shown that over 20% of patients that have undergone meniscectomy procedure show radiological articular cartilage degeneration within 5 years, and that number gets even greater with time [7], [52].

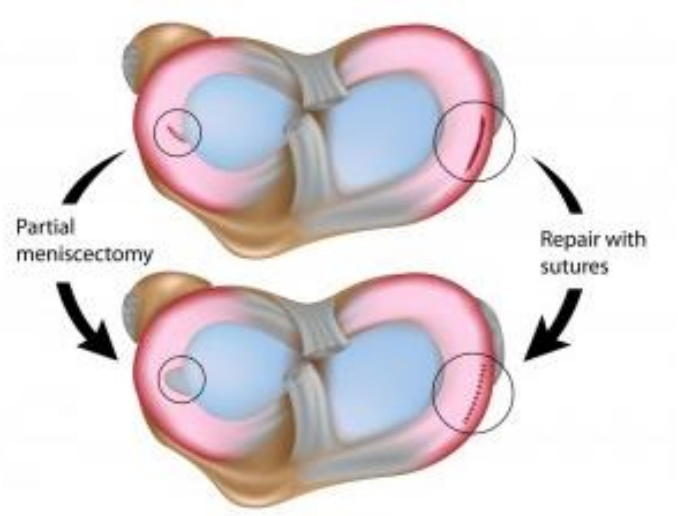

Figure 6: Treatment options for meniscal tears. Part of the meniscus is removed (meniscectomy) when the tear is in the white zone (left). Tears in the red zone can usually be repaired and heal (right). [53]

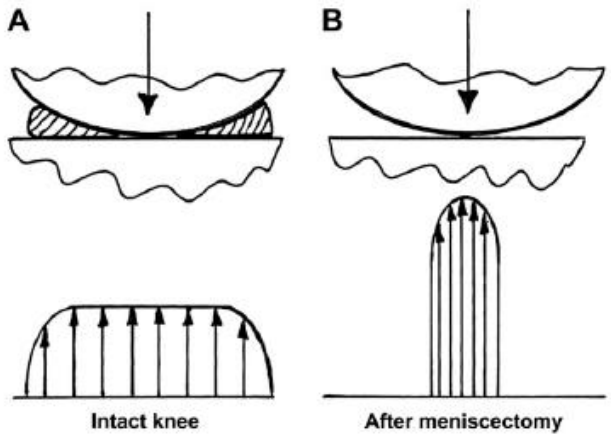

Figure 7: The contact stress on the tibial plateau for an intact knee (A) is concentrated over a smaller area and increases in magnitude following a meniscectomy (B). [7]

1.3.3 Allografts

Patients that undergo multiple partial resections or have very severe tears may require a (sub)total meniscectomy or a complete removal of the damaged meniscus. To relieve pain and prevent advanced osteoarthritis in these patients, meniscal allografts can be implanted to replace the removed meniscus. Although a meniscal allograft is currently the best available treatment for patients with symptomatic meniscectomies, problems associated with this treatment still exist. A meta-analysis of 44 trials representing 1136 grafts was analyzed by ElAttar et al and demonstrated a short to medium term complication rate of 21.3% in a mean follow-up of 4.6 years, the most common complication being a secondary tear [54]. Allografts are known to shrink and undergo collagen remodeling after transplantation, which can compromise their mechanical strength. In addition, problems related to allograft availability, size matching, high cost, and disease transmission prevent this treatment method from being practiced more frequently [25], [55], [56].

1.4 Synthetic Implants

A potential solution to the problems with current treatment would be an implantable meniscal substitute. No such treatment is presently available to patients or FDA approved. Various types of substitutes have been used in experimental and clinical studies including biodegradable scaffolds, permanent synthetic scaffolds, collagen, and completely artificial implants. Current research seems to mainly focus on tissue engineering approaches, but with limited success [25], [57].

1.4.1 Experimental Implants

Some of the earliest attempts of producing a meniscus substitute utilized Teflon and Dacron biomaterials as permanent meniscus replacement materials. However, the material properties of these materials were not suitable for this high-load application and resulted in deformation of the implant and wear particle deposition after testing in a rabbit model [33], [58], [59].

Another substitute that has been researched involves a polyglycolic acid fiber scaffold that is reinforced with poly(lactic-co-glycolic acid) and seeded with allogenic meniscus cells. The scaffold regenerated meniscus-like tissue after implantation into rabbits for 10 weeks, but further analysis of the tissue revealed a significantly decreased modulus value compared to natural tissue [60].

A porous scaffold with a hyaluronic acid and polycaprolactone matrix reinforced with circumferential poly-lactic acid fibers has also been investigated. These implants allowed fibrocartilage tissue ingrowth like the make-up of natural meniscus tissue, and showed little to no signs of cartilage damage in a one-year sheep study. However, implant extrusion out of the joint space was an issue in most cases, and a more rigid fixation to prevent this extrusion lead to dislocation and implant failure [61], [62].

Another porous scaffold made from collagen-hyaluronan reinforced with degradable poly (desaminotyrosyl-tyrosine dodecyl ester dodecanoate) fibers that mimic the collagen fiber arrangement in the meniscus has been studied as a total meniscus replacement [63]. The porous sponge structure allows for cell infiltration and has been shown to exhibit a tensile modulus and ultimate tensile load like the native meniscus prior to implantation. The

device was successful in demonstrating tissue regeneration and protection of articular cartilage compared to meniscectomies for 32 weeks in an ovine model. The device also maintained functional mechanical loads during that time [64]. However, a 52-week study showed that the explants achieved tensile stiffness and ultimate tensile loads that were only about half that of the native tissue and time-zero values. Problems with implant extrusion were also apparent [65].

1.4.1.1 PVA Hydrogel Implants

Polyvinyl alcohol (PVA) hydrogel was one of the first non-scaffold, permanent implants to have been studied for use as a meniscus replacement, and multiple groups have investigated this approach. Early studies by Kobayashi et al. demonstrated the usefulness of the material by showing that its compressive properties and viscoelastic behaviour were very similar to that of the natural meniscus, with no implant fracture or degradation of properties observed after implantation into a rabbit knee for 2 years [66], [67].

Another group evaluated the PVA hydrogel implant in a sheep model. Complete radial tears were observed in the posterior horns of all implants and the implants caused severe damage to the articular cartilage after one year. The authors speculated that size mismatch, inadequate fixation, or structural composition of the implant body could have caused these failures [68].

More recently, polyethylene fiber-reinforced PVA hydrogel implants have been investigated. Holloway et al. showed that incorporation of fibers into the hydrogel matrix can allow tuning of the compressive and tensile moduli to resemble that of the natural meniscus [69]. Since delamination of the hydrophobic fibers from the hydrogel matrix was

an initial concern, they also showed that surface modification of the fibers increased the interfacial strength of the composite [70]. A 4-month sheep study was conducted on implants with polyethylene fiber mats used as the reinforcement, but delamination of the implant still occurred along with implant extrusion and bone tunnel widening (see Figure 8) [71].

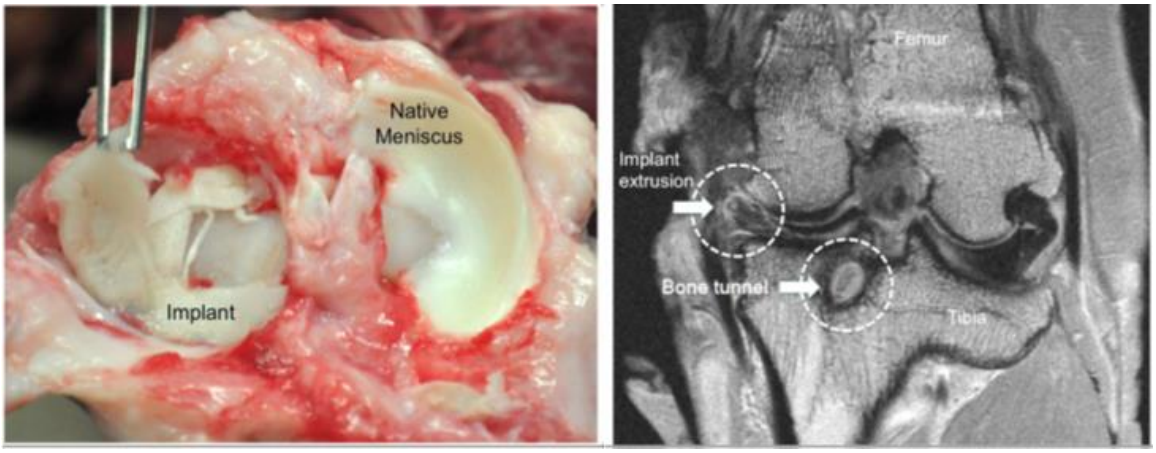

Figure 8: Polyethylene-reinforced PVA hydrogel implant after implantation into a sheep knee. Delamination of the composite (left) and implant extrusion with bone tunnel widening (right) occurred during the study. [71]

1.4.2 Implants in Clinical Use

There are currently two partial and one total meniscal substitute clinically available, but none are presently approved by the FDA. The two partial substitutes are both porous, resorbable implants that stimulate tissue generation and require an intact peripheral meniscal rim, one being made from collagen (CMI®) and the other made from polyurethane (Actifit®). The total substitute is a permanent implant with no bioactivity and

is made from polyethylene reinforced polycarbonate urethane (NUsurface®). Each of these implants have shown promise, but also have their own sets of problems [25].

1.4.2.1 Natural Partial Replacement: CMI®

The collagen meniscus implant (CMI) is made up of bovine type I collagen fibers with glycosaminoglycans and requires the meniscal rim to be intact due to poor mechanical properties and fixation of the scaffold alone [72], [73]. Initially, animal studies demonstrated its safety and ability to regenerate tissue that resembled the meniscus [74]. A clinical study of over 300 patients confirmed the implant's ability to regenerate tissue that resembled the meniscus, but there were no significant improvements in clinical scores compared to the meniscectomy group and the tissue was not pure fibrocartilage but instead a hybrid-type tissue [72]. Another study reported improved clinical scores in the implant group, but again the regenerated tissue was unlike the native meniscus and the mechanisms behind the regeneration process is unclear. In addition, shrinkage and extrusion of the implant was observed during follow-up and persistent pain was noted in 12% of patients [75]–[79].

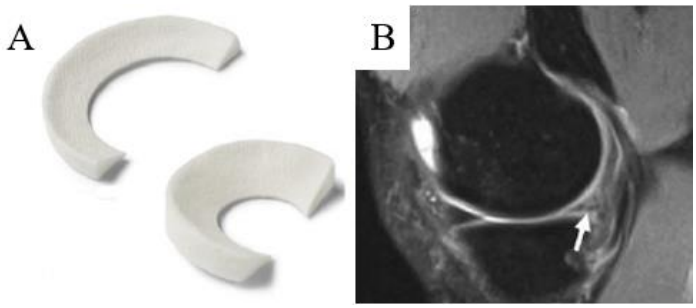

Figure 9: The CMI implant (A) for medial and lateral menisci and MR image of the implant (B) showing shrinkage after implantation (white arrow). [25]

1.4.2.2 Synthetic Partial Replacement: Actifit®

The porous polyurethane scaffold that makes up the Actifit implant was initially studied for use as a total meniscus replacement. It was intended to promote tissue infiltration and differentiation into fibrocartilage, like the tissue that makes up the natural meniscus. A two-year study of the total replacement in dogs showed evidence of tissue ingrowth and produced a structure with similar compressive properties to the natural meniscus, but the collagen orientation was different from the meniscus and the construct was unable to resist the shear forces in the knee joint. These issues could have been the reason the implant was unable to prevent cartilage damage to the joint. Fragmentation in almost all the implants was also reported after 24 months [80], [81]. Based on these results, the implant was considered best suited as a partial replacement.

A partial replacement of the scaffold was implanted into a bovine meniscal defect and promoted fibrous tissue growth without damaging the surrounding cartilage. In addition, the implant helped improve the contact mechanics on the tibia when compared to the defect condition [82], [83]. The implant was also used in human partial meniscectomy knees with a follow up of 24 months. Pain reduction and improved functionality was observed after 6 months due to regeneration of tissue, and 90% of patients demonstrated improved cartilage condition and joint stabilization up to 24 months, but it is important to note that this study did not include a meniscectomy control group for comparison [84]. Another study evaluated patients at a mean of 19 months and showed no progression of osteoarthritis and good structural integrity of the implant, but the tissue gave an oedema-like signal when assessed using MRI as opposed to fibrocartilage tissue [78]. A more recent human study evaluated 67 implanted scaffolds, with 25% needing removal at a mean of 22 months due

to implant extrusion or persisting pain. The total survivorship was only 63.6% at 6 years follow up [85].

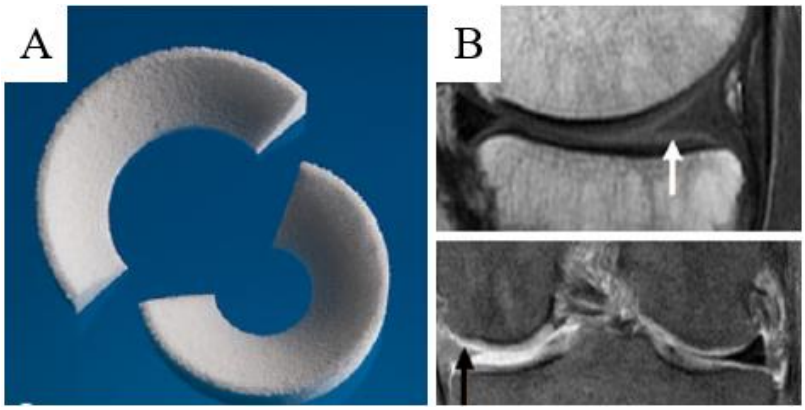

Figure 10: The medial and lateral Actifit Implant (A) and an MRI image after implantation (B) showing an oedema-like signal (black arrow) compared to the natural meniscus (white arrow). [25]

1.4.2.3 Synthetic Total Replacement: NUSurface®

Unlike most of the other meniscal replacements in development, NUSurface from Active Implants is a non-degradable polycarbonate urethane total replacement reinforced with polyethylene fibers that was evaluated initially for biomechanical performance as opposed to biological response. During its development, the free-floating implant was computationally optimized by changing its shape and arrangement of reinforcing fibers to assess pressure distribution and contact area during simulated loading on the tibial plateau, and then the design was validated using cadaver knees [86]. The tests showed comparable contact areas to the native meniscus, but noticeably different distributions. The implant has also been evaluated for viscoelastic properties and the effects of loading the implant on cartilage vitality in vitro [87], [88]. A sheep study revealed no signs of wear or changes in

structural properties of the implant, but slight cartilage damage was observed after 6 months, along with various minor complications [89]. Clinical data is scarce for the implant since it only recently entered clinical trials. One update reports that 19 of 41 implants (46%) had to be removed 2 to 26 months after operation due to either radial tears, dislocation, persistent pain, improper sizing, or synovitis/wear particles. In all, the previous issues or other minor complications occurred in 32 of the implants [85].

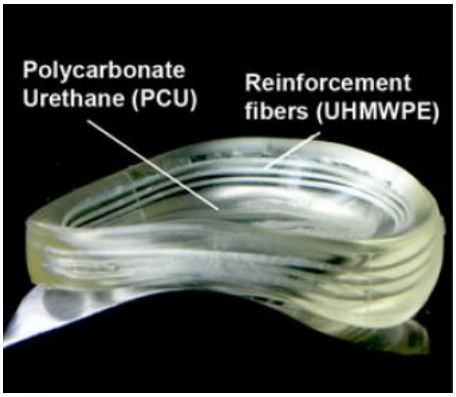

Figure 11: NUsurface meniscus implant [25]**.**

1.4.3 Shortcomings and Lessons Learned

Every current treatment option for meniscus injuries have their own shortcomings and limitations. Repair can only be done is select cases where the tear is in the vascularized region, meniscectomies cause abnormal contact pressures in the joint which can lead to degeneration, and allografts have a range of issues from availability to remodeling and strength reduction. These issues leave a significant clinical need for a reliable treatment option, which could come from the development of an artificial implant for meniscus replacement.

Most previous attempts at developing a meniscus substitute have only focused on biological aspects using tissue engineering approaches or on contact pressure distributions and modulus values. While these are all important parameters to consider, little attention has been given to the evaluation of strength for the implants, which is the reason many of them fail during use.

Since most attempts for a meniscus replacement have been in the form of bioactive scaffolds, resources have been directed to polymer chemistry and cellular interactions [90]. Few have tried to standardize methods to assess mechanical properties and functional performance of the meniscal implants. Information about implant mechanical properties and their ability to function in the knee joint is rarely reported in previous literature. Being in a part of the body exposed to forces up to almost five times body weight and subjected to millions of cycles per year, a standardized mechanical testing evaluation would be very beneficial to the field to ensure safety of the implant prior to implantation [91], [92].

Since the tissue engineering approach has produced implants with limited success due to the previously described issues, a permanent synthetic implant may be a better option. The current permanent implants under development have issues associated with strength and longevity, and have failed by secondary tear, dislocation, or similar failure modes. However, due to the previous work in this area, the development of a synthetic non-resorbable meniscal substitute seems possible with the right combination of material, structure, and strength and would also be worth pursuing due to the large and growing market for meniscal injury.

CHAPTER 2. IMPLANT DESIGN

2.1 Proposed Solution

A synthetic meniscal substitute should be biocompatible and have mechanical requirements like a native meniscus such as compressive properties, flexibility, strength, and wear resistance. It must be able to convert compressive loads into tensile hoop stresses, have proper pressure distribution, and decrease contact pressure on the tibia by increasing contact area. The fixation, surface characteristics, and geometry are also important factors to consider in development [25].

2.1.1 Shape

The shape of a meniscus implant is critical for proper function. The shape will affect the contact area in the joint and therefore the contact mechanics. A high contact area and low contact pressure will help to distribute the force within the knee joint, one of the main functions of the menisci. As such, a meniscus implant should mimic the shape of a natural meniscus, with a concave upper surface for the femoral condyle and a flat bottom surface for the tibial plateau. The size and shape of our implant will be determined using measured values of human menisci obtained from the literature, or will be based on a representative anatomic meniscus model.

Since the medial meniscus is injured 2 to 4 times more often as the lateral meniscus, a medial meniscus implant is our initial focus for implant development [28]. The implant should have an almost semi-circular shape, with an increasing width from anterior to

posterior horn, and wedge cross section with dimensions that are like that of the natural medial meniscus [93], [94].

2.1.2 Need for Composite

The body of the implant should be a relatively flexible material that can conform to the joint space with compressive properties like the natural meniscus so that it has good force dissipation. It will also need to be smooth and wear resistant so no problems arise due to articulation with the femoral condyle. Another important factor to consider for manufacturing is the material's ability to be moulded into a meniscus shape. The material should also be biocompatible so that it will not cause a reaction once implanted into the body. One issue with a flexible, singular bodied implant is that it may deform under load and extrude out of the joint space since there will be no tensile hoop stresses around the periphery to limit the radial displacement under compressive load. For this reason, a composite implant with reinforcements may be needed to convert the compressive load to hoop stresses, as well as provide a means for attaching the implant within the joint to limit excessive movement.

The reinforcements of the implant should be oriented and aligned so that they can convert the compressive forces into tensile stresses to dissipate the load. To accomplish this, reinforcements should be circumferentially aligned with the periphery of the implant to mimic the circumferential collagen fibers in the natural menisci. The circumferential reinforcements should also extend out of the implant at the horns to the attachment points to prevent dislocation from the joint space under load like the native meniscus. Since the natural meniscus also has interwoven radial fibers to provide structural integrity, an implant

should have reinforcements that give the implant radial strength. The radial reinforcements could come in the form of a base layer or weave-like reinforcement that spans across the cross-sectional area of the implant. This base layer would provide strength in all directions and limit implant deformation, as well as provide structural integrity and hold the entire construct together to better avoid tears, ruptures, and any further propagations.

2.1.3 Material Selection

2.1.3.1 Implant Body: PVA Hydrogel

With natural meniscus tissue being composed of mostly water, a material with that same characteristic would make a suitable replacement implant [5], [6]. Hydrogels are hydrophilic polymer networks that swell and trap high amounts of water, allowing them to mimic human tissue more closely than any other synthetic biomaterial [95]. One type of hydrogel that could be - and has been - used for a meniscus implant is polyvinyl alcohol (PVA) hydrogel. It can be synthesized from a dissolved or molten PVA/water solution using a freeze-thaw cycling method, which physically crosslinks the PVA chains to form crystallites and a non-degradable hydrogel network [96]–[99]. They are also very biocompatible if synthesized using this method, partly because the crosslinks are formed without the use of chemical agents [100]. Due to PVA hydrogel's simple synthesis method, these hydrogels can also be molded into complex shapes prior to freeze-thaw cycling to produce their final shape and form.

In addition to having wear resistance even after millions of cycles [101], PVA hydrogel's mechanical properties can be tuned by changing initial PVA molecular weight, PVA concentration in solution, and the number of freeze-thaw cycles, along with numerous other

parameters [71], [97], [98], [102], [103]. PVA hydrogels have been shown to possess similar compressive and viscoelastic properties to that of articular cartilage and meniscus tissue, and have already been used in the development of meniscal implants as mentioned formerly [67], [69], [104]–[106]. Although these previously described PVA-hydrogel meniscus implants had issues associated with them (radial tears, cartilage damage, delamination, extrusion), they show promise as meniscus replacement materials. Tailoring them to the application with a high polymer concentration and sufficient reinforcement can help a PVA-hydrogel meniscal implant to be strong enough to overcome previous failures and serve as a suitable meniscal substitute.

2.1.3.2 Reinforcement: Aramid Fibers

Reinforcements along the entire circumference of a meniscal implant would help to convert the compressive loads on the implant to tensile hoop stresses, like the circumferential fibers of a natural meniscus do within the knee joint. This can be best accomplished by using strong, stiff fibers that are oriented along the circumferential outer periphery and extend from the implant horns for firm attachment within the joint. In addition to the peripheral fibers, a fiber weave could be used as a base reinforcement for strength in all directions and protection from propagating tears and deformation.

Fibers with high strength and stiffness should be used as meniscal implant reinforcements, and the fibers should be able to integrate well into the implant's PVA-hydrogel matrix to prevent delamination when exposed to loading conditions. High strength aramid fibers, such as Kevlar®, have been previously used in biomedical applications. Kevlar fibers and fiber-containing composites have been shown to not induce an inflammatory reaction after

implantation when compared to a PVC positive control in rabbit paravertebral muscles [107], [108]. The fibers also have high damage and fatigue resistance, and they can absorb water unlike hydrophobic polyethylene fibers that have been previously used as PVA-hydrogel meniscus reinforcements [69], [109]. This water absorption could allow for penetration of the initial PVA/water solution into fiber bundles or weaves prior to freeze-thaw cycling to produce a sturdy composite with good interfacial adhesion and integration of fibers within the hydrogel matrix.

2.1.4 Implant Design Summary

This implant is comprised of a hydrogel body component with embedded reinforcements including a fiber mesh at the implant base and reinforcing fibers that follow the implant's outer periphery and extend from the implant to allow for fixation in the joint to hold the implant in place. It is designed with an anatomic geometry for the right medial meniscus and is implanted within the joint space to allow the femur to smoothly articulate against the implant's top surface while it rests on the tibial plateau.

2.2 Risk analysis

2.2.1 Methods

Failure modes and effects analysis (FMEA) is a type of risk analysis performed on a design to identify potential hazards or failure modes, their effects of safety or performance, and possible solutions. Criticality analysis is an extension of FMEA that rates the severity of consequences, probability of occurrence, and probability it will escape detection [110]. In

this analysis, 1 is the most desirable score and 5 is the least desirable score in terms of minimizing risk. The meanings of these ratings are shown in Table 1 to Table 3. The meanings for probability ratings were determined using average failure rates for allografts (about 20%) as the "moderate failures" cutoff, which is the only current approved treatment for meniscus replacement [54]. The three ratings are multiplied to provide a risk priority number (RPN) and a RPN threshold determines which risks are most critical and need to be addressed first [110]. An RPN of 20 will be the threshold value used here.

Table 1: Severity ratings for risk analysis.

Rating	Meaning
1	No Effect – No Danger or reduced performance
2	Minor Effect – May be noticed but function unaffected
3	Moderate Effect – Function affected; User may be inconvenienced or annoyed
4	High – Loss of Function; May cause injury or need for re-op and user is dissatisfied
5	Very High – Hazardous; Can cause permanent injury, complications, or death

Table 2: Probability ratings for risk analysis.

Rating	Meaning
1	No failures
2	Low failures – a <5% incidence
3	Moderate failures – a 5% to 20% incidence
4	High Failures – a 20% to 50% incidence
5	Very High Failures – a >50% incidence

Table 3: Detection ratings for failure analysis.

Rating	Meaning
1	Very High Detection – Patient is fully aware of malfunction or failure; Physician can easily detect issue; Defect is evident by visual examination prior to implantation
2	High Detection – Patient is suspicious of malfunction; Physician can detect through routine examination; Defect can be seen by light manipulation prior to implantation
3	Moderate Detection – Patient unlikely aware of malfunction; Clinician may require targeted investigation; Implant must be tested to find defect
4	Low Detection – Patient unaware of malfunction; Clinician may require non-invasive technique to detect; Implant requires stringent testing to find defect
5	Very Low Detection – Patient unaware of malfunction; Surgical intervention required to detect problem; Defect cannot be determined in preliminary testing

2.2.2 Results

An example of a preliminary failure analysis is shown in Table 4 for issues related to strength of the implant. This list would normally be expanded extensively during development and would include failures associated with other design functions such as attachment, implantation, and other categories. The listed potential failure modes, effects of the failure, and potential causes are mostly based on failures and effects seen in the natural meniscus [30], [111], [112]. Each potential cause of failure would normally be separated into its own row for each effect of failure and would have its own design control, but they are combined into one row after their initial introduction in this condensed version of a FMEA. The current design controls are verification tests that address the potential causes of failure and will be explained in subsequent chapters. The recommended actions are suggested future evaluations for failures modes that have risk priority numbers (RPN) over the threshold value of 20, and these future evaluations will be explained in a later

section. The severity of the effects (S), the probability of the causes (P), and the ability to detect the failure mode (D) are listed to produce the RPN when multiplied.

Table 4: Results of implant design FMEA with severity (S), probability (P), and detection (D) ratings and resulting risk priority number (RPN). Recommended Actions for RPN of 20 or more highlighted in yellow.

Design Function	Potential Failure Mode	Potential Effect(s) of Failure	S	Potential causes of failure	P	Current Design Controls	D	RPN	Recommended actions
Strength	Partial Radial Hydrogel Tear – can be stable	Slight mechanical impairment (popping, catching) from unsmooth implant surface	3	Insufficient longevity of hydrogel	2	Cyclic testing – 1000 cycles of compression and tension load	1	6	None
			3	Insufficient hydrogel strength	2	Impact compression, tensile strength, and shear strength testing	1	6	None
		Propagation risk to large size	4	Insufficient reinforcements throughout hydrogel	2	Implant design - base weave reinforcement	3	24	Optimize reinforcement layout; Composite tear testing
	Large Radial Tear (90% or more)	Accelerated cartilage degeneration from increased contact pressure	4	Insufficient longevity/ strength/ reinforcement	2	Cyclic and strength testing; implant design with reinforcement	2	16	None
		Pain/tenderness from increased contact pressure	4	Insufficient longevity/ strength/ reinforcement	2	Cyclic and strength testing; implant design with reinforcement	1	8	None
		Mechanical impairment (locking, buckling)	4	Insufficient longevity/ strength/ reinforcement	2	Cyclic and strength testing; implant design with reinforcement	1	8	None
	Partial longitudinal tears – can be stable	Slight mechanical impairment (popping, catching)	3	Insufficient longevity/ strength	2	Cyclic and strength testing	1	6	None
		Propagation risk to large size	4	Insufficient reinforcement	2	Implant design – base weave reinforcement	3	24	Optimize reinforcements; Tear testing
	Complete longitudinal tear (bucket handle)	Accelerated cartilage degeneration	4	Insufficient longevity/ strength/ reinforcement	2	Cyclic and strength testing; implant design	2	16	None

		from increased contact pressure				with reinforcement			
		Pain/tenderness from increased contact pressure	4	Insufficient longevity/ strength/ reinforcement	2	Cyclic and strength testing; implant design with reinforcement	1	8	None
		Mechanical impairment (locking, buckling)	4	Insufficient longevity/ strength/ reinforcement	2	Cyclic and strength testing; implant design with reinforcement	1	8	None
	Horizontal tears	Meniscal cysts and local swelling	3	Insufficient longevity/ strength	2	Cyclic and shear strength testing	2	12	None
	Oblique tears	Mechanical impairment (flap catching)	4	Insufficient longevity/ strength	2	Cyclic and strength testing	1	8	None
		Propagation risk to complete longitudinal	4	Insufficient reinforcement	2	Implant design - base weave reinforcement	3	24	Optimize reinforcements; Tear testing
	Scuffing of Hydrogel on articulating surfaces	Incongruent fit – potential increase in contact stress and cartilage damage	3	Insufficient shear strength	2	Shear strength testing	3	18	None
	Hydrogel deformation	Extrusion/ Joint space narrowing – potential increase in contact stress and cartilage damage	3	Insufficient hydrogel longevity/ compressive strength and stiffness	3	Compressive and cyclic testing for deformation	3	27	Fatigue/ Longer cyclic testing and deformation evaluation
	Reinforcement/ attachment fiber break or tear out (partial)	Slight mechanical impairment (popping, catching) from loose fibers	3	Insufficient strength or number of reinforcing fibers	2	Tensile strength testing of composites	1	6	None
			4	Improper layout of reinforcing fibers	2	Fiber tear out testing of implants	1	8	None
		Reduced strength; risk of additional fibers breaking	4	Insufficient strength / number / improper layout of reinforcing fibers	2	Tensile strength and fiber tear out testing	2	16	None
	Reinforcement/ attachment fiber break or tear out (complete)	Mechanical impairment (locking, buckling) from implant dislocation	4	Insufficient strength or number of reinforcing fibers	2	Tensile strength testing of composites	1	8	None
	Delamination of composite (base layer)	Mechanical impairment from loose weave component	4	Insufficient interfacial adhesion/ improper integration	2	Compression testing of composites	1	8	None
		Reduced implant integrity – risk of hydrogel tear	4	Insufficient interfacial adhesion/ improper integration	2	Compression testing of composites	3	24	Optimize reinforcements; weave peel-off testing; tear testing
	Delamination of composite (fibers)	Reduced stress transfer – potential increase	3	Insufficient interfacial adhesion of	2	Fiber tear out testing of implants	3	18	None

		in contact stress and cartilage damage		reinforcing fibers and hydrogel					
			3	Improper integration of fibers into hydrogel matrix	2	Fiber tear out testing of implants	3	18	None
		Mechanical impairment from dislocation of hydrogel component	4	Insufficient interfacial adhesion/ improper integration	2	Fiber tear out testing of implants	1	8	None

CHAPTER 3. FUNCTIONAL REQUIREMENTS AND DESIGN SPECIFICATIONS

Most of the previous attempts at creating a synthetic meniscus replacement have focused on the biological aspects of the implant, with many giving little attention to the implant's mechanical properties, especially related to the implant material's strength. One of the main reasons for failure of these implants is due to a lack of sufficient strength and longevity needed for the high-force environment seen in the knee joint. For this reason, a set of key functional mechanical requirements and design specifications were determined for the development of the meniscal implant proposed here.

3.1 Tensile Properties

3.1.1 Ultimate Tensile Stress

During axial compressive loading, the compressive force is distributed over the meniscus area and causes the meniscus to extrude radially due to its shape. This radial extrusion is resisted by the hoop stresses formed within the circumferential collagen fibers and insertional ligaments at the horns [7], [13]. These circumferential tensile stresses that develop in the menisci under load are believed to dominate their normal function and failure [11]. Although the ultimate tensile stress of anisotropic meniscal tissue varies by region, the mean maximum stress for meniscal tissue has been found to be 18.8 MPa for lateral and 17.6 MPa for medial menisci circumferentially, and around 4 MPa radially [113]. Therefore, an artificial meniscal implant should have an ultimate tensile stress of at

least 19 MPa so that it is able to withstand the same maximum stresses as a natural meniscus, which is a very important requirement that almost all previous developers of artificial meniscus implants have failed to address. This value should be taken from a sample that would be circumferentially oriented around the periphery of the implant, since that is where the tensile hoop stresses develop during loading to resist radial deformation [10], [17].

3.1.2 Tensile Modulus

The tensile modulus is dependent on region and direction within the menisci, so it can vary from about 50 MPa to 300 MPa and can be about 20 MPa to 70MPa radially [11], [113]. This means an artificial meniscus implant should have a tensile modulus above 50 MPa in the circumferential direction and at least 20 MPa in the radial direction to limit deformation and extrusion. The upper limit for the modulus of an implant is not critical since metal is a common material used for spacer devices that have been used clinically and metal spacers would have a modulus much greater than 300 MPa [114]. However, to ensure the implant is as similar to the native meniscus as possible, the modulus should remain within an order of magnitude of the maximum reported value, or less than 1 GPa. These moduli should be taken in a hoop strain region experienced within the natural meniscus, which can be up to about 5% depending on region and flexion angle [115], [116].

3.1.3 Cyclic Tension

Tensile loads develop consistently during gait with each step taken, and have been estimated to peak around 50N during simulated motion at the anteromedial meniscal insertion site and about 65N ± 25 under joint loading in the posterior horn attachment site

[117], [118]. Since the meniscus would realistically experience only one of the attachment site maximums, these values indicate a tensile load of about 90N would be a worst-case value for most individuals. To ensure the integrity of the implant is maintained, a safety factor of about 1.5 times can be added to the specification. This safety factor would make the specification correspond to the added load of both attachments (the 50N anterior load plus the 90N posterior load). Therefore, a requirement of the implant to sustain at least 140N of tensile load for 1000 cycles is chosen. There should also be no significant changes in ultimate tensile strength or tensile modulus following these cycles.

3.2 Compressive Properties

3.2.1 Compressive Modulus

A wide range of compressive moduli have been reported for the menisci and their values are dependent on strain level, loading rate, and test type. Studies have reported values for the compressive modulus of the human meniscus to be from 0.10 to 0.22 MPa under confined compression while others report modulus values from 0.30 to 1.13 MPa under unconfined compression at a physiologic strain and strain rate [119]–[121]. This means that under an unconfined testing protocol, a meniscal implant material should have a modulus of at least 0.30 MPa in a physiologic strain range. Like the tensile modulus specification, the upper limit for the compressive modulus is not critical since metal materials have been used in spacer devices and have moduli much greater than 1.13 MPa. Therefore, the modulus for a flexible prosthetic meniscus should remain within an order of magnitude of the natural meniscus at less than 10 MPa.

3.2.2 High Magnitude Load Resistance

Different activities exert widely various levels of compressive force on the knee joint. The average peak loading on the knee joint during normal activities of daily life has been calculated to be up to 4.5 times body weight, with the medial compartment taking around 80% of the total load during its most heavily loaded times [91], [122]. The average peak forces on the tibia are among the highest in stair climbing, where the tibiofemoral force is sustained for about 0.2 seconds [91]. The menisci normally transmit between 50% to 70% of weight bearing load in the knee joint, but the medial meniscus can transmit up to 85% of the load in the medial compartment when the knee is at a high flexion angle [45], [123]. Assuming a 90th percentile body mass of about 110 kg for men over 20 years old and a mean meniscal area of approximately 620 mm^2 across the tibial plateau, these values taken altogether implies that the medial meniscus must be able to withstand multiple rounds of 5.4 MPa compressive stress for 0.2 seconds without failure [94], [124]. Failure for this specification will be classified as a 5% or greater axial deformation and/or a modulus change that causes the implant material to fall out of its initial compressive modulus specification. This 5.4 MPa "high magnitude" stress value would be a worst-case scenario and is based on Equation 1:

$$\frac{110\ kg\ x\ 9.8\frac{m}{s^2}\ x\ 4.5\ BW\ x\ 0.8\ x\ 0.85}{620\ mm^2} = 5.4\ MPa \quad (1)$$

3.2.3 Cyclic Compression Resistance

An artificial meniscus implant must be able to withstand repeated compressive forces from activities, especially gait, without failure. This means it must maintain its functional size, stiffness, and strength after repeated loading. During gait, the knee joint is loaded to a maximum of about 2.5 times body weight during every step [91]. To ensure the implant can work in most patients after cyclic loading, a 90th percentile body weight of 110 kg will be assessed [124]. During gait, the medial compartment of the knee accounts for about 80% of the total load and 60% of that proportional load falls on the medial meniscus [122], [123]. This means the meniscus must withstand approximately 1300 N of compressive force for every step taken. To ensure continuous success of the meniscal implant, it should be able to withstand a compressive load of 1300 N for at least 1000 cycles. Using Equation 2, this corresponds to a compressive stress of about 2.0 MPa for an average meniscus area of 620 mm^2 [94]. Like the high magnitude loads, failure for this specification will be defined as a 5% or greater change in height and a modulus change that puts it out of its specification range.

$$\frac{110\ kg\ x\ 9.8\frac{m}{s^2}\ x\ 2.5\ BW\ x\ 0.8\ x\ 0.6}{620\ mm^2} = 2.0\ MPa \qquad (2)$$

3.3 Shear Strength

Shear forces in the knee joint are much smaller, by about 10 to 20 times, than compressive forces during daily activities. Although most activities exert much less, these shear forces

can peak at around 60% bodyweight in the posterior direction, especially for high flexion activities or stair climbing [91]. Using a 90th percentile body weight of about 110 kg, the corresponding standing joint load of around 1000N puts the medial meniscus contact area at around 420 mm^2, which is 65% of the total compartment contact area of 640 mm^2 [91], [124], [125]. Using Equation 3 with the meniscus contact area and 60% body weight load, a high estimated shear stress on the natural meniscus can be calculated to be around 1.4 MPa. This is also an over-exaggeration of the shear force, since it assumes all shear force would be in the meniscus area, when it would realistically be exerted on the entire compartment area. Therefore, to withstand the shear forces experienced by the knee joint of most individuals, the material used for a meniscus implant should have a maximum shear stress of at least 1.4 MPa.

$$\tau_{max} = 0.6\, x\, \frac{1000N\ Load}{420\ mm^2\ Area} = 1.4\ MPa \tag{3}$$

3.4 Tear Out Strength

With a fiber reinforced composite serving as an implant, an important failure mode to consider would be the fibers tearing out of the bulk material during functional loading. Since the combined estimated peak force in the attachments of a native meniscus is around 140N as previously described, a meniscal implant should be able to withstand this force without failure of the fiber-hydrogel interface when under physiologic-like loading [117], [118]. This type of loading would have tension being applied to the attachment fibers that

transition into the peripheral reinforcing fibers while the implant is being confined and held stationary in a joint-like space.

3.5 Pressure Distribution in Knee Joint

A major problem with other treatment options, specifically a meniscectomy, include increased contact pressures on the tibial plateau, leading to cartilage degeneration. The peak contact pressure for the natural meniscus under static/standing loads from the literature is about 3 MPa when subjected to a 1000N joint load (1.16 times average BW) and 4 MPa with a 1500 N load (1.73 times average BW), and that pressure increases to over 6 MPa at 1000N joint load following a meniscectomy [124], [125]. The contact pressure on the tibial plateau is even greater during gait. The contact pressure under dynamic gait loading can reach 6.0 MPa and 7.4 MPa with an intact meniscus during the two peak loads of the gait cycle, and the contact pressure rises to almost 10 MPa after a meniscectomy [126]. The peak contact pressure under the same loading conditions for a meniscus implant should certainly remain below the alternative treatment (a meniscectomy) to prevent excessive cartilage damage. Preferably, the implant would remain at the same level or below the peak pressure when the natural meniscus is intact, which would be 3 MPa for a 1000N load, 4 MPa for a 1500N load, and 7.4 MPa for gait loading. Therefore, there will be two specifications and acceptance criteria in relation to contact pressures: peak pressure should be no greater than 3 MPa at 1000N joint load and no greater than 7.4 MPa at a gait load of 2200N (2.5 times average BW) to match the natural condition [91], [124].

3.6 Summary of Design Specifications

A summary of the acceptable values for the design specifications of the artificial meniscus implant can be found in Table 5.

Table 5: Acceptable Values for Artificial Meniscus Implant Properties

Design Specification	Acceptance Criteria	Reference(s)
Tensile Strength	>19 MPa	[113]
Tensile Modulus	50 MPa to 1000 MPa	[11], [113], [115], [116]
Cyclic Tension Resistance	Tensile strength and modulus maintained after 1000 cycles to >140N	[117], [118]
Compressive Modulus	0.30 MPa to 10 MPa	[119]–[121]
High magnitude Load Resistance	<5% change in height and compressive modulus maintained after high magnitude loads to >5.4 MPa	[45], [91], [94], [122], [124]
Cyclic Compression Resistance	<5% change in height and modulus maintained after 1000 cycles to >2.0 MPa	[91], [94], [122]–[124]
Shear Strength	>1.4 MPa	[91], [124], [125]
Fiber Tear Out Strength	>140 N	[116], [118]
Peak Contact Pressure at Static Load	<3 MPa at 1000N joint load	[125]
Peak Contact Pressure at Gait Load	<7.4 MPa at 2200N joint load	[126]

CHAPTER 4. METHODS

4.1 Hydrogel-Fiber Composite Methods

4.1.1 PVA Hydrogel Synthesis and Molding

Granular PVA (>99% hydrolyzed; molecular weight of 146,000-186,000 g/mol) was obtained from Sekisui (Dallas, Texas). PVA solutions were made according to weight percent (10, 25, or 40 wt%) by mixing with deionized (DI) water. For example, a 40 wt% solution is made by adding 33.33g of granular PVA to a beaker, and then 50g of DI water. The mixture was stirred, covered with aluminum foil, and allowed to sit for at least 4 hours. After allowing the granules to absorb some water, the mixture was stirred again and the wet PVA was compacted in the base of the beaker. The beaker was covered with foil, the foil was lightly perforated to allow air to escape, and the beaker was autoclaved at 248°F for 25 min to completely dissolve the PVA granules. The molten PVA solution was removed from the autoclave after the cycle completed, the beakers were wrapped in foil to keep the solutions hot, and molding was performed immediately to prevent excessive viscosity rises from cooling. The 10 and 25 wt% solutions could be applied via injection through a syringe and could also be re-heated in a crockpot after the initial use, but 40 wt% solution quickly became very viscous, similar to a pliable solid and almost putty-like, and could not be injected or reused. Gloved fingers were wet with DI water to prevent sticking during hydrogel molding and the molten hydrogel solution was manually pushed into molds of the desired shape, such as prototypes or mechanical test samples, carefully to avoid creating air bubbles or voids. Once filled, the molds were covered and clamped tightly to compact the hydrogel into the proper shape and to push out any excess from the

mold. All test samples and prototypes were subjected to 6 cycles of freezing at -20°C for at least 1 hour and 5 cycles of thawing at 37°C for about 45 minutes, or until complete phase change where the sample will turn from clear to white during freezing and back to translucent during thawing. After the last freeze cycle, the samples were subjected to a final 6^{th} thaw by submerging in DI water at 25°C for about 1 hour before trimming any flash from molding. All samples and prototypes were stored in DI water at room temperature, for at least 24 hours, until immediately prior to use to prevent drying out.

4.1.2 Composite Mats

Para-aramid fibers, under the trade name Kevlar® 49, were obtained from Fibre Glast Developments (Brookeville, Ohio) in plain weave fabric mats with 17 picks per inch and a fiber denier of 1140. During initial prototype and test sample development, the warp and weft fiber bundles in these mats were prone to moving out of place and unweaving as composite samples were made, so to avoid this problem they were embedded in thin layers of PVA-hydrogel. The fiber mats were laid flat over a pool of molten 10 wt% PVA solution and pressed down to ensure full coverage of bottom surface. More molten PVA solution was poured on top of the fibers and spread evenly across weave. The weave and molten PVA solution were compressed between flat surfaces to ensure even coverage and placed through 2 to 3 freeze/thaw cycles. The hydrogel flash was removed and the composite mats were stored in DI water at room temperature after the 3^{rd} freeze and were cut to size depending on their use. An example of the process to make the composite mats is shown in Figure 12.

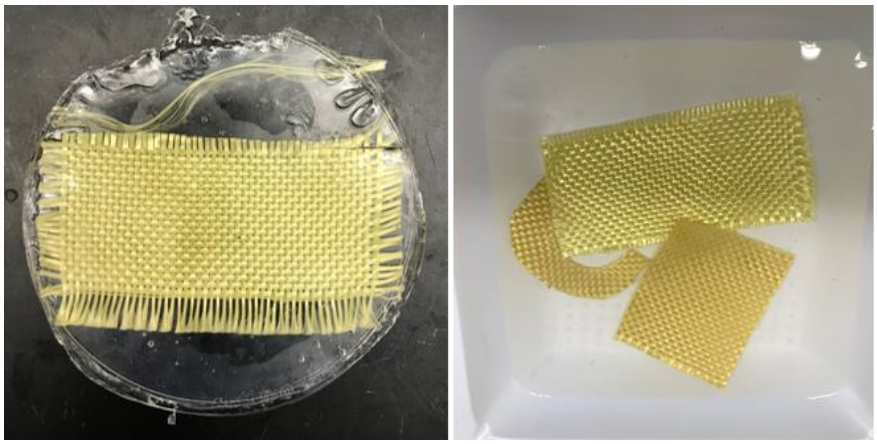

Figure 12: Composite mat fabrication process. Fiber weave mat is embedded in PVA-hydrogel (left) and then cut to size and stored in DI water (right).

4.1.3 Multiple Fiber Bundles

The warp or weft fiber bundles, about 12 inches in length, were removed from the Kevlar® plain weave fabric as shown in Figure 13. Multiple bundles were taped down together on a flat surface at one end, pulled tight ensuring side-by-side alignment, and the opposite ends were taped down together. Then molten 10 wt% PVA solution was applied to each end of the bundles to "glue" all fibers together at the ends (see Figure 13). They were subjected to 2 to 3 freeze/thaw cycles, the excess PVA-hydrogel was trimmed from the ends, and the hydrogel ends were dried out overnight, leaving a group of fiber bundles bonded together at the ends with dry PVA. The fiber bundles were connected at the ends in this way to help prevent misalignment and to make creating samples and prototypes easier, since all fiber bundles could be pulled tight and tensioned together as one when connected.

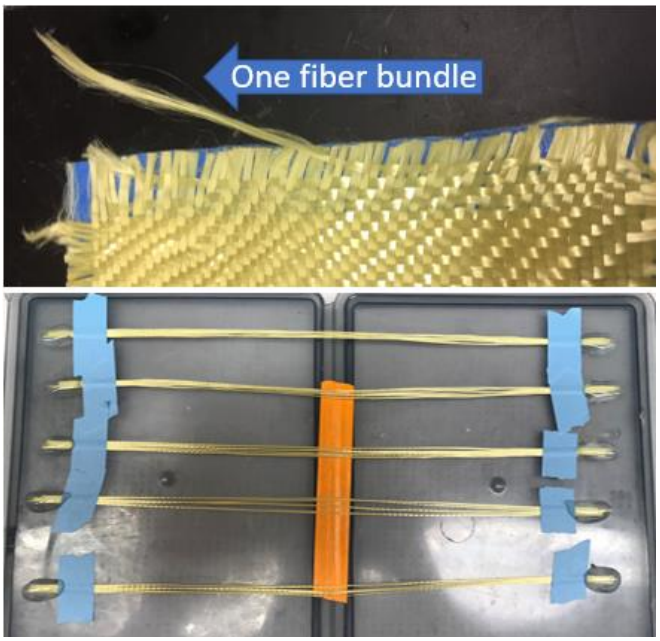

Figure 13: A single fiber bundle from plain weave fabric (top) and the method used to align and connect the ends of five sets of multiple fiber bundles (bottom).

4.1.4 General Mold Manufacturing

Two-part molds, consisting of a mold piece with the proper shape and a flat cover, were designed using Solidworks® V2016 CAD software (Dassault Systèmes Solidworks Corporation, Waltham, MA). The two parts of the mold were designed to be held together using small c-clamps. Since the shape and dimensions of the prototypes and test samples were changed regularly during development, the molds were created through additive manufacturing of PLA filament using a 3D printer (Fablicator FM1, Allentown, PA) due to the low cost and speed of this manufacturing process. The layering of filament during the printing process caused a slightly rough surface on the test samples and prototypes, but

the properties tested here should not be affected by the surface of the samples and rely more on the bulk of the material.

4.2 Implant Prototyping

Prototype molds were designed in CAD software with their dimensions being determined using measurements made on the meniscus from a functional knee joint model (Somso NS 50, Coburg, Germany), as seen in Figure 14A, or from values obtained in the literature [94]. An example of a CAD design used for the meniscus implant is shown in Figure 14B and a drawing with its dimensions can be seen in Figure 15. The first step in prototyping was 3D printing the molds with a series of holes in the base of them that followed the outer periphery of the meniscus, leaving about 1 mm of space to the outer wall (see Figure 14C). Small nails were inserted into the holes from the bottom of the mold and taped down to prevent movement. A set of four connected fiber bundles were aligned along the nails in the area between the nails and the outer peripheral wall in the meniscus mold, and the fiber bundle ends exited the mold at the horn area. Then both ends of the fibers were pulled tight against the nails. Four bundles were used because that was the amount needed to provide an acceptable tensile strength in preliminary fiber testing. A molten 25 wt% PVA-hydrogel was applied through a 10-mL syringe around the mold periphery and the fibers were pushed into the PVA-hydrogel using forceps and splayed across the entire height of the mold. The PVA-hydrogel was compacted into all corners of mold periphery to ensure fibers were fully embedded with no air bubbles or voids, as shown in Figure 14D. This initial fiber-hydrogel construct was subjected to one freeze cycle and removed to thaw during the next steps. The nails were removed from the mold and the initial composite construct was removed, trimmed of excess hydrogel to leave only a 1 to 2 mm layer around the fibers, and stored

in water until the next step. The initial construct was put into a meniscus mold of the same shape, but without peripheral holes, in a similar configuration around the periphery as the first mold (Figure 14E). Freshly molten 40 wt% PVA-hydrogel from the autoclave was pressed into the mold to fill it around the initial construct while removing any overflowing PVA as it was compacted. A pre-cut composite weave was pressed on top of the molten PVA-hydrogel, ensuring flatness and full encasing (no part of the weave extending beyond the edge of the meniscus area in the mold). Another thin layer of molten 40 wt% PVA-hydrogel was applied over the weave and meniscus area, and the mold was covered and clamped tight before being subjected to 6 freeze thaw cycles. An example of the entire step-by-step process is shown in Figure 14.

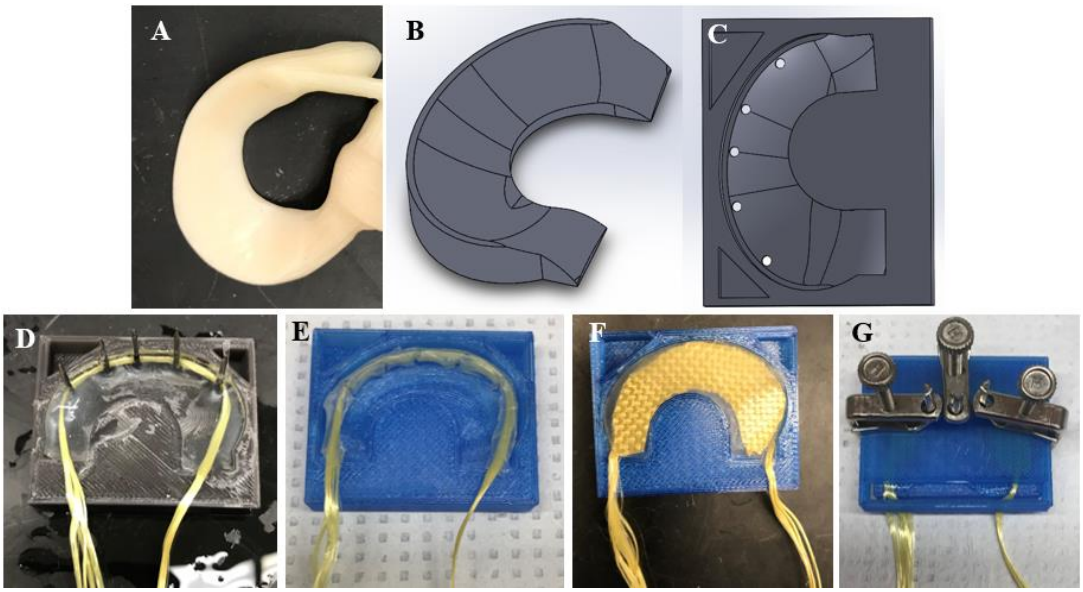

Figure 14: Prototype molding process. Meniscus model (A) used to dimension CAD model (B) and make mold with holes in the base (C). Fiber bundles were aligned on nails, covered with hydrogel (D), and then freeze/thaw cycled and trimmed (E). Mold was filled with hydrogel, composite fiber mat was pressed on top (F), then mold was covered and clamped (G).

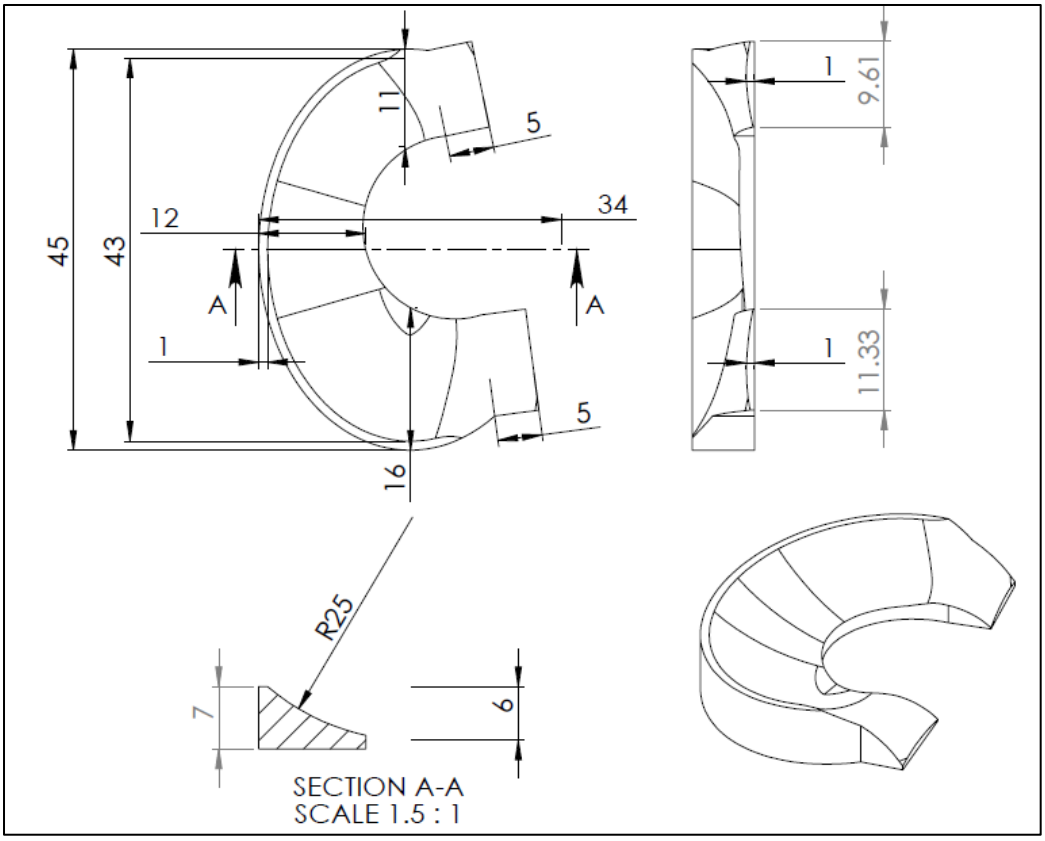

Figure 15: Drawing of the CAD-designed prototype that has a shape and size matched to a meniscus from a functional knee model. All dimensions are in millimeters.

4.3 Ultimate Tensile Strength

4.3.1 Sample Preparation

Samples were made in a similar way to the method previously described. Rectangular 3D printed molds (8mm wide x 2.2mm thick x 30mm long) were used to create the samples. Molten 40wt% PVA was pushed into the bottom of the mold, then 4 connected fiber bundles (determined to be a sufficient number in preliminary testing) were applied side-by-side to the PVA base layer so that all fiber bundles were straight and aligned in the

mold. More molten PVA was added on top of the fibers and the molds were covered and clamped. The opposite ends of the fiber bundles were pulled tight to ensure no slack would be present in the tensile samples and the samples were freeze/thaw cycled. The composite samples consisted of a rectangular PVA portion with 4 embedded fiber bundles that extended about 5 inches from each end axially. To prepare the samples for gripping during the tensile tests, the fiber bundle extensions were wrapped around and glued between two small pieces of wood using cyanoacrylate adhesive, as shown in Figure 16. Samples were made in this way to simulate the periphery of the meniscus implant with the extending fibers being used for attachment.

4.3.2 Mechanical Testing

For all tensile tests, composite samples were pulled in tension using a 15kN load cell on the Model 858 MiniBionix II Testing System (MTS, Eden Prairie, MN). Samples were tested at 10%/min and 100%/min in preliminary testing, and results showed no dependence on strain rate, so the remaining samples were tested at 100%/min to limit time for samples to dry out. The samples were clamped in the grips, preloaded to 1 to 2N tensile load to determine gauge length, and pulled in tension until failure.

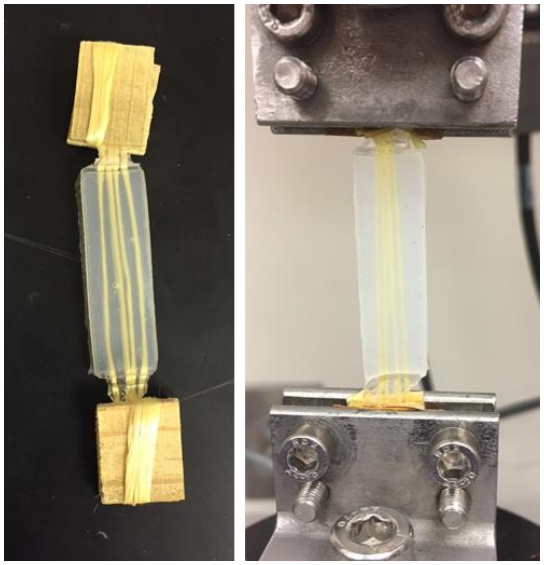

Figure 16: Tensile strength samples before (left) and after (right) loading into tensile grips.

4.4 Tensile Modulus

The tensile modulus was found using data from the ultimate tensile strength samples by calculating the slope of the trendline for the initial linear portion of the stress-strain curves, which usually fell in a segment between 1 to 4% strain. These strain levels also coincide with the physiologic region in a natural meniscus[115], [117].

4.5 Cyclic Tension

Samples were prepared as described previously, but the fiber extensions were not glued to wood. During cyclic testing, the samples were submerged in a tank of DI water at room temperature to prevent drying out, which would significantly weaken the wood-glued gripping method. The method ultimately used involved wrapping the extending fibers tightly around cylinders with through holes drilled into them outside of the wrapping area

so that the bolts from the tensile grips could be inserted to hold the cylinders in place. The grips were tightened to hold the wrapped fibers between the grip walls and cylinders, as shown in Figure 17.

Samples were subjected to a 10-cycle preconditioning to about 5% strain to determine the displacement needed to reach a 140N load. Samples were then loaded at 100%/min for 1000 cycles to a strain level that fell within the physiologic range of the native meniscus [115], which corresponded to a load of at least 140N. Following the cyclic tests, samples were inspected for deformities and/or defects due to cyclic tests, and then pulled in tension to failure to determine if there were any substantial losses in ultimate tensile strength or tensile modulus.

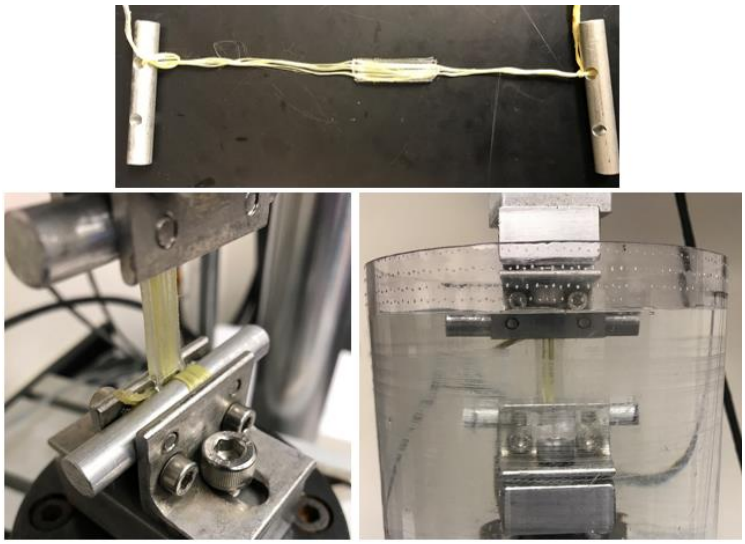

Figure 17: Sample (top) is tied to and wrapped around cylinders that are bolted in tensile grips (left) before being submerged for testing (right).

4.6 Resistance to Compression

4.6.1 Sample Preparation

Samples were created in a similar way as previously described. Molten 40 wt% PVA was pushed into cylindrical 3D printed molds of 3mm height and 10mm diameter. Then a composite mat (see Figure 12) was pressed on top of the molten PVA, ensuring flatness and full coverage of all cylinders. Another thin molten PVA layer was applied and the mold was covered, clamped, and freeze/thaw cycled. An example of a sample can be seen in Figure 18. Samples were made in this way to simulate the bulk of the meniscal implant with a reinforcing base.

4.6.2 Mechanical Testing

All compressive tests were performed using the same machine as the tensile samples in unconfined compression between two flat plates while submerged in a tank of DI water, as shown in Figure 18. The fiber mat reinforced side of the sample rested on the bottom plate, which had a layer of sandpaper to prevent sample movement during testing. For every step of the compression protocol, samples were preloaded to 1 to 2N and tested at 32% strain per second, which corresponds to the native meniscus's physiological strain rate of walking [121]. Prior to testing, a non-test sample was loaded to a very high strain to determine the strain level needed to reach the target specification stress of 5.4 MPa, which represents a worst-case scenario and will be referred to as the high magnitude stress and/or load. Each test sample underwent 10 cycles of "conditioning" to about 15%, which is slightly larger than the estimated physiologic level in the meniscus, to determine initial compressive modulus[116], [121]. The samples were loaded to the high magnitude strain that was

previously found to correspond to 5.4 MPa for 0.2 seconds, which is the time that stress would be experienced in stair climbing, and then unloaded [91]. The change in sample height, which was found using the change in machine crosshead displacement needed to reach the 1 to 2 N preload, was used to determine any axial deformation and another 10 cycles of the conditioning loading was used to determine any change in modulus of the sample. The high magnitude loading with subsequent conditioning loading protocol was repeated 2 more times, for 3 high magnitude loads total, with about 2 minutes between tests. The initial preload height changes were noted between each high magnitude step to determine any axial deformation.

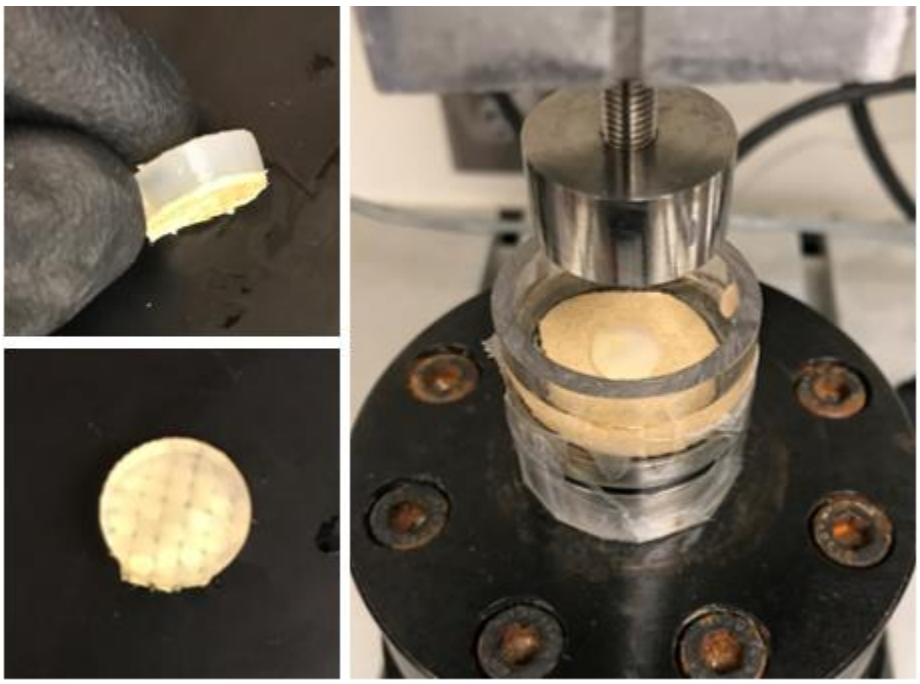

Figure 18: Compression sample side (top left) and top (bottom left) views and the compression test setup (right).

4.7 Cyclic Compression

The same samples from the high magnitude loading tests were used in the cyclic tests with the same test setup. After the third high magnitude load and conditioning cycles, samples were subjected to 1000 cycles of loading at 32%/s to a stress level of at least 2.0 MPa, which corresponds to a stress level the meniscus experiences in normal gait as previously described. This stress level was achieved in the same way as the high magnitude tests, by setting the machine crosshead endpoint to a strain level that corresponded to a stress level greater than 2.0 MPa as determined by preliminary loading to a very high strain. During unloading cycles, the crosshead of the machine was set to a compressive strain level higher than 0% so that a small load would still be applied to the sample to prevent sample motion during cyclic testing. After the cyclic test, samples were subjected to another round of conditioning to determine height changes and modulus data as described previously. Then the samples were subjected to at least one more high magnitude load followed by conditioning loading. The samples were then stored in DI water overnight as a "recovery" period before another conditioning and high magnitude loading was conducted, followed by a final conditioning. Changes in displacements were determined in the same way as before during each conditioning step, during which the data for modulus determination was also collected.

4.8 Compressive Modulus

The compressive modulus for each step in the compression protocol was calculated from the slope of a linear region in the stress-strain curve of the conditioning cycles between 2 and 12% strain, which is within the physiologic region [116], [121]. The average modulus

for the 2nd, 5th, and 10th cycle of each conditioning step was used. The initial 2% strain is excluded because strains lower than that were not always in the linear region of the stress-strain plot. Cycle 1 was not included in the modulus calculation because it always went to a higher stress level and had a different modulus than the remaining 9 cycles, which all overlaid well on a stress-strain plot due to similar responses.

After testing, small decreases in sample height were observed. The height changes caused the stress-strain curves to shift to the right (to a higher strain level) since the same amount of displacement would produce a higher strain and stress levels in shorter samples. This height change altered modulus calculations since the 2 to 12% strains were at different locations and reached different stress levels. To fix this problem, modulus values were also calculated using a linear portion of the stress strain curve that fell between 0.03 MPa and 0.14 MPa of compressive stress so that the samples' moduli could be compared in the same force ranges. Stress was calculated using the original cross-sectional area for each step, so force and stress were proportional for all steps in the loading protocol. The 0.03 MPa value corresponded to the sample's initial stress level at 2% strain, and the 0.14 MPa value corresponded to the stress level at 15% strain for the step in the loading protocol that experienced the lowest maximum stress during its conditioning step.

4.9 Shear Strength

Shear samples were made using a cylindrical 3D printed mold like the compression samples, but with 10 mm height, 10 mm diameter, and no fiber weave reinforcements. No reinforcement was used in these samples since the shear loading the implant would experience in use would mostly be on unreinforced areas, mainly the top surface of the

implant. Samples were tested in shear loading using a custom two-piece plastic testing apparatus, as shown in Figure 19, similar to methods found in the literature [70]. Each piece had a 10 mm diameter, 5 mm deep hole so that half of each hydrogel shear sample could be mounted in them while allowing both pieces to contact each other. The apparatus was mounted in tensile grips using the same test system as before so that the hydrogel samples were held in place between the two contacting pieces. The failure load showed no dependence on strain rate in initial testing, so the samples were tested at a high rate of 50 mm per minute to limit sample dry-out, in a direction perpendicular to the hydrogel's axial axis for shear loading, until failure (see Figure 19). A wrench was used to constrain movement of the plastic pieces to the testing direction. Shear strength, τ_{max}, was calculated using Equation 4, where F_{max} is the maximum force measured and *r* is the sample radius.

$$\tau_{max} = \frac{F_{max}}{\pi r^2} \tag{4}$$

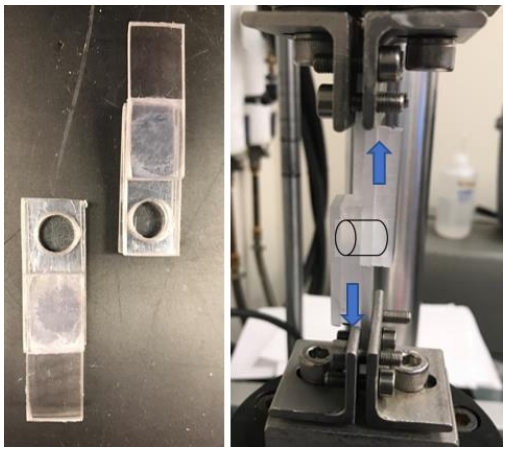

Figure 19: Shear Test setup. The testing apparatus before loading sample (left) and after loading sample, shown as white cylinder, into machine (right) with arrows depicting direction of loading.

4.10 Implant Fiber Tear Out

A custom 3D printed testing apparatus was developed to perform this test to simulate the knee joint environment, with one side being flat to simulate the tibial plateau and one side having curvature to simulate the femoral condyle. The testing apparatus was a modified version of the meniscus prototype mold (simulated curved femur) and cover (simulated flat tibia). The area on each piece of the apparatus where the implant's fibers exited was cleared of any interfering walls so the fibers could be pulled straight in tension. The apparatus also had a rectangular extension to allow mounting in the materials testing machine's tensile grips. This apparatus can be seen in Figure 20, with the CAD model shown in Figure 21 for clarification. Prototype composites were made in a meniscal shape that matched the apparatus shape as previously described, but the base mat layer of reinforcement was not included since the prototype test samples would not be experiencing loading at this area. The prototype samples were inserted in the apparatus and covered and clamped, with some needing trimming at the inner periphery for a tight, secure fit. The extending fibers were gripped using the cylinder wrapping method described for the cyclic tensile testing samples, and the other end of the apparatus was mounted in the bottom grip so that the meniscal prototype samples were oriented vertically to be tested in tension. The apparatus held the PVA portion of the prototype in place while the gripped fiber ends were pulled away in tension, in the opposite direction of the periphery of the meniscus prototype and through the bulk PVA material. The test was run until a sudden decrease in force was observed, and then the test was stopped and the prototype samples were examined for failure mode.

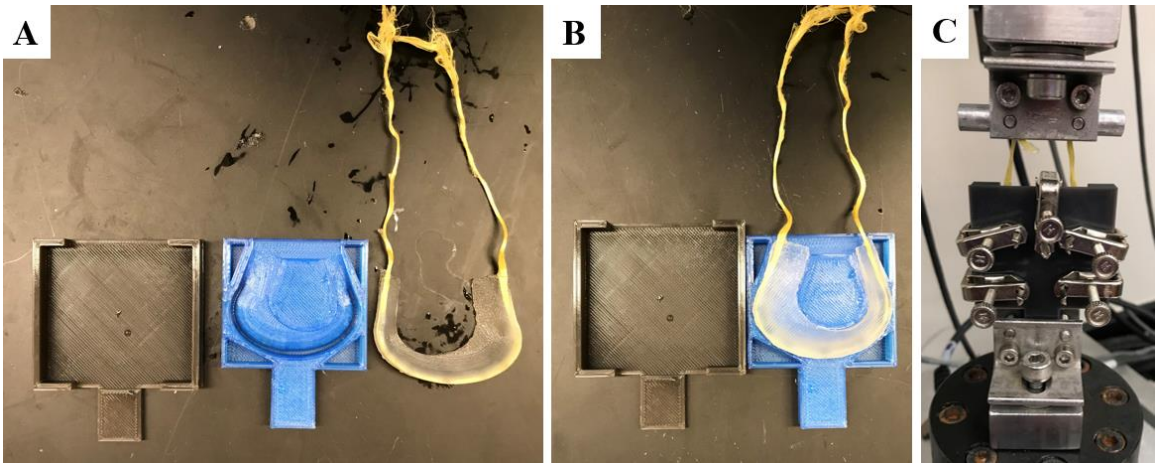

Figure 20: Fiber tear out test setup with two-piece testing apparatus and prototype test sample before (A) and after (B) sample is inserted. The apparatus is assembled and clamped before mounting in testing machine (C).

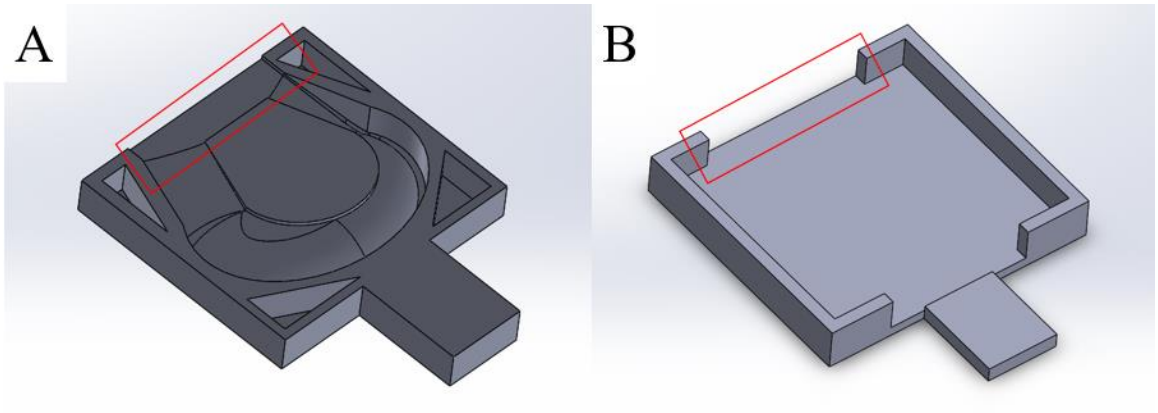

Figure 21: CAD model of fiber tear out apparatus. The mold section (A) has curvature to simulate the femur and the cover section (B) is flat to simulate the tibia. The areas where fibers exit are cleared of interfering walls, outline in red.

4.11 Pressure Distribution in Joint

4.11.1 Sample Preparation

The pressure distributions for different prototypes and conditions were assessed on the tibial plateau of a modified Somso NS 50 functional knee model (Marcus Sommer SOMSO Modelle GmbH, Coburg, Germany) under compressive loading. The functional knee model came equipped with a singular elastic meniscus piece, where the medial and lateral menisci were connected in the middle and inserted into the model by fitting a protrusion at the base of the meniscal piece into a cavity in the center of the tibial plateau. A mold of this model meniscal piece was created so that prototypes with the same shape could be made from the PVA-hydrogel and as a fiber composite. A 3D scan of the model meniscus was obtained using the FaroArm Edge (FARO Technologies, Inc. Lake Mary, FL) portable coordinate measuring machine and was converted to a 3D mesh using Geomagic® Design X (3D Systems, Rock Hill, SC). The highly detailed mesh was then simplified and smoothed using Meshlab open-source mesh processing software [127] and converted to a solid CAD model from which a mold was created in Solidworks V2016 (Dassault Systèmes Solidworks Corporation, Waltham, MA). The mold was 3D printed and prototypes were made in the model shape as previously described. A summary of this process can be seen in Figure 22. Some of the prototypes tested were also made using the original, CAD designed and dimensioned mold shapes as previously described (see Figure 14).

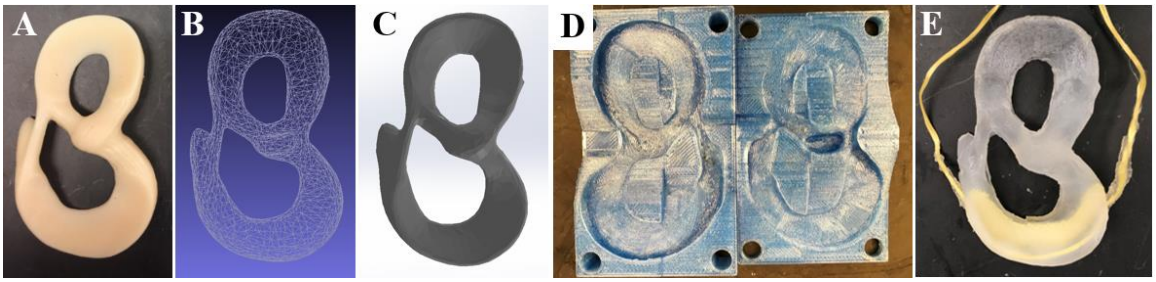

Figure 22: Process of making PVA model-shaped prototype. The model meniscus (A) is scanned to get 3D mesh (B), which is converted to solid CAD model (C) to create a mold to 3D print (D). The PVA prototype (E) is then created.

4.11.2 Testing

The knee model was modified and mounted in the same materials testing machine as all other tests. This modification involved removing most of the ligaments to allow easier implantation of prototypes and addition of threads in the bone sections of the model for mounting in the testing machine, as shown in Figure 23.

The knee model was loaded in full extension to about 1000 N of compressive force for each prototype or condition. This was accomplished by determining the testing machine's displacement set point needed to reach 1000 N prior to measurement for each case, and then setting the machine's endpoint to that displacement value for the tests. A pressure indicating film (Fujifilm PreScale® Super Low, Pressure Metrics LLC, Whitehouse Station, NJ) was wrapped in plastic wrap to prevent it from getting wet from the hydrogel and placed on the medial tibial plateau for each test condition under the prototype being tested (see Figure 27). Then the knee model was loaded at a physiologic strain rate, held for 5 seconds, and then unloaded. The strain rate used for all conditions was 2.25 mm per

second and was determined by assuming all prototypes to be 7 mm thick, which is around the average maximum thickness for medial menisci, and using the physiologic 32% per second strain rate [94], [121]. The load was held for 5 seconds to allow sufficient color development on the film. The film samples were then analyzed using FPD-8010E software (Fujifilm Corporation, Valhalla, NY) to determine pressure distribution values such as pressurized areas, average pressure, and maximum pressure. The film's pressure range was 0.5MPa to 2.5MPa, and any pressure value below 0.5MPa was filtered out of the calculations since these readings were likely due to contact from inserting and removing the film from the setup instead of the actual compression test on the knee model. The conditions tested using this setup are shown in Table 6, with visual depictions of each condition shown in Figure 22 to Figure 29.

Once all the data was collected and analyzed, the prototype that had the best results was tested again to 1500N for comparison with literature values, and then again to 2200N to simulate a normal joint force experienced during gait (2.5x BW for an average person) [91], [124]. The same low pressure indicating film previously mentioned was used in these tests. A second test with another film indicating a higher pressure range of 2.5 MPa to 10 MPa was used to assess whether any high-pressure areas existed. The films for the higher joint load tests were not analyzed using the previously mentioned software. Instead, a Color Correlation Manual (Sensor Products Inc., Madison, NJ) was used to estimate these contact pressures where a darker color indicates a higher contact pressure within the indication range of each film.

Table 6: Conditions tested for contact pressure distribution in the knee model

ID#	Condition or Prototype	Description	Visualization
1	Original Model Meniscus	The meniscus that came with the functional knee model. A protrusion on the meniscus is inserted into a slot in knee model to hold it in place.	Figure 22A, Figure 23, Figure 24
2	Medial Meniscectomy	The medial meniscus of #1 is cut off to leave only the lateral meniscus to be inserted into the slot in the knee model.	Figure 25
3	Unreinforced PVA Model Meniscus	A PVA prototype in the same shape and inserted the same way as #1. It is not reinforced with any fibers.	Figure 26
4	Unattached Composite Model Meniscus	A hydrogel-fiber composite prototype with peripheral fibers and a fiber mat base in the shape of #1. It has the extending fibers for attachment, but is inserted using the slot in the knee model.	Figure 22E, Figure 27
5	Attached Composite Model Meniscus	A hydrogel-fiber composite the same as #4, but the extending fibers are inserted into bone tunnels in the knee joint model and tied tightly around the outside of the bone for firm attachment.	Figure 22E, Figure 28
6	Matched Shape Composite Meniscus	A hydrogel-fiber composite with a flat base and with a shape and dimensions created in CAD software, but matched to the dimensions of #1. It has all reinforcements and is attached like #5. The testing is performed with the lateral meniscus of #2 in the lateral side of the knee model.	Figure 29A
7	Generic Shape Composite Meniscus	A hydrogel-fiber composite with all the same features and conditions as #6, but created in CAD software using generic dimensions from literature.	Figure 29B

Figure 23: Knee model with original model meniscus (#1) mounted in the mechanical testing machine for compression. Most of the ligaments on the model were removed.

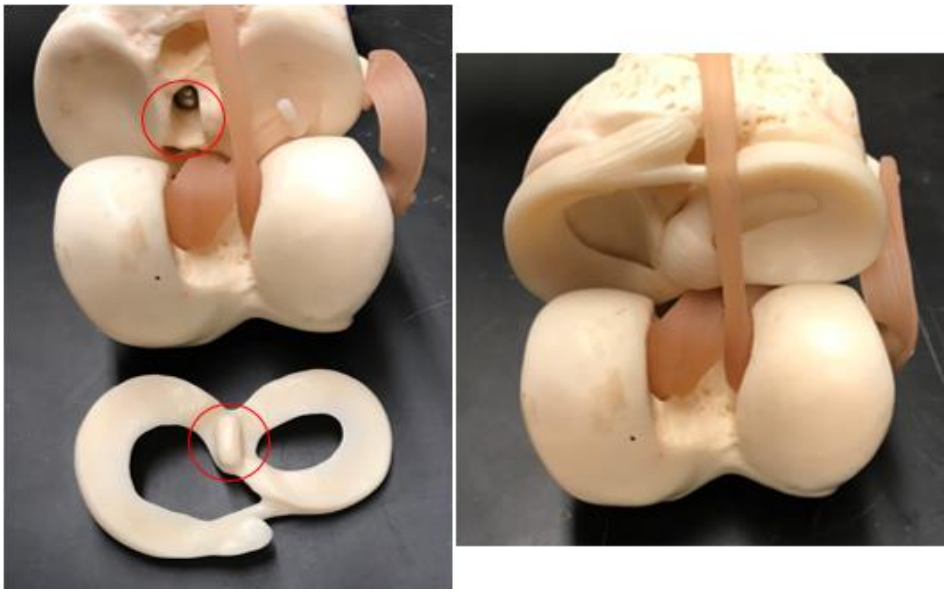

Figure 24: Model meniscus (#1) before (left) and after (right) insertion into the knee model. The protrusion and slot used for insertion are emphasized with red circles.

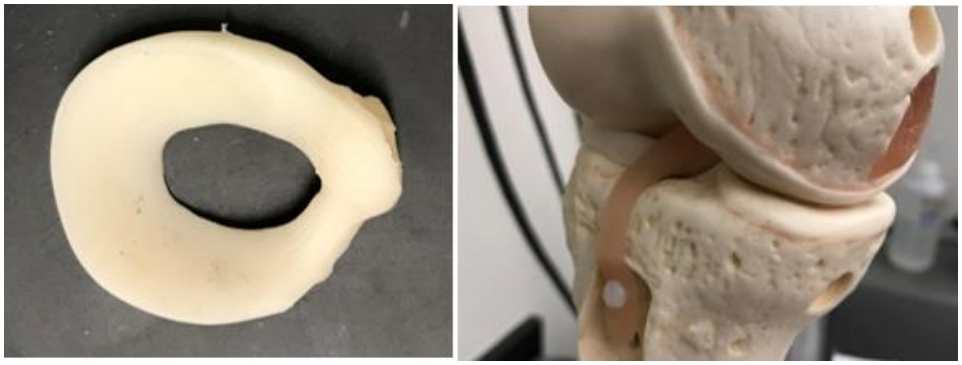

Figure 25: The lateral side of the model meniscus after removal of the medial portion (left) that was used for the medial meniscectomy (#2) test condition (right).

Figure 26: The unreinforced, model-shaped PVA meniscus (#3) before (left) and after (right) insertion into the knee model

Figure 27: Unattached composite model-shaped meniscus (#4) after insertion into the knee model and pressure indicating film placement

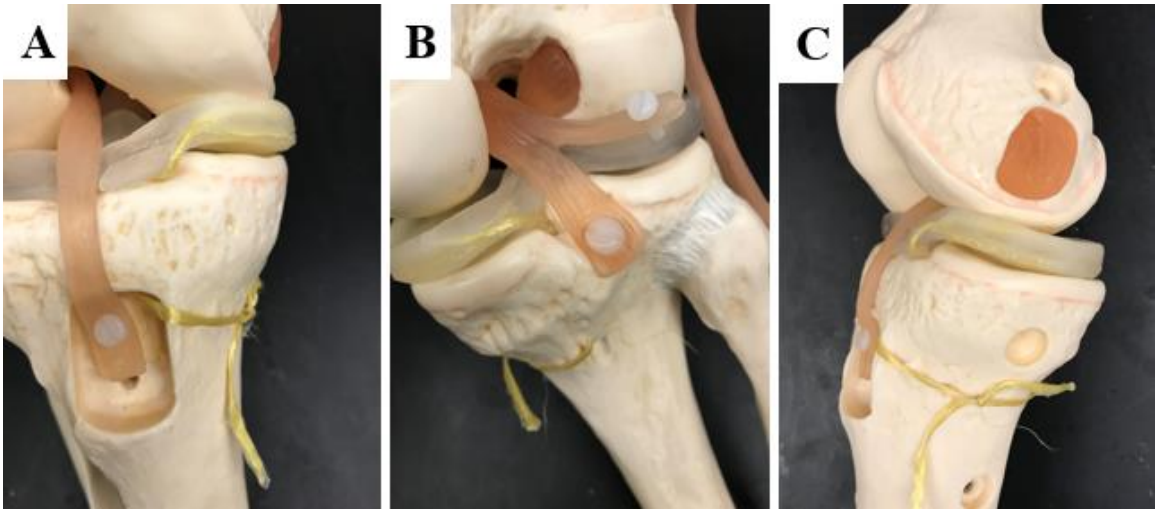

Figure 28: The attachment of the composite model-shaped meniscus (#5). The extending fibers are threaded through bone tunnels in the anterior (A) and posterior (B) areas of the knee model's tibia and tied tightly together on the side (C).

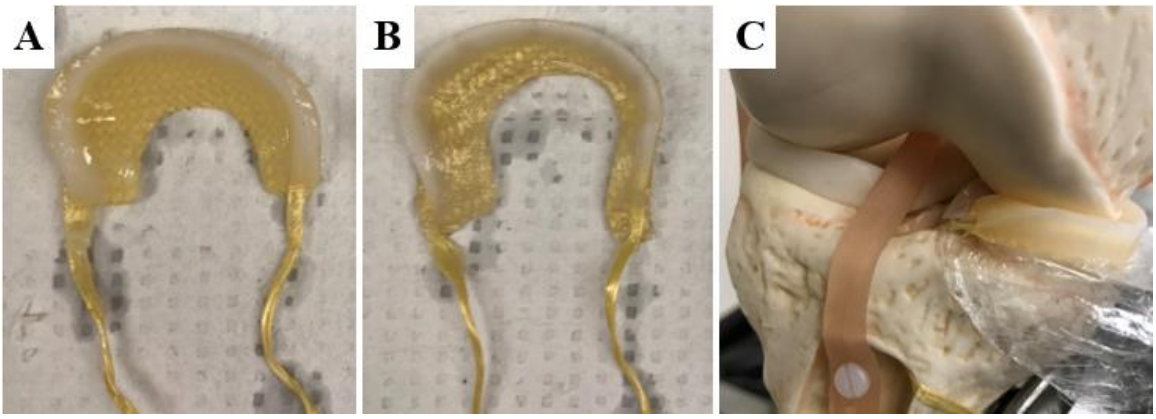

Figure 29: The matched shape, #6 (A), and generic shape, #7 (B), prototypes designed in CAD software, and their attachment in the knee model with the use of the model's lateral meniscus (C).

CHAPTER 5. RESULTS

For all tensile and compressive results, engineering stresses and strains were used. Normal stresses, σ, were calculated according to Equation 5:

$$\sigma = \left|\frac{F}{A_0}\right| \tag{5}$$

where F is the perpendicular force measured at a specific displacement and A_0 is the initial, unstrained cross-sectional area of the specimen. The original cross-sectional area was used in the stress calculations for every step of the compression protocol. Strains, ε, were calculated according to Equation 6:

$$\varepsilon = \left|\frac{\Delta L}{L_0}\right| \tag{6}$$

Where ΔL is the displacement of the testing machine crosshead (or change in axial size of the specimen during testing) and L_0 is the original sample length for tension or original sample height for compression. The L_0 used for all steps in the compression protocol was the original sample height before any high magnitude or cyclic loads. Absolute values are used for these calculations since the compressive tests would give negative values due to the negative force and displacement measurements given by the testing machine software.

Elastic modulus, E, is calculated using Equation 7, and can also be found from the slope in the initial linear portion of a stress-strain curve.

$$E = \frac{\sigma}{\varepsilon} \tag{7}$$

Reported elastic modulus values were calculated in Microsoft Excel® using the slope of the trendline in the initial linear portion of stress-strain plots for both compressive and tensile moduli (see Figure 31 and Figure 33).

5.1 Tensile Properties

5.1.1 Tensile Strength and Modulus

Rectangular composite samples of 40 wt% PVA-hydrogel and four fiber bundles were tested in tension to failure (n = 4). Stress and strain was calculated from the force and displacement data as previously described, and plots were created to determine the Tensile Strength and Modulus values. The tensile strength was defined as the maximum stress value achieved for each sample, and the modulus was found using the slope of the initial linear portion of the stress-strain plot as previously described (see Figure 31). The calculated tensile strength and moduli values are presented in Table 7 with average and standard deviation values.

The samples failed in tension by reinforcing fiber fracture, as seen in Figure 30. Most failed outside of the PVA-H area and at the wood where the fibers were gripped. This likely means that there were stress concentrations at the grip areas or where the fibers were glued to the wood.

The tensile strength and modulus of the samples both met their respective design specifications. The accepted range for the tensile modulus of a meniscus implant was 50 MPa to 1000 MPa. With an average modulus of 589 MPa, the samples tested here fall within that range. The average tensile strength of the samples, 20.2 MPa, was also higher than the minimum specification value for a meniscus implant of 19 MPa.

It is important to note that the tensile strength values can also be increased by addition of more fiber bundles as reinforcements, which would also increase the modulus values. The number of reinforcing fibers is an important parameter for this specification, since they are the main contributor to the tensile strength of the test samples and the implant. The alignment of these fibers also influence the results. If fibers are not properly aligned within the sample, some fibers could prematurely fracture before the rest of them.

Figure 30: Failure mode of the tensile samples by fiber fracture, which occurred at the griped area for most samples.

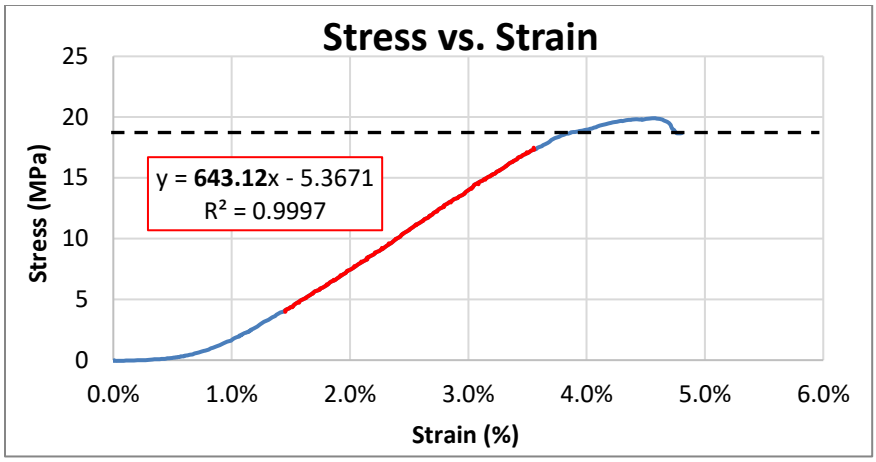

Figure 31: Tensile stress versus strain plot showing linear portion in red with trendline slope value in bold text as the modulus, and the black dashed line showing the tensile strength specification of 19 MPa. Data is taken from sample 2.

Table 7: Tensile strength and modulus values for samples pulled in tension directly to failure.

Sample #	Tensile Strength (MPa)	Tensile Modulus (MPa)
1	19.1	410
2	19.9	643
3	19.7	618
4	22.0	685
Average	**20.2**	**589**
SD	**1.28**	**122**

5.1.2 Cyclic Tension Results

Composite samples of 40 wt% PVA with four fiber bundles were loaded for 1000 cycles to a tensile load greater than 140 N to simulate an extreme case of repeated loading that the native meniscus would experience (n=4). This repeated load was sustained for all 1000 cycles, as seen in Figure 32. As cycling continued, the testing machine did not strain the

samples as much as in earlier cycles, so there is a slight discrepancy in the load that the cycles reached between early and late cycles. The cycling also likely forced water out of the hydrogel during stretching, so the samples became slightly stiffer and reached a higher load at a lower strain level.

After the cycles, samples were pulled in tension to failure to determine tensile strength and tensile modulus. These values, along with the approximate cycle load of each sample for reference, are reported in Table 8 with averages and standard deviations. The samples also failed by fiber fracture near the grips like the other tensile samples.

The average tensile strength (21.9 MPa) and tensile modulus (709 MPa) values for the cyclic samples after being loaded to at least 140 N for 1000 cycles remain within the specification for a meniscus implant, which was >19 MPa tensile strength and 50 MPa to 1 GPa tensile modulus. The values for tensile strength and modulus for the cyclic samples were in fact slightly larger than those of the samples that were tested directly to failure. This could be attributed to the loss of water from the hydrogel mentioned earlier, or could be due to the cyclic samples being slightly smaller in cross-sectional area overall (Poisson ratio effect) than the samples pulled directly to failure. This smaller area would alter the calculations for the stress levels and in turn the tensile modulus.

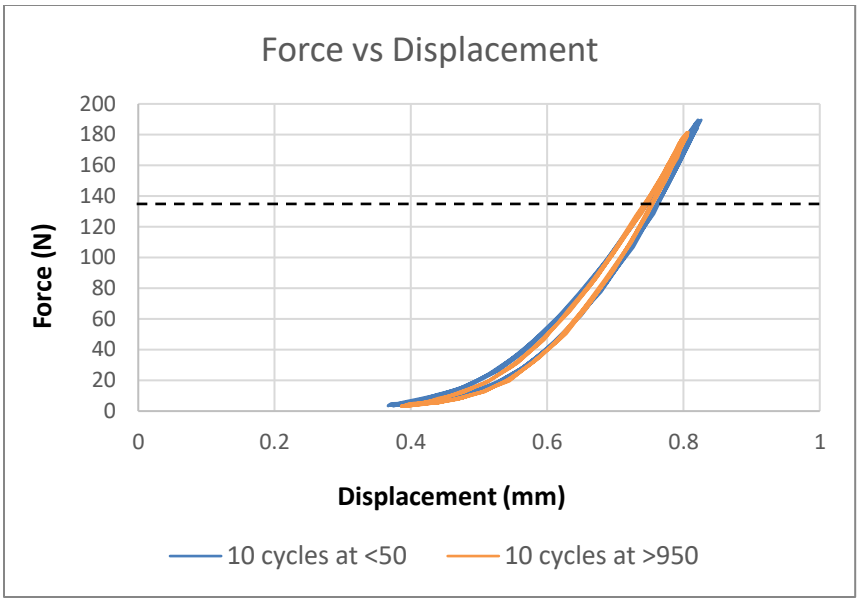

Figure 32: Plot of force versus displacement showing 10 cycles within the first 50 cycles and 10 cycles in the last 50 cycles where the specification load of 140 N, shown as the black dashed line, is sustained during all cycles.

Table 8: Tensile strength and modulus values during pull to failure tests for cyclic samples after cycling, and the approximate cycle loads of each sample.

Sample #	Tensile Strength (MPa)	Tensile Modulus (MPa)	App. Cycle Load (N)
1	19.6	811	180
2	20.0	803	175
3	24.0	562	150
4	24.0	660	170
Average	**21.9**	**709**	**169**
SD	**2.42**	**120**	**13.1**

5.2 Compressive Properties

Cylindrical composite samples of 40 wt% PVA with a reinforcing fiber mat at the base were subjected to a 10-cycle conditioning loading to 15% compressive strain, followed by three high magnitude loads to over 5.4 MPa compressive stress (n=3). Following the three

high magnitude loads, the same samples were subjected to 1000 cycles of compression to at least 2.0 MPa, an additional post-cycle high magnitude load, and another high magnitude load after storage in DI water for at least 24 hours as a recovery period. A conditioning step was performed before and after all steps of the loading protocol. Since the same samples were used for the high magnitude and cyclic loading tests, the results were combined and are presented together. The conditioning steps were used to determine the modulus of the samples before and after each loading step and the modulus was found using the initial linear portion of the stress-strain curve as previously described (see Figure 33). The conditioning steps were also used to determine the change in preload height of each sample (the machine's crosshead position needed to reach 1 N to 2 N of compressive load) which gave the residual axial deformation after each step.

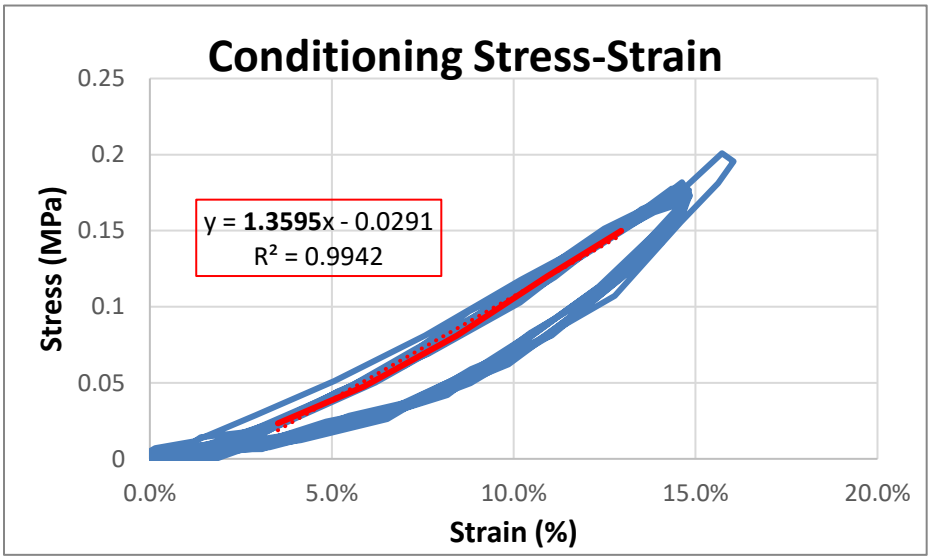

Figure 33: Compressive sample stress-strain plot during 10-cycle conditioning step showing linear portion in red with trendline slope value in bold text as the modulus. Data is taken from sample 3 after one high magnitude load.

5.2.1 Compressive Modulus Changes Using Strain Range

The compressive modulus data using the 2% to 12% strain range for all samples after each step can be seen in

Table 9 with the average and standard deviations for each step, which are also shown in Figure 34. The compressive modulus was highest initially before any loading at 1.63 MPa. The lowest the compressive modulus value reached during the loading protocol was after the 1000 cycles at 0.94MPa and the highest was after recovery at 1.44 MPa. After every step in the loading protocol, the modulus remained well within the acceptable specification range of 0.30 MPa to 10 MPa. The modulus values were also very close to or even below the native meniscus's upper range of 1.13 MPa [121]. A two-tailed paired t-test was performed at a 5% confidence level to assess significant differences in moduli between steps. The modulus after the 1000 cycles was significantly lower than all other points in the loading protocol, except for the modulus after one high magnitude load following the recovery period. The modulus increased again after a subsequent high magnitude loading step and returned to a non-significant difference to the value prior to cycling. The rest of the significant differences are shown in Figure 34, denoted by asterisks. The modulus was significantly higher initially and immediately after the recovery period than after any high magnitude load that followed the same day, but no significant differences between initial modulus and modulus after a recovery period existed. This shows that the hydrogel composite samples regained some of their stiffness during recovery. No significant differences exist between moduli following different high magnitude loads, including those after cyclic compression and after a day of recovery. This shows that after an initial high magnitude load, the hydrogel composite maintains its stiffness after subsequent high

magnitude loads, and that stiffness is also maintained after high magnitude loads following cyclic loading and a recovery. This can be better seen by assessing the percent change between subsequent high magnitude steps, as shown in Table 10.

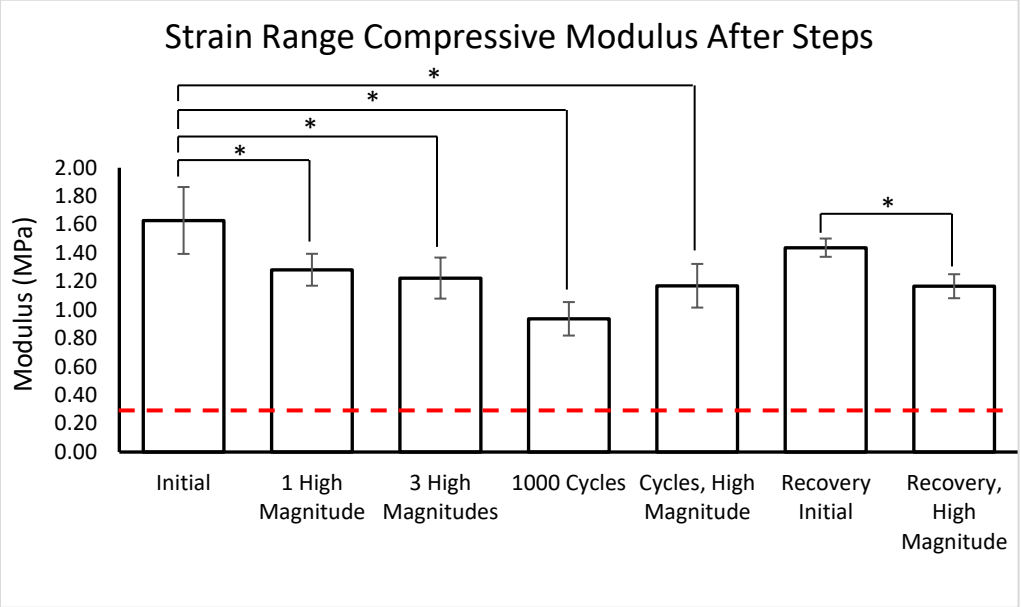

Figure 34: Comparison of compressive moduli after each step in the compression loading protocol using a 2% to 12% strain range. A (*) indicates significance, but the modulus after 1000 cycles was significantly different from all others. The minimum specification of 0.30 MPa is shown in red.

Table 9: Calculated compressive modulus values initially and after each loading step using a 2% to 12% strain range. All moduli remained within the acceptance criteria of 0.30 MPa to 10 MPa.

Sample #	Initial Modulus (MPa)	Compressive Modulus (MPa) After Load Step:					
		One High magnitude	Three High magnitudes	1000 Cycles	Cycles, High magnitude	Recovery Initial	Recovery, High magnitude
1	1.36	1.15	1.06	0.80	1.00	1.51	1.23
2	1.76	1.36	1.29	0.98	1.21	1.39	1.07
3	1.77	1.34	1.32	1.03	1.30	1.42	1.20
Average	**1.63**	**1.28**	**1.22**	**0.94**	**1.17**	**1.44**	**1.17**
SD	**0.24**	**0.11**	**0.14**	**0.12**	**0.15**	**0.06**	**0.08**

Table 10: Percent change in compressive modulus after different high magnitude steps compared to the previous high magnitude step using a 2% to 12% strain range.

Sample #	1 High magnitude vs 3 High magnitudes	3 High magnitudes vs Post Cycle	Post Cycle vs Post Recovery
1	-8.3%	-5.4%	22.6%
2	-4.7%	-6.5%	-11.6%
3	-1.2%	-1.5%	-7.3%
Average	**-4.7%**	**-4.5%**	**1.2%**
SD	**3.5%**	**2.6%**	**18.6%**

5.2.2 Compressive Modulus Changes Using Stress Range

The shift of the stress-strain curves for shorter samples to the right in the later steps of the loading protocol, as described earlier, is shown in

Figure 35: Stress-strain curve shift during different steps of the loading protocol due to samples reducing in height and affecting the strain calculations. Data shown is for sample 1, and modulus values from the trendline equations are in bold font.

. To resolve this issue, compressive modulus values were also calculated in a linear portion of the conditioning stress-strain curves corresponding to a fixed strain range, 0.03 MPa to 0.14 MPa, as mentioned previously. After this fix, modulus values between steps became much closer to each other, as shown in Figure 36 and Table 11. The initial modulus was still the highest at 1.46 MPa. The modulus after 1000 cycles was the lowest at 1.23 MPa and the modulus after recovery was the highest during the loading protocol at 1.39 MPa. Although the same trend for increasing and decreasing of the modulus values between steps exists after this method of modulus calculation, no significant differences exist between

any steps after a two-tailed paired t-test at a 5% confidence level was employed. All moduli also remained within the acceptable range of 0.30 MPa to 10 MPa.

An explanation for the modulus changing phenomena could be attributed to the viscoelastic nature of PVA hydrogel. After the high magnitude loads or cycles, the PVA chains could be shifting to allow channels for water to more easily flow through, reducing the friction of water moving through the matrix and in turn reducing the stiffness. During recovery, the PVA chains shift back to their original conformation and the friction for water motion through the matrix is reintroduced.

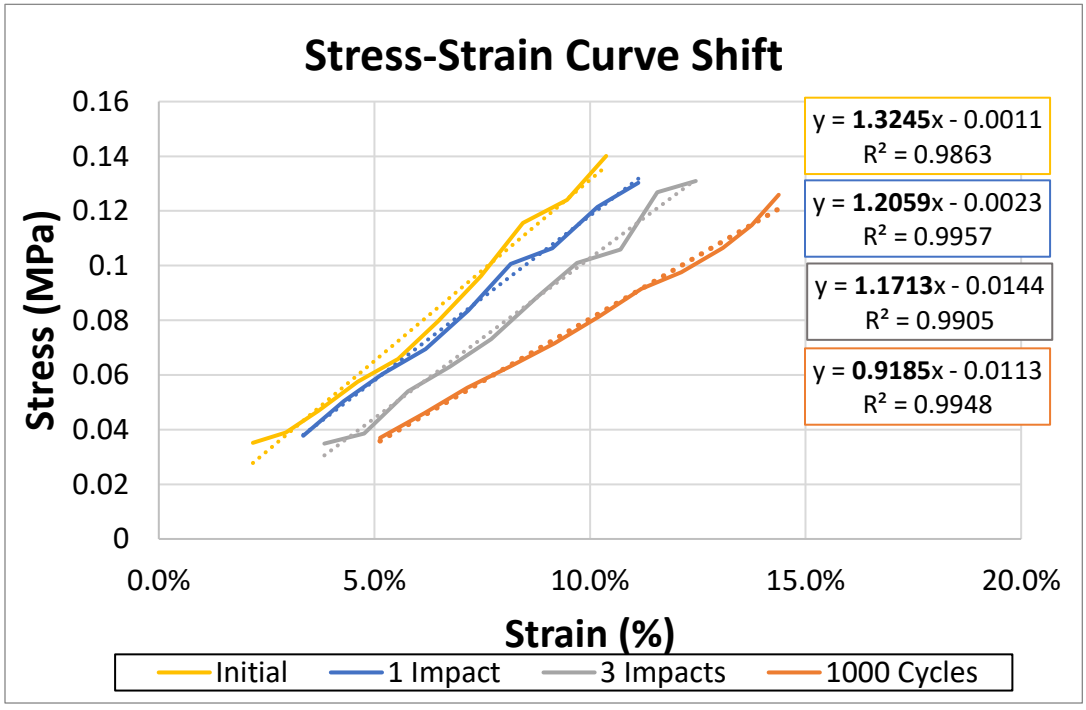

Figure 35: Stress-strain curve shift during different steps of the loading protocol due to samples reducing in height and affecting the strain calculations. Data shown is for sample 1, and modulus values from the trendline equations are in bold font.

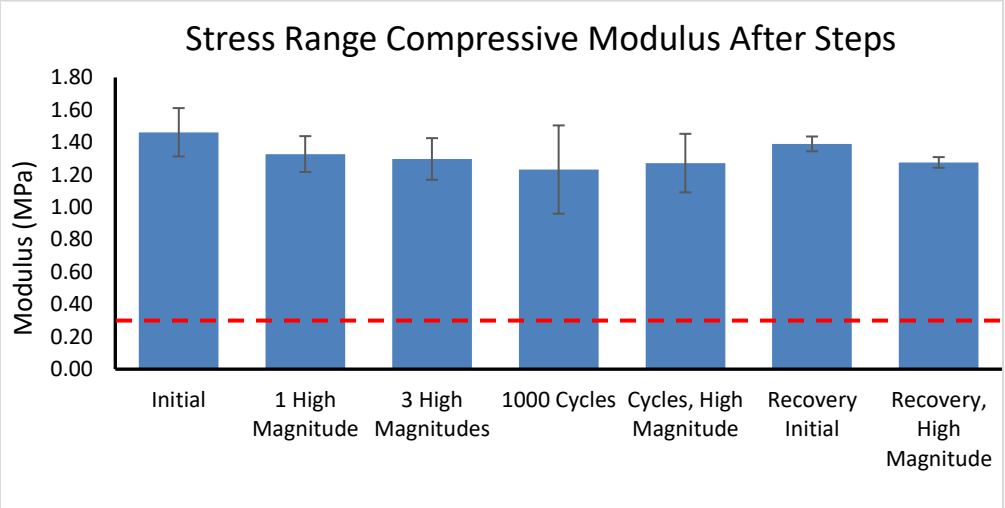

Figure 36: Comparison of compressive moduli after each step in the compression loading protocol using a 0.03 MPa to 0.14 MPa stress range. No significant differences exist between any steps. The minimum specification of 0.30 MPa is shown in red.

Table 11: Calculated compressive modulus values initially and after each loading step using a 0.03 MPa to 0.14 MPa strain range. All moduli remained within the acceptance criteria of 0.30 MPa to 10 MPa.

Sample #	Initial Modulus (MPa)	Compressive Modulus (MPa) After Load Step:					
		One High magnitude	Three High magnitudes	1000 Cycles	Cycles, High magnitude	Recovery Initial	Recovery, High magnitude
1	1.29	1.21	1.17	0.94	1.14	1.37	1.24
2	1.55	1.35	1.29	1.27	1.19	1.36	1.30
3	1.55	1.42	1.43	1.49	1.48	1.44	1.29
Average	**1.46**	**1.33**	**1.30**	**1.23**	**1.27**	**1.39**	**1.28**
SD	**0.15**	**0.11**	**0.13**	**0.27**	**0.18**	**0.05**	**0.03**

5.2.3 Sample Height Changes

The height change data for each sample after the first three high magnitude loads and after 1000 cycles can be found in Table 12. The percent change in height after the high magnitude loads (reduced by 2.8% of initial height) and after the cyclic loading (reduced by 1.6% of initial height) both remain under the acceptable criteria maximum of 5% axial deformation. The total height change when all loading steps are combined (reduced by 4.3%) also remains below the specification. After the 1000 cycles loading, additional high magnitude loads did not cause any more height changes or deformation to any of the samples. This suggests that most, if not all, the height change or deformation occurs in the first few high magnitude and/or cyclic loadings. This could be because any air bubbles or voids in the hydrogel test samples are compacted or pushed out of the hydrogel surface in the initial loadings, or the hydrogel wasn't loaded enough times after the cycles to find that more height change could occur. If the hydrogels in fact do not experience any more deformation after a few initial loadings, an artificial meniscus implant could be conditioned into its final shape and size prior to use in a patient.

Table 12: Height changes of each sample after the first 3 high magnitude loads and after 1000 cycles. No additional height changes occurred following the cycles, and the total height change remains below the specification of 5%.

		After 3 High magnitude Loads		After 1000 Cycles		
Sample #	**Initial Height (mm)**	**Height Change (mm)**	**% Change**	**Height Change (mm)**	**% Change**	**Total % Change**
1	4.50	-0.10	-2.2%	-0.10	-2.2%	-4.4%
2	3.80	-0.10	-2.6%	-0.050	-1.3%	-3.9%
3	4.30	-0.15	-3.5%	-0.050	-1.2%	-4.7%
Average	**4.20**	**-0.12**	**-2.8%**	**-0.067**	**-1.6%**	**-4.3%**
SD	**0.36**	**0.029**	**0.65%**	**0.029**	**0.57%**	**0.36%**

5.2.4 Compressive Stress During High Magnitude Loads

The samples were loaded to at least 5.4 MPa during all high magnitude tests to simulate a worst-case type load on the natural meniscus. While performing the high magnitude tests, the testing machine would occasionally compress the sample farther and impart a higher stress on the sample than intended. To correct for this and to draw comparisons, the high magnitude stress level at a specific strain was found for each sample, which coincided with the lowest-strained step that sample experienced in the loading protocol. For example, if a sample was loaded to 58% strain in one high magnitude load and over 58% strain in the remaining high magnitude loads, the stress level at 58% strain was recorded for each step (see Figure 37). These values are reported for each sample at different high magnitude steps in Table 13, along with the averages and standard deviations among all samples, which is also shown in Figure 38 for comparison. The second high magnitude load for the samples is not reported because little change occurred between the first and third high magnitude loads and the results did not reveal any useful information. Every high magnitude load for all samples exceeded the 5.4 MPa needed to reach the specification, with some reaching as high as 10.8 MPa. A two-tailed paired t-test at a 5% confidence level was performed to determine if the high magnitude stresses were statistically different between the different steps, but none were found to be significant. This indicates that the hydrogel material can withstand these high stress levels repeatedly, and shows that the samples likely had no damage that could not be visually seen after the high magnitude loads and 1000 cycle load.

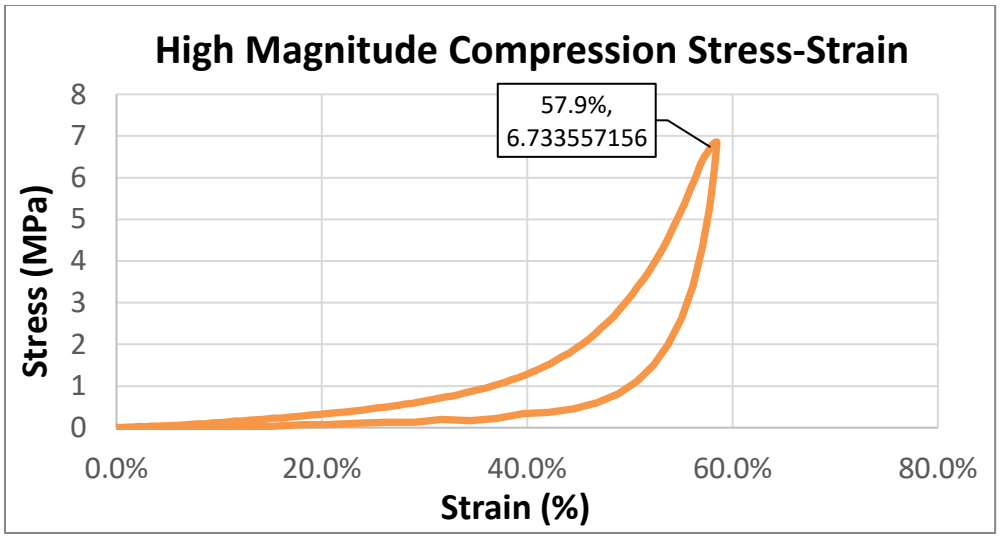

Figure 37: Plot of stress versus strain during a high magnitude load where the high magnitude stress value of 6.73 is extracted at a 57.9% strain. Data is from high magnitude 3 of sample 2.

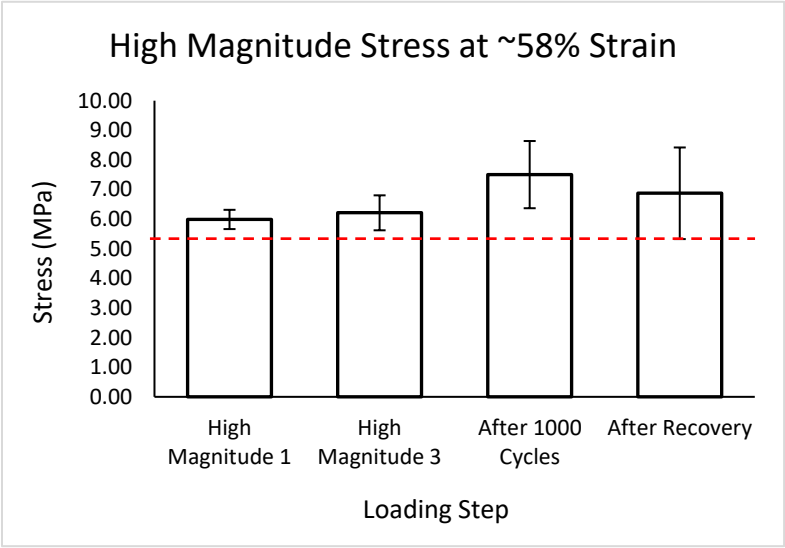

Figure 38: Comparison of the average high magnitude stresses for each step in the loading protocol, with the 5.4 MPa threshold shown as a red dashed line. No significant differences among steps exist.

Table 13: Calculated high magnitude stress values for each sample at different steps in the loading protocol.

	Stress Level (MPa) at approx. 58% strain			
Sample #	**High magnitude 1**	**High magnitude 3**	**After 1000 Cycles**	**After Recovery**
1	6.23	5.57	7.12	8.65
2	5.62	6.73	6.61	5.83
3	6.12	6.34	8.78	6.14
Average	**5.99**	**6.21**	**7.50**	**6.87**
SD	**0.33**	**0.59**	**1.13**	**1.55**

5.2.5 Compressive Stress During Cycles

The samples were loaded to at least 2.0 MPa for 1000 cycles to simulate the load experienced by the medial meniscus during gait. The samples were loaded to a stress level slightly higher than the 2.0 MPa value to ensure that even at the end of the cycles, they were being loaded to the 2.0 MPa specification. The stress level on all samples remained above this value by the end of the cycles, as shown in Figure 39. The slight drop in stress level from early to later cycles is likely due to the samples losing small amounts of axial height from the constantly repeated compression, which temporarily forces water out of the hydrogel matrix to cause the height change. From manual calliper measurements of the samples, the samples recovered some of this height change during the recovery periods (data not shown), but the exact amount is unknown since the change in preload height could not be recorded between different days.

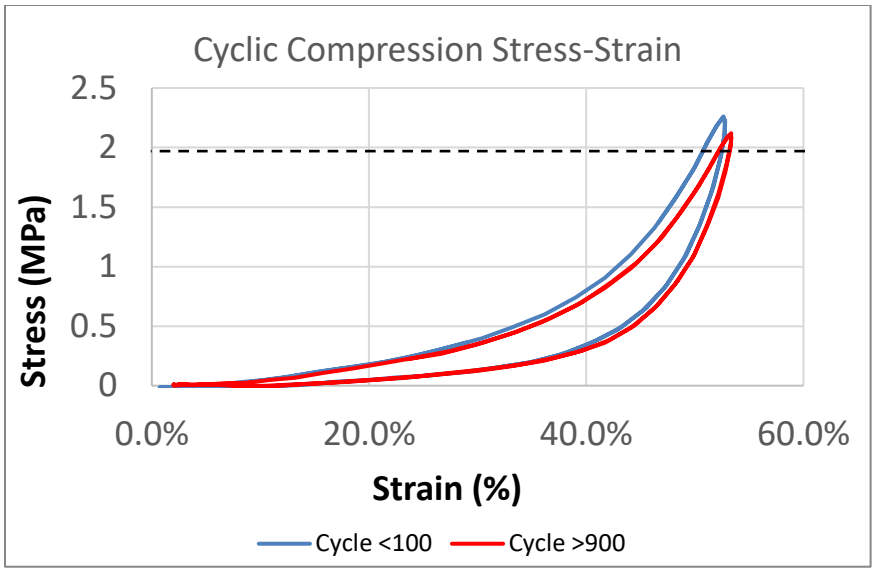

Figure 39: Example plot of stress versus strain for a cycle at less than 100 cycles and a cycle at greater than 900 cycles during cyclic compression testing with the stress level remaining above the 2.0 MPa specification, shown as the black dashed line.

5.3 Shear Strength

Cylindrical samples of 40 wt% PVA were pulled in tension perpendicularly to the sample's axial axis until shear failure using a custom two-piece testing apparatus to determine shear strength. An example plot of the shear data for one sample can be seen in Figure 40, where the maximum shear stress is the shear strength. Failure was confirmed to occur in shear (see Figure 41). The shear strength of each sample, along with the average and standard deviation values, can be found in

Table 14. With an average shear strength of 3.7 MPa, these samples exceed the acceptable criteria of 1.4 MPa for an artificial meniscus implant by over 2 times, so the specification is met.

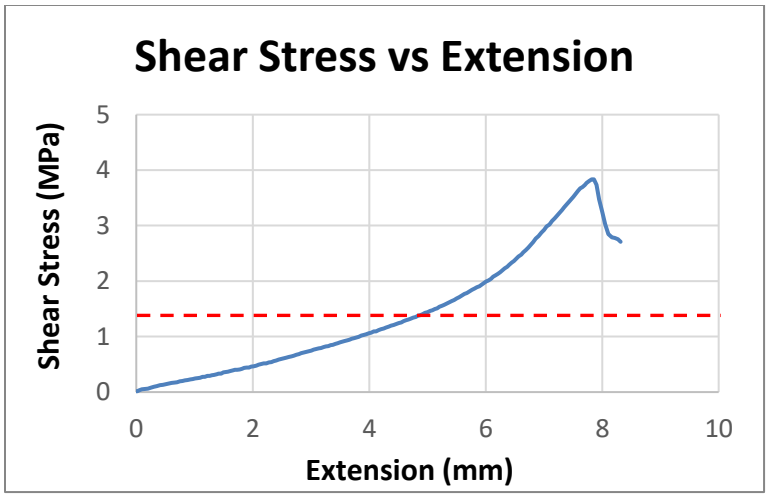

Figure 40: Plot of shear stress versus extension of the test grips, where shear strength is the maximum shear stress value. Data from sample 4. The minimum specification of 1.4 MPa is shown as red dashed line.

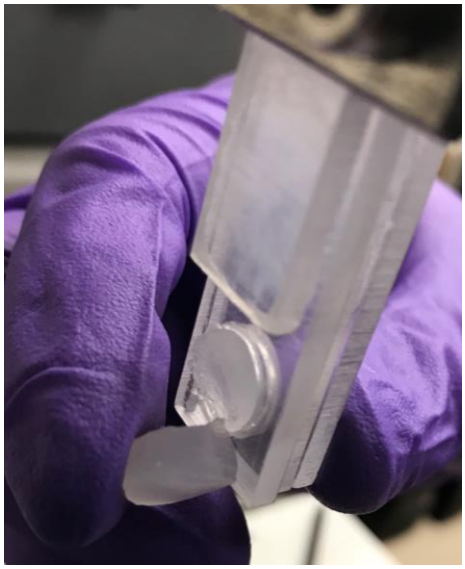

Figure 41: Sample failure mode is shear within the custom testing apparatus when the two pieces are pulled in tension.

Table 14: Shear strength values for each sample calculated from the maximum recorded load and sample cross sectional area.

Sample #	Max Load (N)	Area (mm^2)	Shear Strength (MPa)
1	347.5	84.9	4.09
2	324.3	86.6	3.74
3	277.8	88.2	3.15
4	325.7	84.9	3.83
		Average	**3.70**
		SD	**0.48**

5.4 Fiber Tear Out Strength

Prototype-shaped 40 wt% hydrogel composite samples were pulled by the reinforcing fiber extensions in tension while housed in a custom testing apparatus designed to simulate a knee joint. Samples were pulled in tension this way to mimic the hoop stresses that develop in the meniscus due to its firm attachment at the horns. The fiber tear out strength was assessed by finding the maximum tensile load reached before any plastic deformation in the sample, which was defined as a sudden decrease in force or obvious change in the slope of the force-displacement curve, as shown in Figure 42. All prototype samples failed either by fiber fracture outside of the hydrogel area, or by deformation around the periphery of the prototype, where the originally straight peripheral wall of the implant became concave as the fibers were being pulled away from it and into the bulk hydrogel. An example of a prototype that failed in both ways can be seen in Figure 43. Fiber tear out strength for each sample, along with average and standard deviation values, are reported in Table 15. The 531 N value for average fiber tear out strength easily surpasses the acceptance criteria of 140N, by almost four times. This result suggests that this implant would be able to

withstand the tensile and hoop stresses that are normally present in the meniscus without interfacial composite failure and the reinforcing fibers moving within the hydrogel matrix.

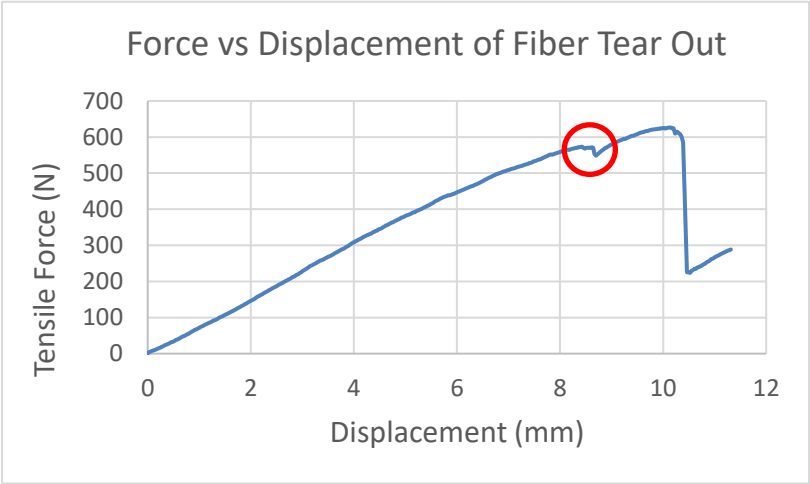

Figure 42: Plot of force versus displacement for a fiber tear out test with the fiber tear out strength defined as the point of plastic deformation, outlined with a red circle. Data shown is for sample 3.

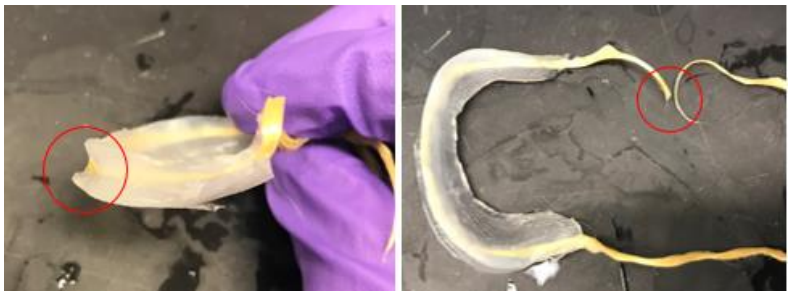

Figure 43: Implant failure modes, highlighted with red circles, of peripheral concavity (left) and fiber fracture (right) from fiber tear out tests.

Table 15: Fiber tear out strength for each sample.

Sample #	Fiber Tear Out Strength (N)
1	642
2	400
3	573
4	511
Average	**531**
SD	**103**

5.5 Pressure Distribution

5.5.1 Visual and Numerical Analyses

Seven different conditions or prototypes were assessed for contact pressure distribution on the tibial plateau of a functional knee model while under a 1000 N compressive joint load. A visual analysis of the pressure distributions for all conditions are shown in Figure 44 and a numerical analysis of the average and maximum pressures for each condition are shown in Table 16, along with the percent of the contact area that had a pressure of 2.5 MPa or greater. The 2.5 MPa value was the upper limit for the visual analysis of the pressure film used, although the maximum pressure could be read up to 3.06 MPa in the numerical analysis (Table 16). In the numerical analysis, the areas of a contact pressure less than 0.5 MPa, shown as green in Figure 44, were removed for the average pressure calculation (see Figure 45). This was done because pressures that low were more likely due to the contact from inserting the film into the setup rather than the actual test, and therefore skewed the results. Any maximum pressure values that are reported as 3.06 MPa are in fact greater than that value, since 3.06 MPa was the highest pressure that the pressure indicating film

could measure. This upper limit for the pressure film also influenced the average pressure calculation. Since 3.06 MPa is the maximum value used in the average pressure calculation, the average pressures for conditions that experienced any area at this maximum would realistically be greater than the reported values.

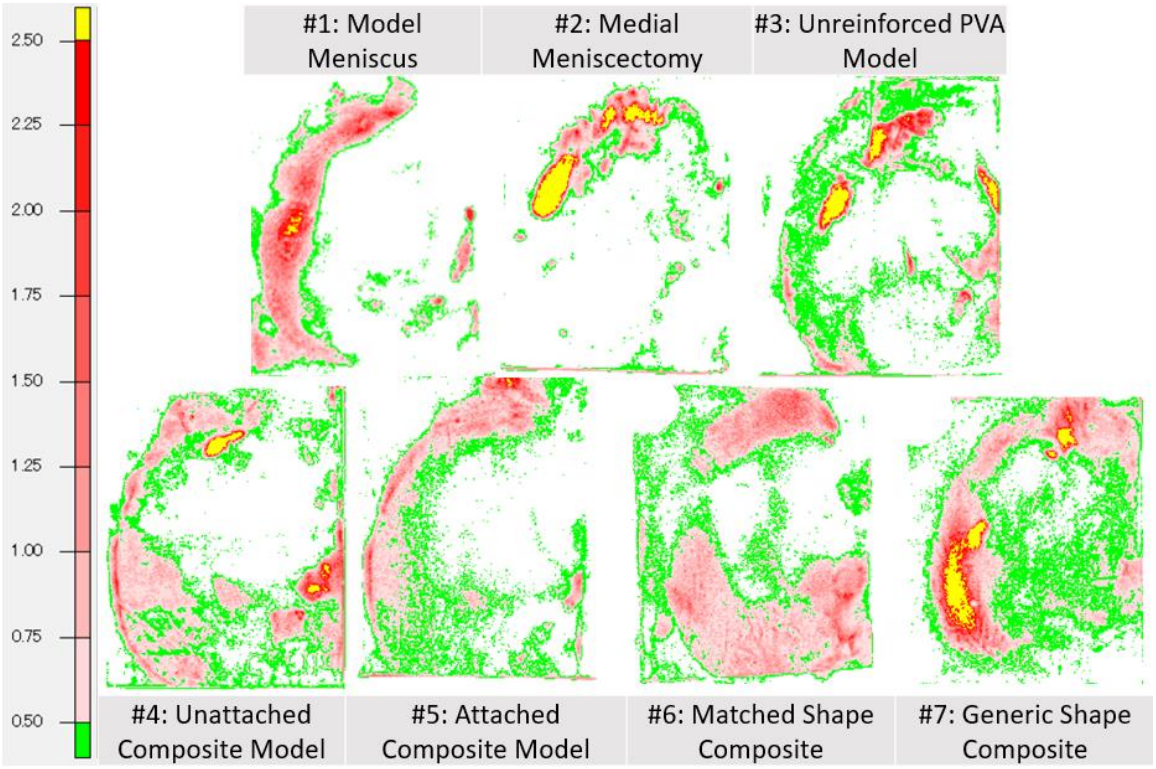

Figure 44: Visual analysis of pressure distribution for each condition and color key for contact pressure in MPa.

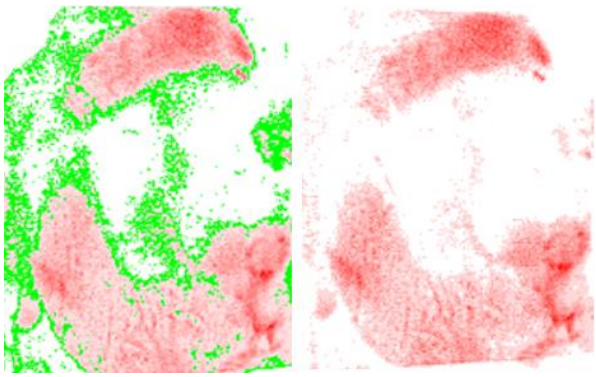

Figure 45: Original visual analysis image #6 with green areas showing less than 0.5 MPa contact pressure (left) and image after green area removal for average pressure calculation (right).

Table 16: Quantitative analysis of conditions for average and maximum pressures, and the percent area of contact pressure greater than 2.5 MPa.

ID #	Condition	Avg Pressure (MPa)	Max Pressure (MPa)	% Area at >2.5MPa
1	Model Meniscus	1.09	3.04	0.82
2	Medial Meniscectomy	1.38	>3.06	18.8
3	Unreinforced PVA Model	1.10	>3.06	8.50
4	Unattached Composite Model	0.89	>3.06	2.23
5	Attached Composite Model	0.80	2.82	0.02
6	Matched Shape Composite	0.89	2.50	0.00
7	Generic Shape Composite	1.08	>3.06	7.53

5.5.2 Comparison Between Conditions

A comparison between all conditions can be seen in Figure 46, showing contact pressure on the left axis and percent area on the right axis. Conditions that had areas at the maximum measurable pressure, 3.06 MPa, have open bars in the top of the chart to depict an unknown maximum value. These conditions included the medial meniscectomy (#2), the

unreinforced PVA model-shaped prototype (#3), the unattached model-shaped composite prototype (#4), and the generic-shaped CAD designed composite prototype (#7). It is important to note that for these four conditions, the reported average pressures are likely higher than those shown here due to the upper limit for pressure film measurement affecting the calculation. There was also noticeable radial extrusion in the unreinforced PVA prototype and in the unattached composite implant. All other composite prototypes experienced slight extrusion, but the attachment of these implants prevented them from extruding very much.

The medial meniscectomy (#2) was the worst overall condition tested, with the highest average pressure at 1.38 MPa, the highest contact area greater than 2.5 MPa pressure at 18.8%, and peak pressure exceeding the maximum measurable value of 3.06 MPa. This result was to be expected since there is no meniscus prototype in the meniscectomy condition to share the load on the medial side.

The unreinforced PVA model (#3) had the second highest average pressure at 1.10 MPa and the second highest percentage of high pressure contact area at 8.50%. This result confirms that no reinforcements in the hydrogel prototype leaves considerable risk for high contact pressure areas and potential cartilage damage.

The generic shaped composite prototype designed in CAD (#7) came in the middle with the fourth highest average at 1.08 MPa, but had the third highest area at high contact pressure with 7.53%. This suggests that size and shape are important parameters to prevent high pressure areas, which can cause damage to the implant or knee joint. The high

percentage of area at the maximum measurable pressure also means the average pressure is probably higher than the 1.08 MPa reported.

The unattached, model-shaped composite prototype (#4) still reached the maximum readable pressure, but had an average pressure of 0.89 MPa (one of the lowest tested) and 2.23% of area at a high contact pressure. Although the average pressure was tied for the second lowest, the areas of maximum pressure would likely make this value increase if the true peak contact pressures could be determined. This shows that even if a hydrogel meniscus implant has reinforcement, risk of high contact pressure is still present if there is no attachment within the joint space.

The original model meniscus (#1) did not reach the maximum measurable pressure, but was very close at 3.04 MPa. Although it had the third lowest percent of high pressure areas at 0.82%, it also had the third highest average pressure at 1.09 MPa. This result shows that even if the shape and size of the prototype is closely fit to the joint, the material of the implant and attachment within the joint are still key parameters for proper pressure distribution.

Only two of the prototypes tested met the preferred acceptance criteria of less than 3 MPa maximum pressure for a 1000N joint load. These were the attached, model-shaped composite (#5) and the CAD-designed, matched shape composite (#6).

The attached, model-shaped composite prototype (#5) had the lowest average pressure at 0.80 MPa, the second lowest maximum pressure at 2.82 MPa, and the second lowest percent of high contact pressure areas at 0.02%. This prototype performed better than all of those previously mentioned in all the categories examined. This shows that a

proper combination of reinforcements, size and shape, firm attachment, and material for a meniscus implant can greatly improve contact mechanics in a knee joint and reduce the risk of cartilage damage over the medial meniscectomy condition.

The matched shape composite prototype designed in CAD (#6), which is the implant proposed in this work, had the second lowest average pressure of 0.89 MPa, the lowest maximum pressure of 2.50 MPa, and an essentially negligible area of contact pressure over 2.50 MPa to give a 0.00% value. Although the average pressure for this prototype was higher than its model-shaped counterpart, the contact pressure was better distributed over a large area and the peak pressure remained below 2.50 MPa everywhere. The high magnitude pressure areas on the articular cartilage are believed to be responsible for the biological changes in the cartilage and bone that may lead to osteoarthritis [128]. Therefore, a lower peak pressure may be more crucial than a lower average pressure for a meniscal implant. The improvement in contact mechanics with this implant when compared to the generic shaped implant (#7) demonstrates that the risk of high contact pressure and resulting cartilage damage can be reduced if a proper implant shape is used. On the other hand, this prototype also performed as well if not better than the model-shaped prototype (#5). The matched shape prototype developed in this work has a flat base and a constant radius of curvature around the concave upper surface, so an exact size and shape match including contours of the upper and lower surfaces of the native meniscus, is not needed for proper contact mechanics. This finding shows that while a meniscus implant cannot just be a generic shape, it also does not need to be customized for each patient. A reasonable number of implant size and shape variations may be sufficient for most patients needing a meniscus replacement.

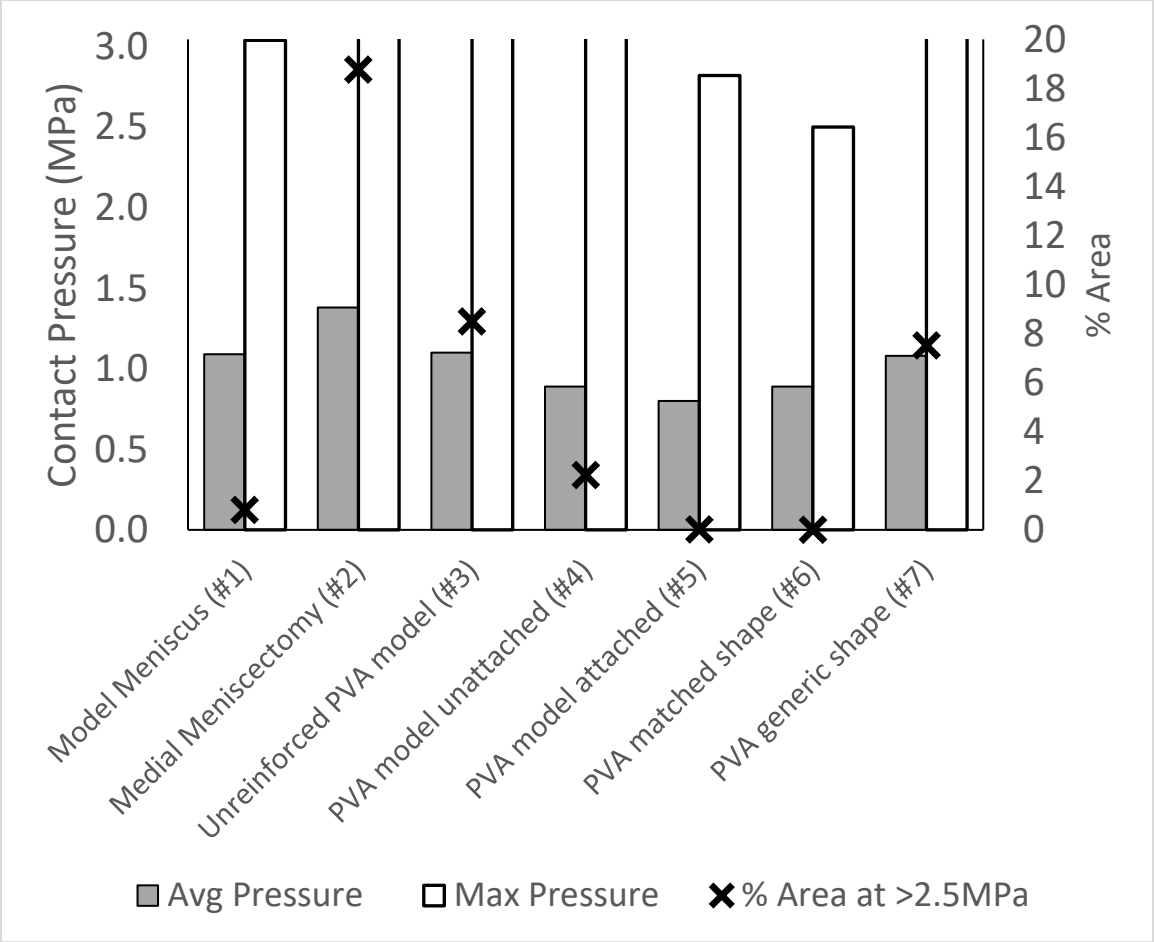

Figure 46: Comparison for all conditions of average and max contact pressures (left axis), where no line at the top of the max pressure bars signifies an unknown value above 3.06 MPa, and the percent of the contact area at a pressure greater than 2.5 MPa (right axis). Results are shown for all conditions described in Table 6.

5.5.3 Higher Joint Loads

The best performing prototype under a 1000 N load in terms of contact mechanics was determined to be the matched-shape, CAD designed implant (#6). To assess its performance under higher, more physiologically relevant gait loads, the prototype was loaded to 1500 N (for comparison with literature values) and to 2200 N (gait load for

average person) using the original pressure indicating film with the range of 0.5 MPa to 2.5 MPa, and with a higher pressure indicating film with the range of 2.5 MPa to 10 MPa. These results are shown in Figure 47, where a color correlation chart was used to estimate the peak contact pressure values instead of a digital analysis. At a load of 1500 N, the higher ranged film shows little to no dark colors, with a maximum pressure value estimated at less than 4 MPa, which is the same as a natural meniscus at a 1500N joint load [125]. At a load of 2200 N, small darker areas can be seen and these spots were estimated to be about 6.5 MPa of contact pressure. These spots of 6.5 MPa peak pressure remain at the same level or below values found in the literature for the natural intact meniscus at peak gait cycle loads and meet the acceptance criteria of less than 7.4 MPa peak pressure [126]. The 6.5 MPa peak pressure for the implant at 2200N is also much less than the peak pressure for meniscectomy conditions at gait loading, which is about 10 MPa [126]. Therefore, the contact mechanics at higher joint loads using the matched shape composite prototype is consistent with the natural meniscus and an improvement over alternative treatment conditions. In addition, these high-pressure spots could potentially be eliminated with more careful attachment of the prototype, since the attachment fibers were just threaded through arbitrary bone tunnels and tied around the outside of the model's tibia in these tests.

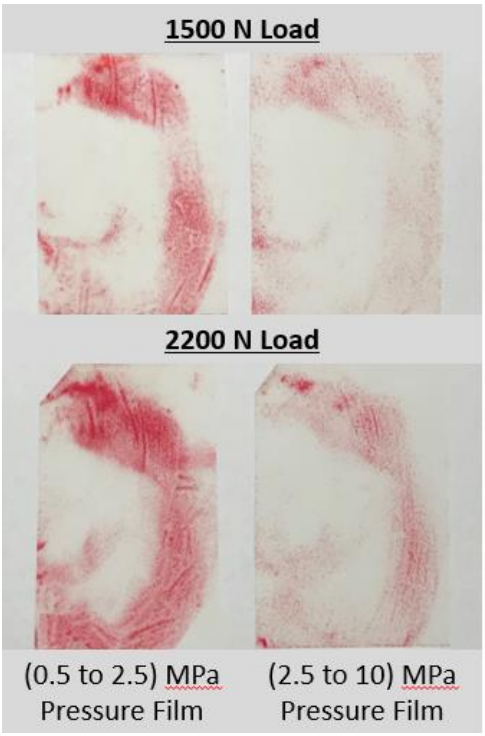

Figure 47: Photo of two ranges of pressure indicating film after testing the matched shape composite prototype at two higher joint loads, such as gait conditions. The 1500N and 2200N (gait) loads produced max contact stresses of about 4 MPa and 6 MPa, respectively, determined by color correlation charts.

CHAPTER 6. IMPLANT AND TESTING EVALUATION

6.1 Design Evaluation and Limitations

All design specifications were met by the implant during verification testing, as shown in Table 17. The design input specifications were directly created from measurements on the natural meniscus or on meniscal tissue from the literature to provide sufficient strength and contact mechanics for the implant to be used as a meniscus replacement. Since all design specifications were met, the implant developed here should be able to withstand the forces it would experience after implantation into the knee joint and serve as a suitable meniscus replacement.

Some problems arose during the early development of this implant design that were solved in the final design, but should be pointed out. Previous versions of the implant prototype had a base reinforcement weave that had to be trimmed from the edges after prototype synthesis and fully encased in hydrogel, with the fiber weave being exposed at the edges of the base of the implant after trimming. The exposed edges were prone to initiate peeling away of the base weave from the implant. When the weave edges became fully encased in hydrogel in later prototypes, this problem could be avoided. Creating prototypes using fibers and weaves that had not been previously embedded in hydrogel also caused issues during prototype synthesis and assembly. The non-embedded, dry fibers and weave would shift and bend during the molding process, causing kinks in the fibers and subsequent deformation of the prototypes while being stored in water after synthesis was complete. Embedding the fibers and weave prior to assembling and creating the prototype ensured

that the fibers were straight and would not cause deformation after storing in and absorbing water.

A limitation of the prototype design presented here is that it was created only in one size, for the right-side medial meniscus. However, the same concepts used in this design could be replicated for an implant used for the other knee joint, the lateral meniscus, and for a range of shapes and sizes. The results of the pressure distribution tests highlighted the importance of size and shape of a meniscus implant since the implant with a generic shape and size produced poor contact mechanics compared to the implant with a shape and size matched to the knee model. The pressure distribution tests also highlighted that a custom, patient-specific implant is not necessary for good contact mechanics since the implant with a size and shape that directly replicated all contours of the knee model did not perform any better than the implant with a size and shape matched to the model that had flat base. The pressure distribution tests also revealed the importance of reinforcement and attachment for the hydrogel implant, showing that contact mechanics are much improved when both reinforcement and attachment are present.

Table 17: Acceptance criteria and measured values from the mechanical evaluation. All specifications were met.

Design Specification	Acceptance Criteria	Measured Value
Tensile Strength	>19 MPa	20.2 MPa
Tensile Modulus	50 MPa to 1000 MPa	589 MPa
Cyclic Tension Resistance (After 1000 Cycles)	*Tensile strength:* >19 MPa *Tensile Modulus:* 50 MPa to 1000 MPa	*Tensile strength:* 21.9 MPa *Tensile Modulus:* 709 MPa
Compressive Modulus	0.30 MPa to 10 MPa	1.63 MPa
High magnitude Load Resistance (After 3 Loadings)	*Height Change*: <5% *Compressive Modulus:* 0.30 MPa to 10 MPa	*Height Change*: 2.8% *Compressive Modulus:* 1.22 MPa
Cyclic Compression Resistance (After 1000 Cycles)	*Height Change:* <5% *Compressive Modulus:* 0.30 MPa to 10 MPa	*Height Change*: 1.6% *Compressive Modulus:* 0.94 MPa
Shear Strength	>1.4 MPa	3.7 MPa
Fiber Tear Out Strength	>140 N	531 N
Peak Contact Pressure at Standing Load	<3 MPa	2.5 MPa
Peak Contact Pressure at Gait Load	<7.4 MPa	6.5 MPa

6.2 Mechanical Evaluation Limitations

The mechanical evaluation of the meniscus implant and the composite material it was made from provided acceptable values for every property and specification that was tested. Due to the lack of literature on the mechanical properties of human meniscal tissue and forces exerted on the meniscus within the body, many of the specifications and force values used in the mechanical evaluation had to be derived by combining measurements from multiple sources. Although the values derived in this work were found through extensive literature review, many factors could have been overlooked or could still be missing and the generated values are not guaranteed to be accurate. Some additional examples of various limitations among the mechanical tests performed are outlined below:

For all tensile and compression tests, stresses and strains were calculated based on dimensions found using the manual technique of calliper measurements. The hydrogel's elasticity and changes from swelling in water also made the measurements more difficult to get exactly right. The variation in manual measurements could have affected some of the calculations for the results, but the small differences in measurement values would likely only have little effects on the reported values for various properties.

The tensile and compressive cyclic tests were only conducted to 1000 cycles to simulate 1000 steps, but people usually take many more steps in any given day. The cyclic tests were conducted for a preliminary assessment of any changes to properties after multiple repeated loadings, but a higher number of cycles would have given a better idea of the longevity of the implant during repeated loads.

The tensile tests were performed on rectangular samples and the samples were loaded unidirectionally in tension. The tensile stresses in the natural meniscus are under a more complex loading pattern in the form of hoop stresses that follow the circumference of the menisci. However, values obtained from the literature were determined using rectangular or dog-bone samples of meniscus tissue in uniaxial tension, so the values measured in the mechanical evaluation of the implant composite material can be compared to these literature values.

The loading of the compression tests was also less complex than the physiologic compressive loading on the meniscus. Cylindrical samples were compressed between two flat plates in unconfined compression, and radial displacement was uncontrolled due to the lack of circumferential reinforcements and subsequent hoop stress development in these

samples. In the wedge shaped natural meniscus, compression occurs between the flat tibial plateau and the curved femur, and radial displacement is resisted by the circumferential collagen fibers to produce hoop stresses. The differences in loading conditions of the samples and the natural meniscus could have influenced the results found here, specifically the level of deformation. In addition, only axial deformation was calculated for the cylindrical hydrogel samples while radial deformation was not assessed.

The setup for the pressure distribution tests utilized an artificial knee model that had to be modified to mount into a materials testing machine. No special care was given to ensure the knee model was mounted to provide an exact match to the alignment in physiologic full extension, and most of the joint ligaments were removed or disconnected. Therefore, the mechanics of the joint could have been different from physiologic conditions and an unknown percentage of the total joint load was transmitted through the implants/conditions tested. However, all conditions were tested in the same situation, so comparisons between them are still valid. The level of attachment for the attached implants could have varied between implants since the attachment fibers were arbitrarily tied as tight as possible after being thread through bone tunnels present in the model, which is likely not the method of attachment that would be used after implantation in a real knee. The bone tunnels were also not necessarily representative of the tunnels that would be used if the implant were used in a patient. The alignment of the knee joint model and the attachment of the implants could have influenced the contact pressure measurements during testing such as magnitude of the pressures, overall distribution of the pressures, and locations of high pressure areas.

6.3 Improvements over Previous PVA Implants

To our knowledge only two other groups have done extensive work on PVA hydrogel meniscus implants. The first implant was developed by Kobayashi et al. and was made from only PVA hydrogel with no reinforcements [66], [67]. Although the non-reinforced implant had sufficient strength for a rabbit meniscal replacement, it failed from radial tears and caused cartilage damage when exposed to the higher force environment of a sheep knee. These failures would likely translate to a human knee since the joint forces are also large.

The second PVA hydrogel implant in the literature was developed by Holloway et al. and was reinforced with polyethylene fiber mats [69]–[71]. This group focused on mechanical properties such as the tensile and compressive elastic moduli, the interfacial strength of the composite, and the pressure distribution when loaded in a knee joint. They did not assess the overall strength of the composite material. After implantation into a sheep knee, the interfacial adhesion proved to be insufficient and delamination still occurred, along with implant extrusion and bone tunnel widening. The bone tunnel widening was likely due to the attachment method used, and the attachment method could have also caused some of the extrusion. The delamination issue, and potentially some of the extrusion, can be attributed to several other factors.

The polyethylene fibers used as reinforcements were hydrophobic and required surface modification to provide good adhesion to the hydrogel matrix. As evidenced by the sheep study, this interfacial adhesion improvement was stiff insufficient and delamination occurred. Our implant developed in this work utilizes aramid fibers that can absorb water

and adhere to a hydrogel matrix without the need for modification. The tensile, compression, and fiber tear out tests performed on the composite material shows that the interface can withstand the high stresses and loads that a meniscus implant would experience in the knee joint after meniscus replacement. Therefore, the risk for delamination after implantation is reduced compared to the polyethylene reinforced implant.

In addition to the differences in fiber interaction with water, the fiber and reinforcement layout used in our implant is different from the reinforcement layout used in the implant developed by Holloway et al. The polyethylene reinforced implant used fiber mats, with no specific orientation, to reinforce the hydrogel matrix. While our implant also utilizes a fiber weave as a base reinforcement, the weave is fully encased in hydrogel which reduces the risk for delamination. The implant also has specifically oriented fiber bundles around its periphery that help convert compressive load to tensile hoop stress and limit radial deformation and subsequent extrusion. This specific fiber orientation and overall reinforcement layout gives the implant strength in all directions and gives the implant enhanced strength in the crucial area around the periphery to prevent extrusion. The fibers being fully encased in hydrogel around the outer periphery also reduces the risk of fiber delamination, especially since the fibers would be pulled toward the bulk of the hydrogel instead of toward the surface during normal loading and use. The fibers also have more surface area in direct contact with the hydrogel than a weave would, which improves interfacial adhesion between the hydrogel and reinforcements.

The hydrogel used in all tests and for all prototypes was made from a single molecular weight of PVA, at a set concentration and number/duration of freeze-thaw cycles. PVA

hydrogel properties can vary significantly when these parameters are changed [source], but the goal of this work was to meet all specifications with the material used, which was accomplished. The number of freeze-thaw cycles has been shown to have little effect on properties after five or six cycles, which was the number of cycles used in this work. The concentration of PVA (or the weight percentage in the initial solution) can impact properties to a greater degree when the hydrogels are subjected to five or more freeze-thaw cycles [69]. The hydrogel used in our implant had a higher concentration of PVA than the previous PVA-hydrogel implants, which likely contributes to its high strength and limits deformation. The high strength that results from the high PVA concentration is part of the reason all specifications could be met, and would likely help this implant succeed where the other PVA implants could not.

6.4 Patent Comparison

A patent search was conducted to determine the prior art in the field for meniscus implants and to assess the patentability of our implant. The search was focused on permanent, total meniscus replacements that seemed similar to our implant. Various patents were found, including some that have not yet been granted, and the claims for the inventions were compared to our implant and are outlined below:

US Patent 6629997 was assigned to Kevin Mansmann and states the following as Claim 1 [129]:

> A non-resorbable Meniscal device designed for surgical emplacement in a mammalian joint, comprising a synthetic non-resorbable hydrogel component and a flexible fibrous mesh component, wherein:

> a. the synthetic non-resorbable hydrogel component provides a smooth and lubricious surface, on at least one surface area which will contact and rub against a natural cartilage surface in the joint;
>
> b. the flexible fibrous mesh component reinforces the smooth and lubricious surface, and provides reinforced means for anchoring the device to tissue which surrounds the joint, and extends throughout essentially all of the hydrogel component other than one or more smooth surfaces,
>
> and wherein the device is non-resorbable, and is designed for surgical implantation without cells embedded within the hydrogel component.

While the first part of the claim (a) matches the description of our implant, the second part (b) highlights several differences. The fibrous mesh described in the claim reinforces the surface that rubs against natural cartilage, but our implant's fibrous mesh reinforces the body of the implant at the base that rests on the tibial plateau. The claim also states that the same fibrous mesh that reinforces the surface provides the means for anchoring device to surrounding tissue, which is described as "fibrous" tissue in the body of the patent. Our implant is anchored by the fibers that extend out of the horns of the implant, which is not a mesh, and is attached through bone tunnels and not fibrous tissue. The claim also states that the fibrous mesh that anchors extends throughout the hydrogel, but our anchoring fibers are exclusively located around the periphery of the implant and our fiber mesh is only located in the central implant base.

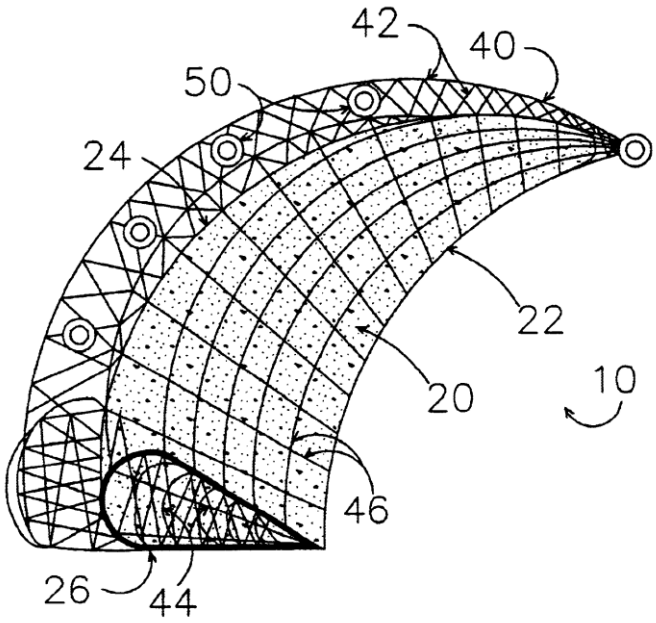

Figure 48: Depiction of implant from US Patent 6629997.

US Patent 9078756 was assigned to Rutgers State University and states the following in Claim 1 [130]:

> An artificial knee meniscus implant comprising:
>
> a c-shaped scaffold having an arcuate middle section extending between an anterior end and a posterior end with a central axis extending through a center of the arcuate middle section and evenly spaced between the anterior and posterior ends; and
>
> a reinforcing network of fibers independent from and embedded in the scaffold, the reinforcing network of fibers defining a matrix having a three-dimensional shape and geometry which is substantially the same as a three-dimensional shape and geometry of the c-shaped scaffold;
>
> wherein fibers of said network fibers exit each end of the scaffold to form respective anterior and posterior attachment segments which extend parallel to the central axis of the scaffold; and said network of fibers is configured to convert an axial compressive force on said scaffold to tensile loads on said attachment points.

The first part of the claim describes a c-shaped scaffold, but our implant is not c-shaped and has a wider posterior section than the anterior section. The claim also describes a reinforcing network of fibers that has a three-dimensional shape that is the same as the scaffold shape. Our implant has a flat base weave reinforcement with separate fibers following the periphery, so the reinforcements are not in the same shape as the hydrogel scaffold. The claim also states that the network of fibers extends parallel to the central axis of the scaffold, but our reinforcing fibers are oriented circumferentially, not in a network, and are in a curved layout.

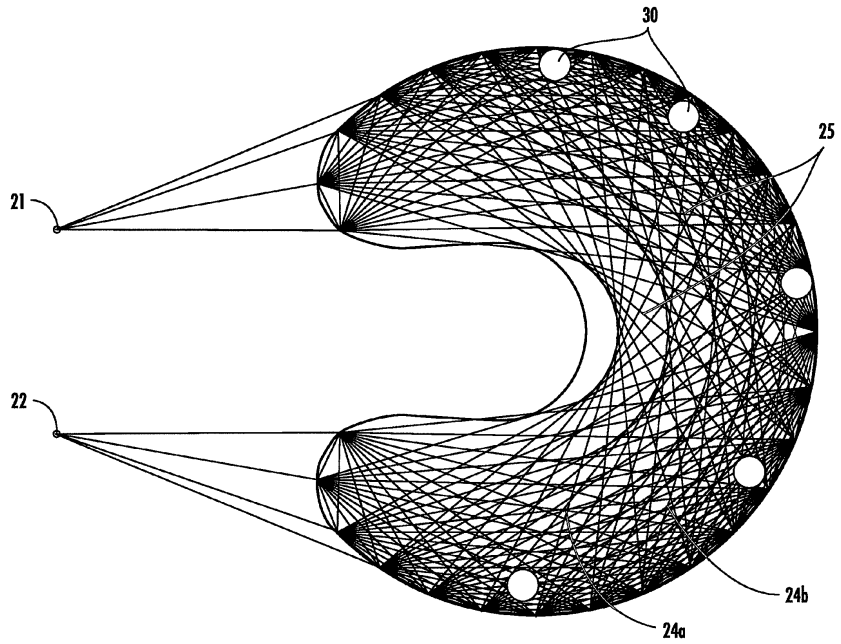

Figure 49: Depiction of implant from US Patent 9078756.

US Patent 9320606 was assigned to Active Implants LLC (the producers of the the NUsurface® implant) and states the following in Claim 1 [131]:

> A prosthetic device for replacing a natural meniscus, the prosthetic device comprising:
>
> a central body portion comprising a flexible polymeric material, the central body portion having an upper articulating bearing surface for movingly engaging a femoral condyle and a lower articulating bearing surface for movingly engaging a tibial plateau;
>
> a perimeter comprising an outer body portion and a boundary, the outer body portion and the boundary together completely surrounding the central body portion, wherein the outer body portion and the boundary each have an increased thickness with respect to the central body portion, wherein the perimeter is configured to limit movement of the femoral condyle with respect to the upper articulating bearing surface of the central body portion, the outer body portion having an increased stiffness with respect to the central body portion, the outer body portion and the boundary having different thicknesses, the boundary extending between first and second ends of the outer body portion;
> wherein the central body portion and the outer body portion comprise a monolithic structure; and
>
> wherein the prosthetic device is configured for implantation without removing any portion of the tibial plateau.

The claim describes a central body portion and a perimeter comprising an outer body portion and a boundary that have increased thicknesses compared to the inner body portion. Our device is a single hydrogel portion, with no specific perimeter or boundary. The claim also states that the central body portion and the outer body portion have a different stiffness and are monolithic. The hydrogel of our implant has the same stiffness throughout the hydrogel portion of the implant until the composite areas with reinforcements, and the structure is no longer monolithic in these composite areas. The claim also describes that the prosthetic device is implanted without removing any portion of the tibial plateau, whereas our implant would likely be attached through bone tunnels.

Active Implants was also assigned US Patent 8778024, which states the following as part of the first claim [132]:

> A meniscus prosthetic device for use in a knee joint, the meniscus prosthetic device comprising:
>
> a central portion having an upper surface for engagement with a portion of a femur and an opposing lower surface for engagement with a portion of a tibia, the central portion comprising a resilient polycarbonate polyurethane

This claim describes an implant made from polycarbonate polyurethane, but our implant is made from PVA hydrogel.

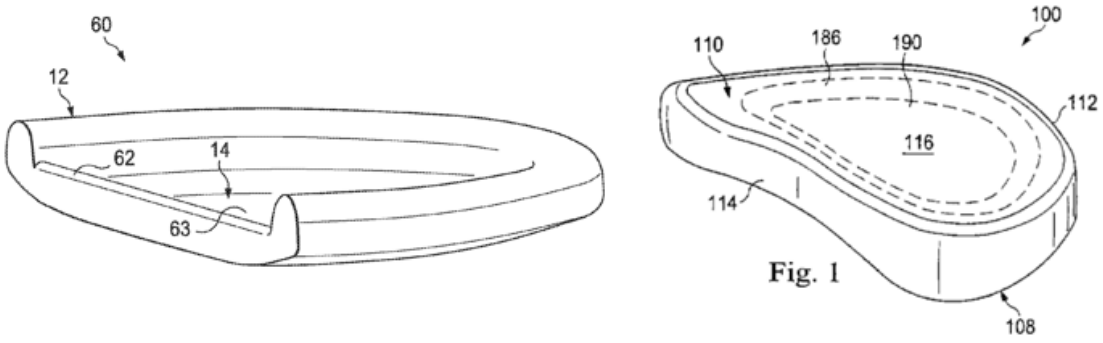

Fig. 1

Figure 50: Depiction of implant from US Patent 9320606 (left) and US Patent 8778024 (right).

US Patent Application 0288199 was assigned to Drexel University (where the polyethylene reinforced PVA hydrogel implant was developed) and New York Society for Relief of

Ruptured and Crippled. The application has since been abandoned, but it states the following in Claim 1 [133]:

> A fiber-reinforced hydrogel composite that mimics a native tissue of a mammal and is suitable for implantation in the mammal, comprising:
>
> at least one fibrous component forming part of a fiber volume fraction;
>
> a polymer fraction comprising poly(vinyl alcohol) (PVA) and poly(acrylic acid) (PAA);
>
> wherein the ratio of PVA to PAA is altered to control the mechanical properties of the composite.

The claim states the polymer fraction of the fiber-reinforced hydrogel composite is comprised of PVA and poly(acrylic acid), but our implant is exclusively made from PVA-hydrogel and the reinforcement fibers.

None of the patents or applications described above, nor any other patents found in the search, directly interfere with our implant. Therefore, we believe we have freedom to operate and have a novel design due to the unique reinforcement layout that could warrant a patent in the future.

6.5 Future Directions

To help researchers and developers create meniscus implants that can function properly, the natural meniscus tissue should be more thoroughly evaluated to provide a basis for comparison. Although meniscal tissue has been studied for multiple properties, the characterization of the tissue is far from complete. Comprehensive mechanical testing of natural meniscus tissue, the tissue's behaviour and the forces it experiences in vivo, and a standardization of the test methods to find the tissue's mechanical properties would

significantly improve the ability of researchers to develop suitable implants and evaluate them as meniscus replacements.

In addition to the characterization of natural tissue, more testing and optimization of the implant developed here could be useful. Although multiple iterations of reinforcing fiber configurations were attempted during development, an optimization of the fiber layout could help find a weave and fiber combination that improves the implant's function and properties. The current reinforcement orientation used in the developed implant met all specifications and performed well, but a fiber orientation that replicates the collagen fibers found in the natural meniscus could provide a superior performing implant. Alternatively, finite element modelling or experimentation using prototypes with different fiber and weave configurations could highlight which fiber orientations and locations are most important for proper function.

Another aspect of the implant that could be optimized is the size and shape of the bulk hydrogel matrix. Different dimensions, such as width, thickness, and curvature of the articulating surfaces could be evaluated using modelling or experimentation of various prototypes by changing these values individually. The overall size is also important, since people have a wide range of knee joint sizes. Meniscal size data could be compiled to determine what sizes would be appropriate if the implant were produced on a larger scale. Although no two people have identical menisci, a select number of different sizes and shapes could potentially be used in most patients. This would allow for an off-the-shelf meniscal replacement that comes in a variety of sizes and shapes without the need for a completely custom implant for each patient.

Some examples of extra mechanical evaluation that could still be done on this implant include tear tests, more long-term cyclic or fatigue tests, and compressive point loading tests. These tests were not performed due to the lack of values for the natural meniscus to compare the results to. Another evaluation that would be helpful would be long-term swelling studies on the composite, since the hydrogel and fiber reinforcements would likely experience different degrees of swelling after long periods of submersion.

The attachment and implantation method of this implant was also not fully developed. The pressure distribution testing showed that attachment is important for contact mechanics, but the method of attachment was crude on the artificial knee model and would need to be altered if the implant were to be implanted into an actual patient. With the attachment method also comes the need to figure out how to insert the implant into the joint, whether it be minimally invasive or through open knee surgery.

The attachment method, as well as in vivo performance would be best determined through animal models. Although no animal can directly replicate the human knee joint, they can tell how an implant would respond to a biologic environment and would help with implantation and attachment methods. However, controversy still exists as to the best animal model to use [90].

6.6 Conclusion

The PVA-hydrogel and aramid fiber composite material and implant was shown to be suitable for the application of a meniscus replacement. The composite showed a tensile strength, tensile modulus, compressive modulus, shear strength, and fiber tear out strength that is within the ranges specified for the implant based on values from the natural meniscus

condition. The material also showed resistance to property changes after cyclic tensile loading, cyclic compressive loading, and high magnitude loadings. Furthermore, an implant made from the composite material demonstrated contact mechanics that resembled the natural meniscus when the size and shape of the implant were similar to, but not an exact replicate of the dimensions of the native meniscus. Therefore, a range of sizes and shapes for implants made from the PVA-hydrogel/fiber composite material developed in this work could provide a superior treatment option for patients in need of a meniscus replacement.

REFERENCES

[1] T. Kusayama, C. D. Harner, G. J. Carlin, J. W. Xerogeanes, and B. A. Smith, "Anatomical and biomechanical characteristics of human meniscofemoral ligaments.," *Knee Surg. Sports Traumatol. Arthrosc.*, vol. 2, no. 4, pp. 234–7, 1994.

[2] K. R. Stone, A. Freyer, T. Turek, A. W. Walgenbach, S. Wadhwa, and J. Crues, "Meniscal Sizing Based on Gender, Height, and Weight," *Arthrosc. - J. Arthrosc. Relat. Surg.*, vol. 23, no. 5, pp. 503–508, 2007.

[3] C. R. Clark and J. A. Ogden, "Development of the menisci of the human knee joint. Morphological changes and their potential role in childhood meniscal injury.," *J. Bone Joint Surg. Am.*, vol. 65, no. 4, pp. 538–47, Apr. 1983.

[4] S. P. Arnoczky and R. F. Warren, "Microvasculature of the human meniscus," *Am. J. Sports Med.*, vol. 10, no. 2, pp. 90–95, Mar. 1982.

[5] C. S. Proctor, M. B. Schmidt, R. R. Whipple, M. A. Kelly, and V. C. Mow, "Material properties of the normal medial bovine meniscus," *J. Orthop. Res.*, vol. 7, no. 6, pp. 771–782, 1989.

[6] J. Herwig, E. Egner, and E. Buddecke, "Chemical changes of human knee joint menisci in various stages of degeneration.," *Ann. Rheum. Dis.*, vol. 43, no. 4, pp. 635–40, Aug. 1984.

[7] I. D. McDermott, S. D. Masouros, and A. A. Amis, "Biomechanics of the menisci of the knee," *Curr. Orthop.*, vol. 22, no. 3, pp. 193–201, 2008.

[8] A. Beaupré, R. Choukroun, R. Guidouin, R. Garneau, H. Gérardin, and A. Cardou, "Knee menisci. Correlation between microstructure and biomechanics.," *Clin. Orthop. Relat. Res.*, no. 208, pp. 72–5, Jul. 1986.

[9] P. G. Bullough, L. Munuera, J. Murphy, and A. M. Weinstein, "The strength of the menisci of the knee as it relates to their fine structure.," *J. Bone Joint Surg. Br.*, vol. 52, no. 3, pp. 564–7, Aug. 1970.

[10] A. J. S. Fox, A. Bedi, and S. A. Rodeo, "The Basic Science of Human Knee Menisci," *Sport. Heal. A Multidiscip. Approach*, vol. 4, no. 4, pp. 340–351, 2012.

[11] D. C. Fithian, M. A. Kelly, and V. C. Mow, “Material properties and structure-function relationships in the menisci.,” *Clin. Orthop. Relat. Res.*, no. 252, pp. 19–31, Mar. 1990.

[12] D. L. Skaggs, W. H. Warden, and V. C. Mow, “Radial tie fibers influence the tensile properties of the bovine medial meniscus,” *J. Orthop. Res.*, vol. 12, no. 2, pp. 176–185, Mar. 1994.

[13] E. A. Makris, P. Hadidi, and K. A. Athanasiou, “The knee meniscus: Structure-function, pathophysiology, current repair techniques, and prospects for regeneration,” *Biomaterials*, vol. 32, no. 30, pp. 7411–7431, 2011.

[14] A. S. Voloshin and J. Wosk, “Shock absorption of meniscectomized and painful knees: a comparative in vivo study.,” *J. Biomed. Eng.*, vol. 5, no. 2, pp. 157–61, Apr. 1983.

[15] H. Kurosawa, T. Fukubayashi, and H. Nakajima, “Load-bearing mode of the knee joint: physical behavior of the knee joint with or without menisci.,” *Clin. Orthop. Relat. Res.*, no. 149, pp. 283–90, Jun. 1980.

[16] I. M. Levy, P. A. Torzilli, and R. F. Warren, “The effect of medial meniscectomy on anterior-posterior motion of the knee.,” *J. Bone Joint Surg. Am.*, vol. 64, no. 6, pp. 883–8, Jul. 1982.

[17] K. Messner and J. Gao, “The menisci of the knee joint. Anatomical and functional characteristics, and a rationale for clinical treatment.,” *J. Anat.*, vol. 193 (Pt 2), pp. 161–78, Aug. 1998.

[18] W. R. Krause, M. H. Pope, R. J. Johnson, and D. G. Wilder, “Mechanical changes in the knee after meniscectomy.,” *J. Bone Joint Surg. Am.*, vol. 58, no. 5, pp. 599–604, Jul. 1976.

[19] R. S. Jones *et al.*, “Direct measurement of hoop strains in the intact and torn human medial meniscus.,” *Clin. Biomech. (Bristol, Avon)*, vol. 11, no. 5, pp. 295–300, Jul. 1996.

[20] K. A. Athanasiou and J. Sanchez-Adams, *Engineering the Knee Meniscus*. Morgan & Claypool, 2009.

[21] M. Drakos and A. Allen, “Meniscal Structure, Function, Repair, and Replacement,” *Oncology and Basic Science*, 2016. [Online]. Available: https://oncohemakey.com/meniscal-structure-function-repair-and-replacement/. [Accessed: 08-Apr-2018].

[22] A. A. Amis, A. M. J. Bull, and I. D. McDermott, “Caracteristiques biomecaniques des ligaments et des menisques du genou [Biomechanical function of knee ligaments and menisci],” in *Pathologie ligamentaire du genou*, no. 2, Springer Verlag, 2004, pp. 45–60.

[23] W. E. GarrettJr. *et al.*, “American Board of Orthopaedic Surgery Practice of the Orthopaedic Surgeon: Part-II, Certification Examination Case Mix,” *J. Bone Jt. Surg.*, vol. 88, no. 3, p. 660, Mar. 2006.

[24] M. Majewski, H. Susanne, and S. Klaus, “Epidemiology of athletic knee injuries: A 10-year study,” *Knee*, vol. 13, no. 3, pp. 184–188, Jun. 2006.

[25] A. C. T. Vrancken, P. Buma, and T. G. Van Tienen, “Synthetic meniscus replacement: A review,” *Int. Orthop.*, vol. 37, no. 2, pp. 291–299, 2013.

[26] A. B. Nielsen and J. Yde, “Epidemiology of acute knee injuries: a prospective hospital investigation.,” *J. Trauma*, vol. 31, no. 12, pp. 1644–8, Dec. 1991.

[27] T. D. Lauder, S. P. Baker, G. S. Smith, and A. E. Lincoln, “Sports and physical training injury hospitalizations in the army.,” *Am. J. Prev. Med.*, vol. 18, no. 3 Suppl, pp. 118–28, Apr. 2000.

[28] J. C. Jones, R. Burks, B. D. Owens, R. X. Sturdivant, S. J. Svoboda, and K. L. Cameron, “Incidence and risk factors associated with meniscal injuries among active-duty US Military service members,” *J. Athl. Train.*, vol. 47, no. 1, pp. 67–73, 2012.

[29] P. E. Greis, D. D. Bardana, M. C. Holmstrom, and R. T. Burks, “Meniscal injury: I. Basic science and evaluation.,” *The Journal of the American Academy of Orthopaedic Surgeons*, vol. 10, no. 3. pp. 168–176, 2002.

[30] N. Maffulli, U. G. Longo, S. Campi, and V. Denaro, “Meniscal tears.,” *Open access J. Sport. Med.*, vol. 1, pp. 45–54, Apr. 2010.

[31] L. S. Lohmander, P. M. Englund, L. L. Dahl, and E. M. Roos, “The Long-term Consequence of Anterior Cruciate Ligament and Meniscus Injuries,” *Am. J. Sports Med.*, vol. 35, no. 10, pp. 1756–1769, Oct. 2007.

[32] I. D. McDermott and A. A. Amis, “The consequences of meniscectomy,” *J. Bone Joint Surg. Br.*, vol. 88–B, no. 12, pp. 1549–1556, Dec. 2006.

[33] K. Messner and J. Gillquist, “Prosthetic replacement of the rabbit medial meniscus,” *J. Biomed. Mater. Res.*, vol. 27, no. 9, pp. 1165–1173, Sep. 1993.

[34] P. Verdonk and P. Vererfve, “Traumatic Lesions: Stable Knee, ACL Knee,” in *The Meniscus*, Berlin, Heidelberg: Springer Berlin Heidelberg, 2010, pp. 45–49.

[35] I. P. Terzidis, A. Christodoulou, A. Ploumis, P. Givissis, K. Natsis, and M. Koimtzis, “Meniscal Tear Characteristics in Young Athletes with a Stable Knee,” *Am. J. Sports Med.*, vol. 34, no. 7, pp. 1170–1175, Jul. 2006.

[36] M. T. Hirschmann and N. F. Friederich, “Classification: Discoid Meniscus, Traumatic Lesions,” in *The Meniscus*, Berlin, Heidelberg: Springer Berlin Heidelberg, 2010, pp. 241–246.

[37] F. A. Barber and J. E. McGarry, “Meniscal Repair Techniques,” *Sports Med. Arthrosc.*, vol. 15, no. 4, pp. 199–207, Dec. 2007.

[38] P. Beaufils and N. Pujol, “Meniscal repair: Technique,” *Orthop. Traumatol. Surg. Res.*, vol. 104, no. 1, pp. S137–S145, Feb. 2018.

[39] S. C. Mordecai, N. Al-Hadithy, H. E. Ware, and C. M. Gupte, “Treatment of meniscal tears: An evidence based approach.,” *World J. Orthop.*, vol. 5, no. 3, pp. 233–41, Jul. 2014.

[40] S. P. Arnoczky and R. F. Warren, “Microvasculature of the human meniscus,” *Am. J. Sports Med.*, vol. 10, no. 2, pp. 90–95, Mar. 1982.

[41] R. Seil and D. Pape, “Meniscal Repair: Biomechanics,” in *The Meniscus*, Berlin, Heidelberg: Springer Berlin Heidelberg, 2010, pp. 107–117.

[42] B. E. Baker, A. C. Peckham, F. Pupparo, and J. C. Sanborn, “Review of meniscal

injury and associated sports," *Am. J. Sports Med.*, vol. 13, no. 1, pp. 1–4, Jan. 1985.

[43] A. Hede, D. B. Jensen, P. Blyme, and S. Sonne-Holm, "Epidemiology of meniscal lesions in the knee. 1,215 open operations in Copenhagen 1982-84.," *Acta Orthop. Scand.*, vol. 61, no. 5, pp. 435–7, Oct. 1990.

[44] T. J. Fairbank, "KNEE JOINT CHANGES AFTER MENISCECTOMY," *J. Bone Joint Surg. Br.*, vol. 30–B, no. 4, pp. 664–670, Nov. 1948.

[45] A. M. Ahmed and D. L. Burke, "In-vitro measurement of static pressure distribution in synovial joints - Part I: Tibial surface of the knee," *J. Biomech. Eng.*, vol. 105, no. 3, pp. 216–225, 1983.

[46] M. E. Baratz, F. H. Fu, and R. Mengato, "Meniscal tears: The effect of meniscectomy and of repair on intraarticular contact areas and stress in the human knee," *Am. J. Sports Med.*, vol. 14, no. 4, pp. 270–275, Jul. 1986.

[47] J.-M. Fayard, H. Pereira, E. Servien, S. Lustig, and P. Neyret, "Meniscectomy: Global Results-Complications," in *The Meniscus*, Berlin, Heidelberg: Springer Berlin Heidelberg, 2010, pp. 177–190.

[48] J. L. Cook, "The current status of treatment for large meniscal defects.," *Clin. Orthop. Relat. Res.*, no. 435, pp. 88–95, Jun. 2005.

[49] A. Hede, E. Larsen, and H. Sandberg, "The long term outcome of open total and partial meniscectomy related to the quantity and site of the meniscus removed.," *Int. Orthop.*, vol. 16, no. 2, pp. 122–5, 1992.

[50] H. Roos, M. Lauren, T. Adalberth, E. M. Roos, K. Jonsson, and L. S. Lohmander, "Knee osteoarthritis after meniscectomy: Prevalence of radiographic changes after twenty-one years, compared with matched controls," *Arthritis Rheum.*, vol. 41, no. 4, pp. 687–693, Apr. 1998.

[51] M. Englund and L. S. Lohmander, "Risk factors for symptomatic knee osteoarthritis fifteen to twenty-two years after meniscectomy," *Arthritis Rheum.*, vol. 50, no. 9, pp. 2811–2819, Sep. 2004.

[52] I. D. McDermott and A. A. Amis, "The consequences of meniscectomy," *J. Bone Jt. Surg. - Br. Vol.*, vol. 88–B, no. 12, pp. 1549–1556, 2006.

[53] H. Luks, “Recovery After Meniscal Tear Surgery,” *Orthopedic Surgery and Sports Medicine*, 2018. [Online]. Available: https://www.howardluksmd.com/meniscal-tear-recovery-surgery/. [Accessed: 08-Apr-2018].

[54] M. ElAttar, A. Dhollander, R. Verdonk, K. F. Almqvist, and P. Verdonk, “Twenty-six years of meniscal allograft transplantation: Is it still experimental? A meta-analysis of 44 trials,” *Knee Surgery, Sport. Traumatol. Arthrosc.*, vol. 19, no. 2, pp. 147–157, 2011.

[55] Y. Wada, M. Amiel, F. Harwood, H. Moriya, and D. Amiel, “Architectural remodeling in deep frozen meniscal allografts after total meniscectomy.,” *Arthroscopy*, vol. 14, no. 3, pp. 250–7, Apr. 1998.

[56] B.-S. Lee, J.-W. Chung, J.-M. Kim, W.-J. Cho, K.-A. Kim, and S.-I. Bin, “Morphologic Changes in Fresh-Frozen Meniscus Allografts Over 1 Year,” *Am. J. Sports Med.*, vol. 40, no. 6, pp. 1384–1391, Jun. 2012.

[57] T. G. van Tienen, G. Hannink, and P. Buma, “Meniscus Replacement Using Synthetic Materials,” *Clin. Sports Med.*, vol. 28, no. 1, pp. 143–156, Jan. 2009.

[58] K. Messner, “Meniscal substitution with a Teflon-periosteal composite graft: a rabbit experiment,” *Biomaterials*, vol. 15, no. 3, pp. 223–230, Feb. 1994.

[59] K. Sommerlath, M. Gallino, and J. Gillquist, “Biomechanical characteristics of different artificial substitutes for rabbit medial meniscus and effect of prosthesis size on knee cartilage,” *Clin. Biomech.*, vol. 7, no. 2, pp. 97–103, May 1992.

[60] S.-W. Kang *et al.*, “Regeneration of whole meniscus using meniscal cells and polymer scaffolds in a rabbit total meniscectomy model,” *J. Biomed. Mater. Res. Part A*, vol. 78A, no. 3, pp. 638–651, Sep. 2006.

[61] C. Chiari *et al.*, “A tissue engineering approach to meniscus regeneration in a sheep model,” *Osteoarthr. Cartil.*, vol. 14, no. 10, pp. 1056–1065, Oct. 2006.

[62] E. Kon *et al.*, “Tissue engineering for total meniscal substitution: animal study in sheep model--results at 12 months.,” *Tissue Eng. Part A*, vol. 18, no. 15–16, pp. 1573–82, Aug. 2012.

[63] E. Balint, C. J. Gatt, and M. G. Dunn, “Design and mechanical evaluation of a novel

fiber-reinforced scaffold for meniscus replacement," *J. Biomed. Mater. Res. Part A*, vol. 100A, no. 1, pp. 195–202, Jan. 2012.

[64] A. R. Merriam, J. M. Patel, B. M. Culp, C. J. Gatt, and M. G. Dunn, "Successful Total Meniscus Reconstruction Using a Novel Fiber-Reinforced Scaffold," *Am. J. Sports Med.*, vol. 43, no. 10, pp. 2528–2537, Oct. 2015.

[65] J. M. Patel, A. R. Merriam, B. M. Culp, C. J. Gatt, and M. G. Dunn, "One-Year Outcomes of Total Meniscus Reconstruction Using a Novel Fiber-Reinforced Scaffold in an Ovine Model," *Am. J. Sports Med.*, vol. 44, no. 4, pp. 898–907, 2015.

[66] M. Kobayashi, J. Toguchida, and M. Oka, "Development of an artificial meniscus using polyvinyl alcohol-hydrogel for early return to, and continuance of, athletic life in sportspersons with severe meniscus injury. I: Mechanical evaluation," *Knee*, vol. 10, no. 1, pp. 47–51, 2003.

[67] M. Kobayashi, Y. S. Chang, and M. Oka, "A two year in vivo study of polyvinyl alcohol-hydrogel (PVA-H) artificial meniscus," *Biomaterials*, vol. 26, no. 16, pp. 3243–3248, 2005.

[68] B. T. Kelly *et al.*, "Hydrogel meniscal replacement in the sheep knee: Preliminary evaluation of chondroprotective effects," *Am. J. Sports Med.*, vol. 35, no. 1, pp. 43–52, 2007.

[69] J. L. Holloway, A. M. Lowman, and G. R. Palmese, "Mechanical evaluation of poly(vinyl alcohol)-based fibrous composites as biomaterials for meniscal tissue replacement," *Acta Biomater.*, vol. 6, no. 12, pp. 4716–4724, 2010.

[70] J. L. Holloway, A. M. Lowman, M. R. Vanlandingham, and G. R. Palmese, "Interfacial optimization of fiber-reinforced hydrogel composites for soft fibrous tissue applications," *Acta Biomater.*, vol. 10, no. 8, pp. 3581–3589, 2014.

[71] J. L. Holloway, "Development and Characterization of UHMWPE Fiber-Reinforced Hydrogels For Meniscal Replacement," Drexel University, 2012.

[72] W. G. Rodkey *et al.*, "Comparison of the Collagen Meniscus Implant with Partial Meniscectomy," *J. Bone Jt. Surgery-American Vol.*, vol. 90, no. 7, pp. 1413–1426, Jul. 2008.

[73] P. Buma, N. N. Ramrattan, T. G. van Tienen, and R. P. H. Veth, “Tissue engineering of the meniscus.,” *Biomaterials*, vol. 25, no. 9, pp. 1523–32, Apr. 2004.

[74] K. R. Stone, W. G. Rodkey, R. Webber, L. McKinney, and J. R. Steadman, “Meniscal regeneration with copolymeric collagen scaffolds,” *Am. J. Sports Med.*, vol. 20, no. 2, pp. 104–111, Mar. 1992.

[75] J. C. Monllau, X. Pelfort, and M. Tey, “Collagen Meniscus Implant: Technique and Results,” in *The Meniscus*, Berlin, Heidelberg: Springer Berlin Heidelberg, 2010, pp. 373–382.

[76] J. C. Monllau *et al.*, “Outcome After Partial Medial Meniscus Substitution With the Collagen Meniscal Implant at a Minimum of 10 Years’ Follow-up,” *Arthrosc. J. Arthrosc. Relat. Surg.*, vol. 27, no. 7, pp. 933–943, Jul. 2011.

[77] A. Ginés, P. Hinarejos, M. Tey, and J. C. Monllau, “COLLAGEN MENISCUS IMPLANT. OUTCOMES AFTER 4 TO 7 YEARS,” *Orthop. Proc.*, vol. 88–B, no. SUPP_II, p. 329, May 2006.

[78] S. J. Spencer, A. Saithna, M. R. Carmont, M. S. Dhillon, P. Thompson, and T. Spalding, “Meniscal scaffolds: Early experience and review of the literature,” *Knee*, vol. 19, no. 6, pp. 760–765, Dec. 2012.

[79] E. Genovese *et al.*, “Follow-up of collagen meniscus implants by MRI,” *Radiol. Med.*, vol. 112, no. 7, pp. 1036–1048, Oct. 2007.

[80] T. G. Tienen *et al.*, “Replacement of the Knee Meniscus by a Porous Polymer Implant,” *Am. J. Sports Med.*, vol. 34, no. 1, pp. 64–71, Jan. 2006.

[81] R. T. C. Welsing *et al.*, “Effect on Tissue Differentiation and Articular Cartilage Degradation of a Polymer Meniscus Implant,” *Am. J. Sports Med.*, vol. 36, no. 10, pp. 1978–1989, Oct. 2008.

[82] S. A. Maher *et al.*, “Evaluation of a Porous Polyurethane Scaffold in a Partial Meniscal Defect Ovine Model,” *Arthrosc. J. Arthrosc. Relat. Surg.*, vol. 26, no. 11, pp. 1510–1519, Nov. 2010.

[83] R. H. Brophy, J. Cottrell, S. A. Rodeo, T. M. Wright, R. F. Warren, and S. A. Maher, “Implantation of a synthetic meniscal scaffold improves joint contact mechanics in

a partial meniscectomy cadaver model," *J. Biomed. Mater. Res. - Part A*, vol. 92, no. 3, pp. 1154–1161, Mar. 2010.

[84] P. Verdonk *et al.*, "Successful Treatment of Painful Irreparable Partial Meniscal Defects With a Polyurethane Scaffold," *Am. J. Sports Med.*, vol. 40, no. 4, pp. 844–853, Apr. 2012.

[85] C. Van Der Straeten, B. Doyen, C. Dutordoir, W. Goedertier, S. Pirard, and J. Victor, "SHORT- AND MEDIUM-TERM RESULTS OF ARTIFICIAL MENISCAL IMPLANTS," *Orthop. Proc.*, vol. 98–B, no. SUPP_4, p. 91, Jan. 2016.

[86] J. J. Elsner, S. Portnoy, G. Zur, F. Guilak, A. Shterling, and E. Linder-Ganz, "Design of a Free-Floating Polycarbonate-Urethane Meniscal Implant Using Finite Element Modeling and Experimental Validation," *J. Biomech. Eng.*, vol. 132, no. 9, p. 095001, 2010.

[87] M. Shemesh, R. Asher, E. Zylberberg, F. Guilak, E. Linder-Ganz, and J. J. Elsner, "Viscoelastic properties of a synthetic meniscus implant," *J. Mech. Behav. Biomed. Mater.*, vol. 29, pp. 42–55, 2014.

[88] R. Pöllänen, A.-M. Tikkanen, M. J. Lammi, and R. Lappalainen, "The effect of loading and material on the biomechanical properties and vitality of bovine cartilage in vitro.," *J. Appl. Biomater. Biomech.*, vol. 9, no. 1, pp. 47–53, 2011.

[89] G. Zur *et al.*, "Chondroprotective effects of a polycarbonate-urethane meniscal implant: Histopathological results in a sheep model," *Knee Surgery, Sport. Traumatol. Arthrosc.*, vol. 19, no. 2, pp. 255–263, 2011.

[90] S. A. Maher, S. A. Rodeo, H. G. Potter, L. J. Bonassar, T. M. Wright, and R. F. Warren, "A Pre-Clinical Test Platform for the Functional Evaluation of Scaffolds for Musculoskeletal Defects: The Meniscus," *HSS J.*, vol. 7, no. 2, pp. 157–163, 2011.

[91] I. Kutzner *et al.*, "Loading of the knee joint during activities of daily living measured in vivo in five subjects," *J. Biomech.*, vol. 43, no. 11, pp. 2164–2173, 2010.

[92] C. Tudor-Locke *et al.*, "How many steps/day are enough? For adults.," *Int. J. Behav. Nutr. Phys. Act.*, vol. 8, p. 79, Jul. 2011.

[93] A. C. T. Vrancken *et al.*, "3D geometry analysis of the medial meniscus--a statistical shape modeling approach.," *J. Anat.*, vol. 225, no. 4, pp. 395–402, Oct. 2014.

[94] K. Bloecker *et al.*, "Revision 1 Size and position of the healthy meniscus, and its Correlation with sex, height, weight, and bone area- a cross-sectional study," *BMC Musculoskelet. Disord.*, vol. 12, pp. 1–9, 2011.

[95] A. M. Lowman and N. A. Peppas, "Hydrogels," *Encycl. Control. drug Deliv.*, vol. 1, pp. 397–418, 1999.

[96] C. M. Hassan and N. A. Peppas, "Structure and Morphology of Freeze/Thawed PVA Hydrogels," *Macromolecules*, vol. 33, no. 7, pp. 2472–2479, Apr. 2000.

[97] V. I. Lozinsky, L. G. Damshkaln, I. N. Kurochkin, and I. I. Kurochkin, "Study of cryostructuring of polymer systems: 28. Physicochemical properties and morphology of poly(vinyl alcohol) cryogels formed by multiple freezing-thawing," *Colloid J.*, vol. 70, no. 2, pp. 189–198, Apr. 2008.

[98] R. Ricciardi, F. Auriemma, C. Gaillet, C. De Rosa, and F. Lauprêtre, "Investigation of the Crystallinity of Freeze/Thaw Poly(vinyl alcohol) Hydrogels by Different Techniques," *Macromolecules*, vol. 37, no. 25, pp. 9510–9516, Dec. 2004.

[99] T. Hatakeyema, J. Uno, C. Yamada, A. Kishi, and H. Hatakeyama, "Gel–sol transition of poly(vinyl alcohol) hydrogels formed by freezing and thawing," *Thermochim. Acta*, vol. 431, no. 1–2, pp. 144–148, Jun. 2005.

[100] C. M. Hassan and N. A. Peppas, "Structure and Applications of Poly(vinyl alcohol) Hydrogels Produced by Conventional Crosslinking or by Freezing/Thawing Methods," in *Biopolymers · PVA Hydrogels, Anionic Polymerisation Nanocomposites*, Berlin, Heidelberg: Springer Berlin Heidelberg, 2000, pp. 37–65.

[101] A. JOSHI *et al.*, "Functional compressive mechanics of a PVA/PVP nucleus pulposus replacement," *Biomaterials*, vol. 27, no. 2, pp. 176–184, Jan. 2006.

[102] N. A. Peppas, "Turbidimetric studies of aqueous poly(vinyl alcohol) solutions," *Die Makromol. Chemie*, vol. 176, no. 11, pp. 3433–3440, Nov. 1975.

[103] S. R. Stauffer and N. A. Peppast, "Poly(vinyl alcohol) hydrogels prepared by freezing-thawing cyclic processing," *Polymer (Guildf).*, vol. 33, no. 18, pp. 3932–

3936, Sep. 1992.

[104] K. L. Spiller, S. J. Laurencin, D. Charlton, S. A. Maher, and A. M. Lowman, "Superporous hydrogels for cartilage repair: Evaluation of the morphological and mechanical properties," *Acta Biomater.*, vol. 4, no. 1, pp. 17–25, Jan. 2008.

[105] M. I. Baker, S. P. Walsh, Z. Schwartz, and B. D. Boyan, "A review of polyvinyl alcohol and its uses in cartilage and orthopedic applications," *J. Biomed. Mater. Res. - Part B Appl. Biomater.*, vol. 100 B, no. 5, pp. 1451–1457, 2012.

[106] Y.-S. Chang, H.-O. Gu, M. Kobayashi, and M. Oka, "Comparison of the bony ingrowth into an osteochondral defect and an artificial osteochondral composite device in load-bearing joints," *Knee*, vol. 5, no. 3, pp. 205–213, Jun. 1998.

[107] J. D. Henderson, R. H. Mullarky, and D. E. Ryan, "Tissue biocompatibility of kevlar aramid fibers and polymethylmethacrylate, composites in rabbits," *J. Biomed. Mater. Res.*, vol. 21, no. 1, pp. 59–64, Jan. 1987.

[108] E. Salernitano and C. Migliaresi, "Composite materials for biomedical applications: a review.," *J. Appl. Biomater. Biomech.*, vol. 1, no. 1, pp. 3–18, 2003.

[109] M. Jassal and S. Ghosh, "Aramid fibres - An overview," *Indian J. Fibre Text. Res.*, vol. 27, pp. 290–306, Sep. 2002.

[110] F. Franceschini and M. Galetto, "A new approach for evaluation of risk priorities of failure modes in FMEA," *Int. J. Prod. Res.*, vol. 39, no. 13, pp. 2991–3002, Jan. 2001.

[111] A. Bedi *et al.*, "Dynamic Contact Mechanics of the Medial Meniscus as a Function of Radial Tear, Repair, and Partial Meniscectomy," *J. Bone Jt. Surgery-American Vol.*, vol. 92, no. 6, pp. 1398–1408, Jun. 2010.

[112] J. Babu, R. M. Shalvoy, and S. B. Behrens, "Diagnosis and Management of Meniscal Injury.," *R. I. Med. J. (2013)*, vol. 99, no. 10, pp. 27–30, Oct. 2016.

[113] M. Tissakht and A. M. Ahmed, "Tensile stress-strain characteristics of the human meniscal material," *J. Biomech.*, vol. 28, no. 4, pp. 411–422, 1995.

[114] D. Bruni, F. Iacono, I. Akkawi, M. Gagliardi, S. Zaffagnini, and M. Marcacci, "Unicompartmental knee replacement: A historical overview," *Joints*, vol. 1, no. 2, pp. 45–47, 2013.

[115] R. Spencer Jones *et al.*, "Direct measurement of hoop strains in the intact and torn human medial meniscus," *Clin. Biomech.*, vol. 11, no. 5, pp. 295–300, 1996.

[116] M. Freutel *et al.*, "Medial meniscal displacement and strain in three dimensions under compressive loads: MR assessment," *J. Magn. Reson. Imaging*, vol. 40, no. 5, pp. 1181–1188, 2014.

[117] A. Seitz, R. Kasisari, L. Claes, A. Ignatius, and L. Dürselen, "Forces acting on the anterior meniscotibial ligaments," *Knee Surgery, Sport. Traumatol. Arthrosc.*, vol. 20, no. 8, pp. 1488–1495, 2012.

[118] K. L. Markolf, S. R. Jackson, and D. R. McAllister, "Force measurements in the medial meniscus posterior horn attachment: Effects of anterior cruciate ligament removal," *Am. J. Sports Med.*, vol. 40, no. 2, pp. 332–338, 2012.

[119] M. A. Sweigart *et al.*, "Intraspecies and interspecies comparison of the compressive properties of the medial meniscus," *Ann. Biomed. Eng.*, vol. 32, no. 11, pp. 1569–1579, 2004.

[120] M. D. Joshi, J. -K Suh, T. Marui, and S. L. -. Woo, "Interspecies variation of compressive biomechanical properties of the meniscus," *J. Biomed. Mater. Res.*, vol. 29, no. 7, pp. 823–828, 1995.

[121] H. N. Chia and M. L. Hull, "Compressive moduli of the human medial meniscus in the axial and radial directions at equilibrium and at a physiological strain rate," *J. Orthop. Res.*, vol. 26, no. 7, pp. 951–956, 2008.

[122] D. Kumar, K. T. Manal, and K. S. Rudolph, "Knee joint loading during gait in healthy controls and individuals with knee osteoarthritis," *Osteoarthr. Cartil.*, vol. 21, no. 2, pp. 298–305, 2013.

[123] B. B. Seedhom, D. Dowson, and V. Wright, "Proceedings: Functions of the menisci. A preliminary study.," *Ann. Rheum. Dis.*, vol. 33, no. 1, pp. 111–111, 1974.

[124] M. McDowell, C. Fryar, C. Ogden, and K. Flegal, "Anthropometric reference data

for children and adults: United States, 2003-2006," *Natl. Health Stat. Report.*, no. 10, pp. 2003–2006, 2008.

[125] T. Fukubayashi and H. Kurosawa, "the contact area and pressure distribution pattern of the knee: A study of normal and osteoarthrotic knee joints," *Acta Orthop.*, vol. 51, no. 1–6, pp. 871–879, 1980.

[126] A. Bedi *et al.*, "Dynamic contact mechanics of the medial meniscus as a function of radial tear, repair, and partial meniscectomy," *J. Bone Jt. Surg. - Ser. A*, vol. 92, no. 6, pp. 1398–1408, 2010.

[127] P. Cignoni *et al.*, "MeshLab: an Open-Source Mesh Processing Tool," *Sixth Eurographics Ital. Chapter Conf.*, pp. 129–136, 2008.

[128] L. McCann, E. Ingham, Z. Jin, and J. Fisher, "Influence of the meniscus on friction and degradation of cartilage in the natural knee joint," *Osteoarthr. Cartil.*, vol. 17, no. 8, pp. 995–1000, Aug. 2009.

[129] K. Mansmann, "Meniscus-type implant with hydrogel surface reinforced by three-dimensional mesh," 6629997, 27-Mar-2001.

[130] C. Gatt, A. Merriam, and M. Dunn, "Implantable device and method to replace the meniscus of the knee and other body structures," 9078756, 15-Mar-2013.

[131] H. Fox, "Meniscus prosthetic device," 9320606, 25-May-2012.

[132] A. Shterling, E. Linder-Ganz, and A. Danino, "Tensioned meniscus prosthetic devices and associated methods," 8778024, 09-Sep-2011.

[133] A. Lowman, G. Palmese, S. Maher, R. Warren, T. Wright, and J. Holloway, "Fiber-Hydrogel Composite for Tissue Replacement," 0288199, 19-May-2010.